inorganics

MDPI

Review

Role of Silver Nanoparticles in Wound Healing: Mechanisms, Efficacy, and Clinical Applications

Paul Cătălin Balaure [1,*], Adelina-Gabriela Niculescu [1,2], Daniela Anghel [3,4], Alexandru Mihai Grumezescu [1,2] and Adina Alberts [5]

[1] Faculty of Chemical Engineering and Biotechnology, National University of Science and Technology Politehnica Bucharest, 011061 Bucharest, Romania; adelina.niculescu@upb.ro (A.-G.N.); agrumezescu@upb.ro (A.M.G.)
[2] Research Institute of the University of Bucharest—ICUB, University of Bucharest, 050657 Bucharest, Romania
[3] Department of Internal Medicine 2, Central Military Emergency University Hospital 'Dr. Carol Davila', 010825 Bucharest, Romania
[4] Department of Medico Surgical and Prophylactic Disciplines, 'Titu Maiorescu' University, 031593 Bucharest, Romania
[5] Faculty of Medicine, Carol Davila University of Medicine and Pharmacy, 050474 Bucharest, Romania
* Correspondence: paul.balaure@upb.ro

Abstract

Wound healing is a complex biological process involving haemostasis, inflammation, cellular proliferation, and remodelling. The use of silver nanoparticles (AgNPs) in wound care has gained significant attention due to their potent antimicrobial, anti-inflammatory, and tissue-regenerating properties. This review provides a comprehensive analysis of the role of AgNPs in wound healing, focusing on their mechanisms of action, efficacy, and clinical applications. The antimicrobial activity of AgNPs helps prevent infections in both acute and chronic wounds, while their ability to modulate inflammation and promote angiogenesis accelerates tissue repair. Various AgNP-based delivery systems, including hydrogels, nanofiber dressings, and composite biomaterials, are explored in the context of wound management, with special emphasis on smart, stimuli-responsive wound dressings. Additionally, clinical evidence supporting the effectiveness of AgNPs in treating chronic, burn, and surgical wounds is reviewed, along with considerations of their safety, cytotoxicity, and regulatory challenges. Although AgNPs present a promising alternative to conventional wound dressings and antibiotics, further research is needed to optimize their formulations and ensure their long-term safety. This review aims to provide insights into current advancements and future perspectives of AgNP-based wound-healing therapies.

Keywords: wound healing; silver nanoparticles; AgNPs; antimicrobial activity; anti-inflammatory; tissue regeneration; angiogenesis; hydrogels; nanofiber dressings; composite biomaterials; smart wound dressings; chronic wounds; burns; surgical wounds; cytotoxicity; safety; clinical applications; regulatory challenges; tissue repair; nanotechnology in medicine

Academic Editors: Eduardo Padilla-Camberos and Angélica Sofía González-Garibay

Received: 30 October 2025
Revised: 28 November 2025
Accepted: 2 December 2025
Published: 6 December 2025

Citation: Balaure, P.C.; Niculescu, A.-G.; Anghel, D.; Grumezescu, A.M.; Alberts, A. Role of Silver Nanoparticles in Wound Healing: Mechanisms, Efficacy, and Clinical Applications. *Inorganics* **2025**, *13*, 401. https://doi.org/10.3390/inorganics13120401

1. Introduction: Wounds and the Wound Healing Process

A wound is an injury that disrupts the integrity of the skin, mucous membranes, or deeper tissues, resulting from accidental trauma, surgical procedures, or certain underlying medical conditions. Wounds can be classified by aetiology and appearance. According to aetiology, wounds can be acute and chronic [1,2]. Acute wounds occur suddenly and heal normally, while chronic wounds are characterized by a delayed or impaired healing

process, resulting in persistent inflammation and pain, infectious processes including biofilm development, and the presence of non-viable tissue. The appearance of wounds varies widely depending on aetiology, but roughly speaking, wounds can be open or closed. In open wounds (abrasions, lacerations, incisions, punctures, avulsions, burns), the integrity of the protective skin barrier or mucosal surface is disrupted, exposing the underlying tissue and increasing the risk of infection. On the other hand, in closed wounds (contusions, blisters, seromas, hematomas, crush injuries), the skin remains intact, but the underlying tissues and/or blood vessels are damaged [3–5].

Regardless of the wound type, the normal healing process consists of four sequential, overlapping stages involving a complex network of signalling molecules and cells, closely interconnected within the wound-healing cascade. The four phases of wound healing are: haemostasis, inflammation, proliferation, and tissue remodelling [6,7].

Haemostasis is the body's immediate response to injury, aiming to prevent excessive bleeding by forming a clot. Basically, adhesion and aggregation of platelets at the damaged site form an initial plug, which is further stabilized by a fibrin mesh, a protein produced during the clotting cascade.

The key aim of the inflammation phase of the wound healing process is to prevent infection. Besides their essential role in clotting, platelets also produce a plethora of growth factors and cytokines, which act as chemical signals regulating the healing cascade. For instance, the release of transforming growth factor beta (TGF-β) and platelet-derived growth factor (PDGF) by platelets plays a dual role. On one hand, these proteins initiate chemotaxis of neutrophils and macrophages, which destroy debris and bacteria, and on the other hand, they stimulate the immune blood cells to secrete additional cytokines like the fibroblast growth factor (FGF), PDGF, TNF-α (tumour necrosis factor alpha), and IL-1 (interleukin-1) [6–8].

Once the inflammatory response is balanced and the debris is removed, the proliferation phase begins to repair the defect. The proliferative stage encompasses several simultaneously occurring processes, namely angiogenesis, fibroblast migration, epithelialization, and wound retraction [6,7].

The final remodelling phase of wound healing involves strengthening and refining the newly developed tissue. This stage is characterized by the replacement of the initial type III collagen by the stronger type I collagen, decreased vascularity, and scar formation. However, full restoration of the original tissue's tensile strength is never achieved [7].

Classical wound care faces several critical challenges, particularly in the treatment of chronic wounds and burn wounds [9–11]. One major issue is the dynamic changes in the wound environment during healing [12–14]. Local factors such as hypoxia, ischemia, oxidative stress, enzymatic degradation of growth factors by matrix metalloproteinases (MMPs), infection, pathogenic biofilm formation, moisture imbalance, and the development of necrosis all pose serious threats to the patient's health. In many cases, conventional treatments are unable to effectively address and overcome these risks. The clinical picture is even more complicated by systemic factors in diabetic, elderly, malnourished, or chronically ill patients. Achieving homeostasis (a stable, well-balanced internal environment) in each stage of wound healing is crucial for successful wound repair [7]. During the haemostasis stage, transient hypoxia resulting from vasoconstriction and increased oxygen demand during clotting triggers the production of reactive oxygen species (ROS) and activates hypoxia-inducible factor (HIF-1). HIF-1, in turn, regulates the expression of vascular endothelial cell growth factor (VEGF), stimulating neovascularization. HIF-1 also induces expression of nitric oxide synthase (NOS) genes and the production of nitric oxide (NO) [15]. NO, a potent vasodilator, counterbalances vasoconstriction, restores blood flow and oxygen delivery, and helps prevent ischemia. It also inhibits platelet aggregation, helping prevent

excessive blood clotting. Although acute hypoxia in the early phase of wound healing is beneficial, prolonged or unbalanced hypoxia is detrimental to later stages of the process. On the other hand, ROS such as the superoxide radical anion $(O^{2-})^{\cdot}$ increases fibrin deposition during the haemostasis stage, while H_2O_2 induces the recruitment of monocytes and neutrophils [16]. ROS play important roles not only during haemostasis but also along the whole wound repair process. During inflammation, ROS activate immune cells and help prevent infection by destroying pathogens. ROS modulate cellular signalling pathways involved in the proliferation stage, promoting angiogenesis and the proliferation, migration, and differentiation of fibroblasts and keratinocytes. Eventually, ROS contributes to collagen remodelling in the final stage of wound repair [17,18]. However, excessive ROS levels lead to oxidative stress, which damages tissues and disrupts the healing process, resulting in chronic wounds. The remodelling stage requires a delicate, continuously regulated balance between the breakdown of damaged extracellular matrix (ECM)—including collagen and other proteins—by MMPs, and the synthesis of new collagen by fibroblasts to rebuild the ECM [19]. Strict control of proteolytic activity is therefore crucial for successful tissue repair, and this is achieved by tissue inhibitors of metalloproteinases (TIMPs) [13,20]. An imbalance between proteolytic enzymes and their inhibitors underlies the abnormal healing seen in chronic ulcers.

Silver nanoparticles (AgNPs) are emerging as a valuable therapeutic option for wound care due to their antimicrobial and anti-inflammatory properties, as well as their ability to support the normal progression of acute wound healing through all four stages and to prevent delayed or impaired tissue repair and chronic wound formation [21–23].

This paper aims to provide an up-to-date overview of the complex role of AgNPs in wound healing, including mechanistic insights based on current knowledge. It also reviews currently available AgNPs-based nanomaterials—such as AgNPs-coated wound dressings, nanofibers, hydrogels, and nanocomposite semipermeable film dressings—and their performance in preclinical studies and clinical trials. Safety concerns, risks, and limitations, as well as future challenges and perspectives in the development of AgNPs-based wound care strategies, are also addressed.

2. Effects of AgNPs on Wound Healing with Mechanistic Insights

2.1. Antimicrobial and Anti-Biofilm Activities

The antimicrobial properties of silver and its compounds have been recognized for centuries. Even in ancient times, diluted silver salt solutions were used to treat eye infections in newborns and burn wounds [21–25]. As a result of the recent rapid and significant advances in metallic nanoparticle research, the effects and applications of AgNPs in wound care have received growing, widespread attention. Silver-based nanomaterials are used in wound dressings for their ability to effectively prevent and control bacterial colonization and pathogenic biofilm formation, as well as to manage infections, thereby facilitating and promoting wound healing. Although the precise mechanism underlying the antimicrobial effects of AgNPs has not yet been fully elucidated, several key molecular and cellular targets have been identified, and the effects of AgNPs on these targets have been partially clarified [21–23,26,27].

The first step in the complex antibacterial mechanism of AgNPs involves the attachment of nanoparticles to the negatively charged bacterial cell wall and membrane, primarily driven by electrostatic attraction to the positively charged silver ions [28–30]. Various mechanisms underlie the antimicrobial activity of AgNPs, including the release of silver ions, the generation of ROS in vivo, increased oxidative stress, alterations in important cellular and molecular structures such as the cell membrane and ribosomes, and impacts on protein synthesis, DNA, and intracellular metabolic pathways.

2.1.1. Oxidative Dissolution of AgNPs in Biological Media and the Effect of Some Important Physicochemical Characteristics of AgNPs on the Rate of Silver Ions Release and Antibacterial Activity

There is ongoing scientific debate about whether the antibacterial activity is primarily due to the intrinsic properties of the metallic particles (Ag^0NPs) themselves, or to the Ag^+ ions released through oxidative dissolution of AgNPs in biological aqueous environments, as described by the following chemical processes [31]:

$$4Ag + O_2 \rightarrow 2Ag_2O \quad (1)$$

$$2Ag_2O + 4H^+ \rightarrow 4\ Ag^+ + 2H_2O \quad (2)$$

Several studies suggest that silver ions (Ag^+) are responsible for the cytotoxic effects of AgNPs, as their bactericidal activity is significantly reduced under anaerobic conditions. Consequently, the role of AgNPs would be only that of a reservoir releasing Ag^+ ions that exert the observed antibacterial effects [32–35]. In vivo, AgNPs might release Ag^+ ions by interaction with H_2O_2 [36,37].

The kinetics of ion release—and the resulting antibacterial activity—strongly depend on physicochemical features of AgNPs, such as morphology (size, shape, and crystallinity), surface functionalization, and charge [35,38,39].

Smaller nanoparticles dissolve faster than larger ones, thereby releasing more Ag^+, resulting in greater antibacterial activity [38]. Several methods are available today for producing AgNPs with controlled dimensions. Wu et al., synthesized AgNPs by reducing $AgNO_3$ with $NaBH_4$ in the presence of citric acid (CA) as a capping agent. By adjusting the pH of the reaction medium, they produced nanoparticles of different sizes: 2 nm at pH 11, 12 nm at pH 9, and 32 nm at pH 7 [40]. Green-synthesized AgNPs were obtained by Skandalis and co-workers [41] using a phenolic- and flavonoid–rich aqueous extract of the plant *Arbutus unedo* as both reducing and stabilizing agent. They obtained AgNPs of two different sizes (40 nm and 58 nm) by tuning the amount of the fresh leaf extract used in the synthesis. In a similar approach, Balu et al. [42] reported the synthesis of AgNPs using an extract from *Rosa indica* petals as a reducing and stabilizing agent. They investigated the influence of the extraction solvent on nanoparticle size and found that acetone and ethanol extracts produced AgNPs of approximately 12 nm and 18 nm, respectively, whereas water as the solvent resulted in significantly larger nanoparticles, around 700 nm.

Differently, Hileuskaya and co-workers [43] used three types of pectin polysaccharides—high-methoxyl (PectHM), low-methoxyl (PectLM), and amidated low-methoxyl (PectA)—to synthesize spherical AgNPs coated with a stabilizing pectin shell. The nanoparticle diameter varied depending on the degree of pectin esterification and the presence of specific functional groups. TEM micrographs of high- and low-methoxyl pectin-capped nanoparticles showed sizes in the 8–13 nm range, whereas the amidated low-methoxyl pectin–Ag nanocomposite exhibited a larger average diameter of 28 ± 7 nm. Ji et al. [44] synthesized AgNPs capped with a thermo-responsive copolymer of N-isopropylacrylamide (NIPAM) and 5-(2-methacryloylethoxymethyl)-8-hydroxyquinoline (MQ), denoted as p(NIPAM-co-MQ), by reducing silver nitrate with sodium borohydride in the presence of the copolymer. By varying the molar ratio of the copolymer to the Ag precursor, they were able to control the nanoparticle size, producing three samples with average diameters of approximately 3.91 nm, 2.29 nm, and 1.59 nm, respectively. The larger the above ratio, the smaller the size of the obtained AgNPs and the narrower the size distribution of AgNPs. The AgNPs with a higher content of thermo-responsive copolymer and smaller particle size exhibited the most potent antibacterial activity against kanamycin-resistant *Escherichia coli* at 28 °C—below the copolymer's lower critical solution temperature (LCST), where the polymer shell re-

mains in a hydrophilic, swollen state. At this temperature, 1.59 nm AgNPs stabilized by the copolymer completely inhibited *E. coli* growth within 72 h at a concentration of 16.2 μg/mL. However, when the temperature increased to 37 °C, the antibacterial activity pattern reversed: the largest nanoparticles with the lowest content of the thermo-responsive copolymer became the most effective. This shift was attributed to the temperature-induced hydrophobic collapse of the copolymer shell, which reduced bacterial contact and hindered silver ion release [44], nicely illustrating the impact of AgNPs' surface properties on their antibacterial performance.

Surface charge also plays a critical role. Hadari et al. [45] synthesized ultrasmall AgNPs (<3 nm) functionalized with the polycationic polymer chitosan and compared their antibacterial and anti-biofilm activities to those of identically sized AgNPs with a negatively charged surface. The chitosan-coated AgNPs exhibited superior performance in both antibacterial and antibiofilm tests. To demonstrate the effect of surface functionalization on Ag^+ ion release rate, Kittler et al. [46] investigated the oxidative dissolution of AgNPs capped with either citrate or polyvinylpyrrolidone (PVP) in aqueous suspension at various temperatures. They found that the uncharged, PVP-functionalized AgNPs had a higher dissolution rate than the negatively charged citrate-coated AgNPs, because the latter's surface charge acted as a barrier to silver cation release. Additionally, the release rate increased with temperature, consistent with the rise in kinetic energy.

In addition to size, the shape of nanoparticles can influence their antibacterial activity by affecting surface energy, surface area, and, thereby, the degree of contact with the bacterial cell membrane and surface charge distribution [38]. Currently, several synthetic methods for non-spherical AgNPs are available, including chemical and bio-based syntheses [38,47,48]. Hong and co-workers prepared AgNPs in the form of nanospheres, nanocubes, and nanowires by microwave-assisted reduction of $AgNO_3$ with ethylene glycol in the presence of PVP and varying amounts of NaCl [49]. The antibacterial activity of the differently shaped AgNPs against *E. coli* was evaluated using optical density (OD) measurements, growth curve analysis, and minimum inhibitory concentration (MIC) assays. Nanocubes exhibited the strongest antibacterial activity, followed by nanospheres and nanowires [49]. TEM analysis revealed that nanocubes and nanospheres had closer contact with the bacterial surface compared to nanowires. The enhanced antibacterial activity of nanocubes relative to nanospheres was attributed to differences in the surface energy of their crystal facets. Nanocubes have higher surface energy, leading to greater reactivity. Goyal et al. [50] synthesized anisotropic, plate-like AgNPs of identical size but with different edge morphologies—sharp versus rounded—and compared their antibacterial activity. They found that the sharper-edged nanoparticles exhibited higher antibacterial activity than those with round corners. This enhancement was attributed to the higher charge density at sharp corners. A higher charge density renders AgNPs more able to disrupt bacterial cell membrane permeability [50]. Another nice example of morphological influences on antibacterial activity was provided by Seyedpour and co-workers [51]. They synthesized, characterized, and studied the antibacterial activity of supramolecular self-assembled coordination polymers obtained by stirring at room temperature an aqueous solution of $AgNO_3$ with a previously sonicated ethanolic solution of three different imidazole ligands, namely imidazole, 2-methylimidazole, and benzimidazole. The morphology of the resulting nanocrystalline coordination polymers, denoted as Ag-Imid, Ag-2-Imid, and Ag-Benz, respectively, was investigated by TEM analysis, which revealed an organic ligand-dependent morphology: octahedral and hexagonal sheets for Ag-2-Imid and Ag-Imid, respectively, and nanoribbons for Ag-Benz. X-ray photoelectron spectroscopy (XPS) revealed that the silver content in the three hybrid nanostructures decreased in the following order: Ag-2Imid > Ag-Imid > Ag-Benz. This trend also matched the decreasing

antibacterial activity observed against *E. coli* and *Bacillus subtilis*, as determined using a cell staining assay with the propidium iodide (PI)/SYTO9 fluorescent dye kit. The authors conclude that the above antibacterial efficiency order was determined by the silver concentration and specific nanocrystal structure [51].

The above-presented effects of the physicochemical characteristics of various types of AgNPs on their antimicrobial efficacy are summarized in the tables below. Specifically, Table 1 emphasizes the differences in antibacterial activity depending on AgNP size; Table 2 highlights the effects on NP shape; and Table 3 overviews the effects of surface functionalization and charge.

Table 1. The effects of AgNPs' size on their antibacterial activity.

Type of AgNPs	Method of Preparation	Size	Targeted Microorganisms	Magnitude of the Antibacterial Activity	Ref.
Citrate-capped AgNPs of different sizes depending on pH	Reduction of $AgNO_3$ by $NaBH_4$ in the presence of citrate as the capping agent	2 nm 12 nm 32 nm	*E. coli* *Staphylococcus aureus*	The smaller the NPs, the stronger the activity	[40]
AgNPs of different sizes, depending on the amount of fresh leaf extract	Reduction of $AgNO_3$ by an aqueous extract of *Arbutus unedo*	40 nm 58 nm	*E. coli* *Pseudomonas aeruginosa* *Bacillus subtilis* *Staphylococcus epidermidis*		[41]
AgNPs of different sizes, depending on the nature of the extraction solvent	Reduction of $AgNO_3$ by the petals extract of *Rosa Indica*	12 nm 18 nm 700 nm	*E. coli* *S. aureus* Observation: good biocompatibility assessed by haemolysis assay		[42]
AgNPs of different sizes, depending on the degree of pectin esterification and specific functional groups	Reduction of $AgNO_3$ by pectin in alkaline medium	8–13 nm 28 ± 7 nm	*Bacillus subtilis* *Bacillus pumilus* *E. coli*		[43]
Thermo-sensitive co-polymer-capped AgNPs	Reduction of $AgNO_3$ by $NaBH_4$ in the presence of a thermos-responsive copolymer as the capping agent	1.59 nm 2.29 nm 3.91 nm	*E. coli* *S. aureus* Kanamycin-resistant *E. coli* Observation: No toxicity against mammalian cells		[44]

Table 2. The effects of AgNPs' shape on their antibacterial activity.

Type of AgNPs	Method of Preparation	Shape	Targeted Microorganisms	Magnitude of the Antibacterial Activity	Ref.
AgNPs of different shapes	Microwave-assisted reduction of $AgNO_3$ by ethylene glycol in the presence of PVP and varying amounts of NaCl	Nanocubes Nanospheres Nanowires	*E. coli*	The antimicrobial activity decreased in the order Nanocubes > Nanospheres > Nanowires.	[49]
AgNPs with different edge morphologies	Solvothermal method involving the reduction of $AgNO_3$ in dimethylformamide in the presence of PVP	Anisotropic plate-like NP with: - sharp edges - round edges	*E. coli* *S. aureus* *Bacillus* (MTCC 1789) *Streptococcus pyogenes* *Vibrio cholerae*	The AgNPs with sharp edges and corners showed greater antibacterial activity than those with rounded edges and corners.	[50]

Table 2. *Cont.*

Type of AgNPs	Method of Preparation	Shape	Targeted Microorganisms	Magnitude of the Antibacterial Activity	Ref.
Nanocrystals of supramolecular coordination polymers of different shapes, depending on the type of imidazole ligands	Mixing at room temperature an aqueous solution of $AgNO_3$ with previously sonicated ethanolic solutions of three different imidazole ligands	Octahedral Hexagonal Nanosheet Nanoribbon	*E. coli* *B. subtilis*	The antibacterial activity decreased in the order: Ag-2Imid (octahedral nanocrystals) > Ag-Imid (hexagonal nanostructures > Ag-Benz (nanoribbons).	[51]

Table 3. The effects of AgNPs' surface functionalization and charge on their antibacterial activity.

Type of AgNPs	Method of Preparation	Targeted Microorganisms	Magnitude of the Antibacterial Activity	Ref.
Polycationic silver nanoclusters	Reduction of $AgNO_3$ in the presence of chitosan as both a reducing and capping agent	*Fusobacterium Nucleatum* *Streptococcussanguinis*	Positively charged AgNPs enhance penetration to the bacterial cell membrane compared to the corresponding negatively charged counterparts.	[45]
Negatively charged MSA-coated AgNPs	Reduction of $AgNO_3$ by $NaBH_4$ in the presence of mercaptosuccinic acid (MSA or thiomalic acid)			
Neutrally PVP-capped AgNPs	Reduction of $AgNO_3$ by glucose in the presence of PVP	-	The neutral PVP-capped AgNPs have a higher dissolution rate than citrate-coated AgNP.	[35,46]
Negatively charged citrate-capped AgNPs	Reduction of $AgNO_3$ by sodium citrate			

2.1.2. Disruption of Bacterial Cell Membrane

A well-documented cytotoxic effect of silver-based nanomaterials on pathogenic bacteria is their ability to disrupt the integrity of the cell membrane barrier, thereby altering its permeability. In addition to its protective function, the bacterial cell membrane also serves as the site of key metabolic pathways, including the electron transport chain and oxidative phosphorylation. The attachment of metal nanoparticles to bacterial cell membranes is driven by various intermolecular forces, such as electrostatic attractions, van der Waals forces, receptor–ligand interactions, and hydrophobic effects [29,52–54].

The denaturing action of metallic nanoparticles and metallic ions on the cell membrane begins as soon as they attach to the bacterial surface. Several microscopy techniques demonstrated that even brief contact with AgNPs can cause severe damage to the bacterial cell wall, leading to the formation of dense pits [55–60]. Comparative transmission and scanning electron microscopy (TEM and SEM) images of AgNPs-exposed and untreated bacterial cells revealed striking morphological differences in the cell wall. In AgNPs-treated cells, large disruptions, irregular pits, and apparent leakage of cytoplasmic content were observed. In sharp contrast, untreated cells displayed smooth, intact cell walls and a homogeneous distribution of cytoplasmic material [60]. Altered permeability of the bacterial cell wall and membrane disrupts the cell's ability to regulate its internal environment, leading to lysis and eventual cell death.

Both positively charged AgNPs and their released Ag^+ ions easily interact with the sulfhydryl groups of proteins in the bacterial cell wall and membrane [61–63] as well as with the phosphate groups in the phospholipid bilayer forming complexes that disrupt the structural integrity of the cell membrane leading to increased permeability, enhanced

uptake of toxic substances like antibiotics, and leakage of vital ions like H^+ and K^+. Protons from the extracellular environment enter the cell through damaged or permeabilized membrane regions, and this uncontrolled influx of H^+ dissipates the proton gradient across the membrane (the proton motive force, PMF). As a result, the exergonic electron transport chain (ETC) becomes uncoupled from oxidative phosphorylation, since protons leak across the membrane without passing through ATP synthase. This deprives the endergonic ATP synthesis process of its energy source, leading to rapid depletion of cellular ATP levels, which in turn impairs other bacterial defence mechanisms, such as efflux pumps [64].

By embedding into the cell membrane, AgNPs disrupt lipid packing and create pores, allowing the extracellular leakage of intracellular K^+ and leading to the collapse of the electrochemical gradient across the membrane. As a result, the membrane potential drops, the membrane becomes depolarized, and the electric double layer surrounding the negatively charged bacterial surface shrinks. The zeta potential decreases [65], and all these changes are associated with increased membrane permeability and a diminished ability of the cell to regulate ion transport into and out of the cell. Consequently, the delicate and vital electrochemical balance that cells maintain across their membranes is disrupted. Moreover, AgNPs and silver ions interact with membrane-bound proteins of the ETC [66–68], forming disruptive complexes that denature and inhibit key enzymes such as cytochrome c oxidase and succinate dehydrogenase. These interactions also impair the function of coupled proton pumps, as do membrane ATPases. As a result, the bacterial cell loses its ability to restore membrane potential, and its energetic metabolism is disrupted as well. In addition, AgNPs' interaction with the ETC promotes excess production of ROS, which, in turn, initiates lipid peroxidation, further damaging the cell membrane.

Antibacterial activity is also dependent on the bacterial cell wall and cell membrane characteristics. In general, Gram-negative bacteria are more susceptible to AgNPs than Gram-positive bacteria, a difference attributed to structural differences in their cell wall composition. The cell wall of Gram-negative bacteria consists of an inner phospholipid bilayer (the plasma membrane), a thin intermediate peptidoglycan layer approximately 8 nm thick, and an outer phospholipid membrane containing numerous porin channels. This outer membrane is further coated with a 1–3 μm thick layer of negatively charged lipopolysaccharides (LPS). In contrast, the cell wall of Gram-positive bacteria lacks an outer membrane and, consequently, does not possess an LPS coating. Instead, it features a much thicker peptidoglycan layer (over 80 nm) enriched with covalently bound, negatively charged teichoic and teichuronic acids [69]. This thick, porin-free layer is thought to act as a barrier that sequesters positively charged AgNPs through strong electrostatic interactions. In Gram-negative bacteria, the outer membrane contains a negatively charged LPS layer that attracts AgNPs, while the abundant, water-filled porin channels facilitate the entry of hydrophilic species such as Ag^+ ions and ultrasmall AgNPs [70,71]. Although larger AgNPs cannot pass through the porins, their accumulation on the membrane surface can disrupt membrane integrity and generate larger pores, eventually allowing them to enter the cell, as previously discussed. The involvement of porins in Ag^+ ion transport [72] was demonstrated by the finding that *E. coli* expressing mutated porin proteins is less susceptible to silver ions, as shown by Li [73] and Radzig [74]. *E. coli* mutant strains deficient in OmpF or OmpC porins were 4–8 times more resistant to AgNPs when compared to the wild strain [74].

2.1.3. Effects of AgNPs on Bacterial Proteins

AgNPs denature bacterial cell membrane proteins, including ETC enzymes, and intracellular proteins involved in key metabolic pathways, ultimately leading to cell damage and death. Electrophilic silver deactivates important transmembrane enzymes underlying cellular energy generation and ion transport by forming stable S-Ag bonds with the

nucleophilic thiol groups of the cysteine residues in those proteins. Silver catalyses the formation of disulfide bridges in the reaction of cellular oxygen with thiol groups, thereby altering the native three-dimensional structure of cellular enzymes and disturbing their function. Denaturation of respiratory enzymes halts ATP production [75].

The expression of key proteins and enzymes—including the 30S ribosomal subunit protein S2, succinyl-CoA synthetase, the maltose transporter MalK, and fructose bisphosphate aldolase—was altered in cells treated with a 900 ppb Ag^+ solution [76–79]. These findings can be explained as follows: silver ion–induced downregulation of ribosomal protein S2 destabilizes the ribosome, impairing translation and protein synthesis. This disruption ultimately leads to cell death by suppressing key biosynthetic steps catalysed by essential metabolic enzymes, such as fructose bisphosphate aldolase in glycolysis and succinyl-CoA synthetase in the tricarboxylic acid (TCA) cycle. Both pathways are critical for ATP production in *E. coli* [79].

AgNP-induced disruption of the proton gradient, membrane potential, and proton motive force (PMF) inhibits the activity of bacterial efflux pumps, which are responsible for expelling antibiotics from the cell. Efflux pumps, along with other adaptive defence mechanisms, contribute significantly to the widespread emergence of multidrug resistance (MDR) in bacteria. These pumps are transmembrane transport proteins, and at least six distinct types have been identified in bacteria. Among them is one ATP-binding cassette (ABC) transporter, which is directly powered by ATP hydrolysis, and five secondary active transporters that utilize the electrochemical gradient across the membrane as their energy source [80]. Using an ethidium bromide (EtBr) accumulation assay, Behdad et al. measured the MIC of EtBr in MDR *Acinetobacter baumannii* clinical isolates treated with AgNPs synthesized via the reduction of $AgNO_3$ using an ethanolic leaf extract of *Acroptilon repens*. Compared to untreated cultures, the MIC values of EtBr were two to four times lower in the AgNP-treated cultures, indicating that the synthesized AgNPs inhibited efflux pump activity [81]. Moreover, using quantitative real-time PCR, the authors showed that, in isolates carrying efflux pump genes, expression levels of these genes were significantly reduced following treatment with sub-MICs of AgNPs [81] AgNPs by reducing $AgNO_3$ with $NaBH_4$ in the presence of glutamic acid and subsequently functionalized them by grafting with thiosemicarbazide (TSC). The resulting Ag-TSC-conjugated nanoparticles were evaluated for their ability to downregulate the expression of the *MexA* and *MexB* efflux pump genes in ciprofloxacin-resistant *Pseudomonas aeruginosa*. Using quantitative PCR, the authors found that strains exposed to both Ag-TSC NPs and ciprofloxacin showed 6.0-fold and 2.75-fold reductions in MexA and MexB expression, respectively, compared with control strains treated with ciprofloxacin alone [82]. Similar results were reported by Madhi et al., who showed that expression of the efflux pumps AdeB in A. baumannii and MexB in *P. aeruginosa* decreased after exposure to AgNPs loaded with antibiotics [83,84].

2.1.4. Generation of Reactive Oxygen Species

One proposed explanation for the strong bactericidal effect of Ag^+ is that silver ions bind to low redox-potential enzymes in the bacterial respiratory chain, impeding efficient electron flow to the terminal oxidoreductase, thereby leading to overproduction of ROS and increased oxidative stress [66]. It should be noted that ROS are not inherently harmful; they are produced at physiological levels as a normal consequence of aerobic metabolism and play essential roles in redox signalling. However, when ROS production exceeds the cell's antioxidant capacity, they become toxic. Cells possess defence mechanisms to maintain ROS within safe physiological limits. Two antioxidant enzymes act as ROS scavengers: superoxide dismutase (SOD) transforms the superoxide radical anion into hydrogen peroxide, while catalase (CAT) converts hydrogen peroxide to water and oxygen.

Oxidative stress occurs when this balance is disrupted, with ROS levels overcoming the cell's ability to neutralize them. For instance, elevated levels of hydrogen peroxide damage biomolecules and trigger an inflammatory response.

ROS such as hydrogen peroxide, superoxide radical anion, hydroxyl radical, singlet oxygen, and hypochlorous acid are highly reactive and attack and damage key biomolecules, including lipids, proteins, and nucleic acids, as well as critical cellular structures such as the cell membrane and ribosomes [75]. Chemical transformations of targeted biomolecules, such as lipid peroxidation, oxidative carbonylation of proteins, oxidative alteration of DNA bases, and strand excision, severely harm bacteria by disrupting membranes, inhibiting enzymes, and damaging DNA. These alterations can ultimately trigger mutations, metabolic failure, and cell death via apoptosis or necrosis.

In addition to its destructive effect on cell membranes, lipid peroxidation of polyunsaturated fatty acids (PUFAs) ultimately produces toxic metabolites that contribute to oxidative stress and genotoxicity. Notable examples include malondialdehyde (MDA), the end product of arachidonic acid peroxidation, and 4-hydroxynonenal (4-HNE), which originates from linoleic acid. These aldehydic products further promote protein carbonylation and oxidative modifications of DNA bases, potentially leading to mutations. Hydroxyl radicals and other ROSs generated during normal metabolism and inflammation attack deoxyribose sugar and possibly nucleobases in DNA, generating several electrophilic products with genotoxic potential [85–87]. For instance, 4′-hydrogen atom abstraction on the deoxyribose moiety by hydroxyl radicals or other activated oxygen species leads to the formation of base propenals. On the other hand, malondialdehyde, a major product of lipid peroxidation, reacts with bases in DNA to form several adducts, the most prominent being M1dG (pyrimidopurinone adduct of deoxyguanosine), which is known to be mutagenic. Because base propenals are structural analogues of malondialdehyde, Dedon et al. [85] investigated whether base propenals could also form M1dG adducts. They confirmed this hypothesis, showing that 9-(3-oxoprop-1-enyl)adenine (adenine-propenal) reacts with DNA to form the M1dG adduct even more efficiently than malondialdehyde itself. Thus, oxidative DNA damage—whether directly caused by ROS or indirectly via lipid peroxidation products such as MDA and 4-HNE—contributes significantly to the mutagenic burden in bacterial cells. Similarly, elevated ROS levels can lead to protein carbonylation, either directly—through the oxidation of amino acid side chains such as proline, arginine, lysine, and threonine—or indirectly, via reactive lipid peroxidation end products [88].

AgNPs may increase ROS levels in bacteria by inactivating the detoxifying enzymes SOD and CAT [89].

2.1.5. Interaction with DNA

Studies on *E. coli* have shown that exposure to AgNPs can cause DNA strand breaks and potentially induce mutations in critical DNA repair genes. One of the most common oxidative DNA lesions is the formation of 8-oxoguanine (8-oxoG) [87]. Radzig et al., investigated how mutations in genes of the base excision repair (BER) system affect *E. coli* susceptibility to AgNPs. The MutM DNA glycosylase repairs 8-oxoG lesions by excising the oxidized purine base, while MutY and MutS remove adenine residues that were erroneously incorporated opposite to 8-oxoG. MutT, on the other hand, prevents incorporation of oxidized nucleotides by hydrolytically removing 8-oxodGTP from the nucleotide pool. The study found that *E. coli* strains deficient in these repair genes were 2- to 10-fold more susceptible to $AgNO_3$ exposure, depending on the specific mutation. These findings indicate that the BER pathway plays a critical role in repairing oxidative DNA damage and suggest that the genotoxic effects of AgNPs may overwhelm or compromise this repair system in susceptible *E. coli* strains [74,75,90,91].

AgNPs can induce a transition of DNA from its relaxed state to a condensed state, thereby preventing replication or suppressing the transcription of some genes [74,75,92]. Ag^+ ions released from AgNPs intercalate between base pairs, disrupting hydrogen bonding and forming coordination complexes with the nitrogen and oxygen atoms in nucleobases, rather than binding to phosphate groups. At the G≡C base pair, linear bidentate coordination complexes such as O-Ag^+-N, N-Ag^+-N, and N-Ag^+-O can form. Similarly, N-Ag^+-O, and N-Ag^+-N complexes may appear at A=T pairs loci [93].

2.1.6. Antibiofilm Activity

Biofilms are complex and dynamic sessile bacterial communities composed of single or multiple strains embedded in a sheltering self-produced extracellular polymeric substance (EPS) matrix. The EPS consists primarily of water, polysaccharides, proteins, nucleic acids, ions, and various inorganic substances. It plays multiple roles: facilitating intercellular signalling, promoting horizontal gene transfer—both of which are critical for the MDR development—and forming a physical barrier that protects bacteria within the biofilm from variations in osmotic potential and pH fluctuations, while also limiting the penetration of antibiotics and host immune cells, thereby helping the bacteria evade phagocytic clearance [94]. A striking feature of biofilms compared to planktonic bacteria is their remarkable resistance to antibiotic treatment, often leading to recurrent infections [94–96]. A biofilm's life cycle progresses through four sequential stages: initial attachment to a biotic or abiotic surface, proliferation, maturation, and, eventually, dispersion and migration to new sites to be colonized, thereby restarting the cycle. A mature biofilm typically contains a heterogeneous population of bacterial cells, including sessile (attached) cells, free-floating (planktonic) cells, persister dormant (antibiotic-tolerant) cells, and dead cells. These coexist within the EPS matrix, along with signalling molecules and structured water channels [97].

AgNPs exert their antibiofilm activity by interacting with the protein, nucleic acid, polysaccharide, and lipid components of the EPS. Tian et al. provided evidence supporting the hypothesis that AgNPs suppress biofilm formation by interacting with small regulatory RNAs (sRNAs) and altering RNA expression [98,99]. Small regulatory RNAs are short, non-coding RNAs that modulate gene expression post-transcriptionally. In bacteria, each sRNA typically contains two functional regions: a target-binding sequence, which hybridizes with a complementary region of the target messenger RNA (mRNA) in an antisense manner, and a scaffold sequence. The scaffold serves dual functions: it stabilizes the sRNA by recruiting the RNA chaperone protein Hfq, which in turn accelerates annealing to the targeted mRNA. Annealing can result in either positive or negative regulation of translation. Positive regulation may result from the remodelling of inhibitory RNA structures or from blocking the binding of negative regulatory elements. In contrast, negative regulation involves inhibition of translation initiation, recruitment of RNases for mRNA degradation, or both. One mechanism of negative regulation engages sRNA binding to the 5′ translation initiation region (TIR) of the target mRNA, typically near the Shine-Dalgarno (SD) sequence. This interaction blocks the base pairing between the SD sequence and the anti-SD sequence of the 16S ribosomal RNA within the small ribosomal subunit, thereby impeding proper ribosome assembly and translation initiation. As a result, expression of the target genes is post-transcriptionally repressed [100,101]. AgNPs may exert their antibiofilm effects either by downregulating sRNAs that normally promote biofilm formation or by upregulating sRNAs that repress biofilm-related genes.

Biofilm formation is closely linked to quorum sensing (QS), a mechanism by which bacteria regulate gene expression in response to cell population density within the biofilm lifestyle. QS is a cell-to-cell communication mechanism. Bacteria produce, release, and

sense chemical signalling molecules called autoinducers (AIs). When the concentration of AIs exceeds a specific threshold, it serves as a signal that triggers changes in bacterial gene expression. Reaching this threshold depends on the bacterial population density—hence the term quorum is used to describe the phenomenon. When AIs accumulate to sufficient concentrations, they are detected by specific receptors located in the bacterial cytoplasm or plasma membrane. The binding of these signalling molecules to their receptors activates intracellular signalling cascades, ultimately leading to changes in gene expression, including the synthesis of adherence molecules, EPS matrix, and virulence factors. Detection of AIs also promotes the expression of genes involved in cooperative bacterial behaviours associated with the biofilm lifestyle. In addition, it upregulates the synthesis of autoinducers themselves through a positive feedback loop. It is important to note that biofilms function as coordinated communities, responding collectively to environmental stimuli rather than behaving as isolated individual cells [94,102]. As a result, bacteria in biofilms gain a competitive advantage in survival and spread compared to their planktonic counterparts. AgNPs can interact with amino acid residues in the binding domains of receptor proteins—such as members of the LuxR family in the QS regulatory cascade—or inhibit AHL synthases responsible for producing acyl-homoserine lactone (AHL) autoinducers in Gram-negative bacteria, thereby disrupting cell-to-cell communication and downstream signalling pathways.

Two main types of polysaccharides are associated with bacterial biofilms: structural polysaccharides that are part of the cell envelope, and EPS polysaccharides, each serving distinct roles in bacterial survival and biofilm development. Cell envelope–associated polysaccharides, such as those in the LPS layer and the capsular polysaccharide (CPS) shell, not only provide mechanical strength and structural stability but are also involved in osmoregulation, contribute to virulence, and protect bacteria from host immune responses and antimicrobial killing [103]. In contrast, EPS polysaccharides are secreted into the ECM and play key roles in maintaining biofilm integrity, protecting against environmental stress, preserving nutrient availability, and promoting intercellular interactions within the microbial community [102]. The interaction of AgNPs with both structural and extracellular polysaccharides, mainly driven by electrostatic forces, enhances their antibacterial activity and disrupts the protective function of the biofilm matrix [102].

In summary, AgNPs appear to act against pathogenic biofilms through mechanisms similar to those by which they affect free-floating (planktonic) bacteria. However, their specific effects on persister cells within the biofilm community remain to be elucidated.

The main antibacterial mechanisms of AgNPs are illustrated in Figure 1.

2.1.7. Comparison of the Antibacterial Activity of Antibiotics and AgNPs

The non-specific antibacterial activity of AgNPs offers a significant advantage over conventional antibiotics in combating multidrug-resistant (MDR) bacteria, which typically act through highly specific mechanisms targeting only one or, at most, a few key molecular or cellular structures (as summarized in Table 4). Although antibiotics may influence multiple biological pathways, their primary mode of action remains narrowly focused [104]. In contrast, AgNPs exert multiple simultaneous damaging effects on bacterial cells, making it more difficult for bacteria to develop effective resistance mechanisms. However, scientific evidence also shows that prolonged exposure to silver-based nanomaterials is detrimental, as it can promote the development of bacterial tolerance to AgNPs. This issue will be further discussed in the section addressing toxicity and safety concerns.

Table 4. Antibiotic targets and mechanisms of action [104].

Antibiotic Classes	Antibiotics	Primary Targets	Genetic and Biochemical Processes That Are Disrupted
Fluoroquinolones (DNA synthesis inhibitors	Nalidixic acid, ciprofloxacin, levofloxacin, gemifloxacin	Topoisomerase II (DNA gyrase), topoisomerase IV	DNA replication, SOS response, cell division, ATP generation, TCA cycle, Fe–S cluster synthesis, ROS formation, redox-responsive two-component systems, and envelope
Trimetropim-sulfamethoxazole (DNA synthesis inhibitor)	Co-trimoxazole	Tetrahydrofolic acid synthesis inhibitors	Nucleotide biosynthesis and DNA replication
Rifamycins (RNA synthesis inhibitors)	Rifamycins, rifampin, rifapentine	DNA-dependent RNA polymerase	RNA transcription, DNA replication, SOS response
β-Lactams	Penicillins (penicillin, ampicillin, oxacillin), cephalosporins (cefazolin, cefoxitin, ceftriaxone, cefepime), carbapenems (imipenem)	Penicillin-binding proteins	Cell wall synthesis, cell division, autolysin activity (regulated by LytSR–VncRS two-component system), SOS response, TCA cycle, Fe–S cluster synthesis, ROS formation, envelope, redox-responsive two-component systems
Glycopeptides and glycolipopeptides (cell wall inhibitors)	Vancomycin, teicoplanin	Peptidoglycan units (terminal D-Ala-D-Ala dipeptide)	Cell wall synthesis, transglycosylation, transpeptidation, and autolysin activation (VncRS two-component system)
Lipopeptides (cell wall synthesis inhibitors)	Daptomycin, polymixin B	Cell membrane	Cell wall synthesis, envelope two-component systems
Aminoglycosides (protein synthesis inhibitors)	Gentamicin, tobramycin, streptomycin, kanamycin	30S ribosome	Protein translation (mistranslation by tRNA mismatching), ETC, SOS response, TCA cycle, Fe–S cluster synthesis, ROS formation, envelope, redox-responsive two-component systems
Tetracyclines (protein synthesis inhibitors)	Tetracycline, doxycycline	30S ribosome	Protein translation (through inhibition of aminoacyl tRNA binding to ribosome)
Macrolides (protein synthesis inhibitors)	Erythromycin, azythromycin	50S ribosome	Protein translation (through inhibition of elongation and translocation steps) and free tRNA depletion
Streptogramins (protein synthesis inhibitors)	Pristinamycin, dalfopristin, quinupristin	50S ribosome	Protein translation (through inhibition of initiation, elongation, and translocation steps) and free tRNA depletion
Phenicols (protein synthesis inhibitor)	Chloramphenicol	50S ribosome	Protein translation (through inhibition of the elongation step)

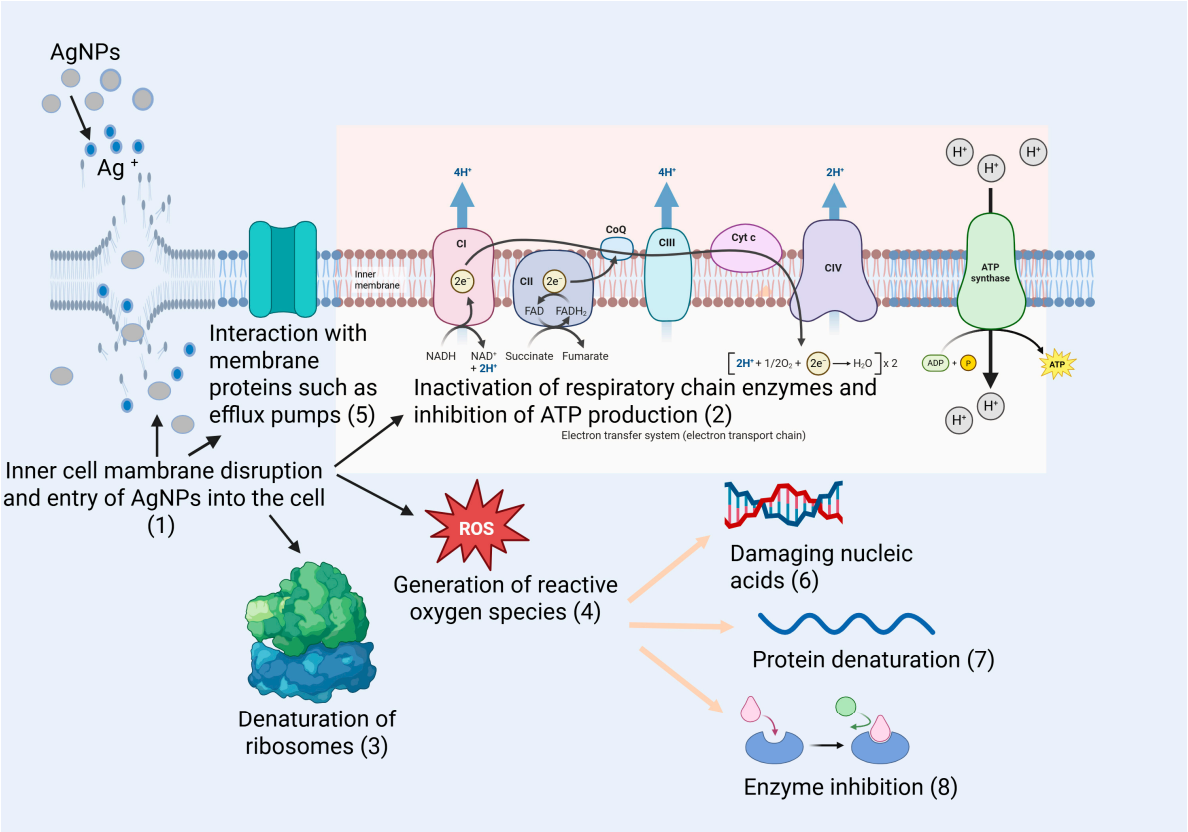

Figure 1. Antibacterial mechanisms of AgNPs. The main molecular targets of AgNPs and Ag^+, along with the resulting cellular effects, are indicated in the figure by numbers (1–8).

2.2. The Role of Silver Nanoparticles in Modulating Inflammation and Promoting Wound Healing

2.2.1. Anti-Inflammatory Activity

Beyond their antibacterial effects, AgNPs' potent anti-inflammatory properties are particularly important for mitigating excessive inflammation and supporting tissue repair. The oxidative dissolution of AgNPs leads to the release of Ag^+ ions and the generation of ROS, such as hydrogen peroxide (H_2O_2). At moderate levels, these ROS can inhibit the NF-κB signalling pathway, thereby reducing the expression of pro-inflammatory mediators, including tumour necrosis factor-α (TNF-α), interleukin-1β (IL-1β), interleukin-6 (IL-6), as well as inducible nitric oxide synthase (iNOS) and cyclooxygenase-2 (COX-2) [105,106]. In addition, AgNPs interfere with intracellular signalling pathways involving key kinase proteins, such as the mitogen-activated protein kinase (MAPK) cascade (ERK, JNK, p38) and the phosphatidylinositol 3-kinase (PI3K)/protein kinase B (Akt) pathway. Through these interactions, AgNPs help regulate oxidative stress by reducing levels of ROS and reactive nitrogen species (RNS), thereby attenuating inflammatory responses.

The anti-inflammatory effects of AgNPs have been demonstrated in both in vitro and in vivo studies. Jalil et al. [107] showed, using a murine carrageenan-induced hind paw edema model, that both AgNPs and Ag-amoxicillin nanoconjugates exhibited superior anti-inflammatory efficacy compared to conventional treatments such as diclofenac and high-dose amoxicillin. Five hours after administration at a dose of 10 mg/kg, the inflammation inhibition rates were 64% for AgNPs and 65% for Ag-amoxicillin, whereas diclofenac—administered at a twofold higher dose of 20 mg/kg—achieved only 56% inhibition. However, diclofenac exhibited stronger anti-inflammatory effects during the acute phase (1–3 h post-induction). In this early stage, AgNPs are thought to inhibit mast cell degranulation and reduce the release of vasoactive compounds, thereby decreasing capillary

permeability. In the later phase, they are believed to target COX–2–catalyzed prostaglandin synthesis, thereby mitigating inflammation. Moldovan et al. [108] synthesized AgNPs using a green biosynthetic method, in which *Viburnum opulus* L. fruit extract—rich in polyphenols—served as the reducing agent for $AgNO_3$. The anti-inflammatory properties of these AgNPs were evaluated both in vitro, using UVB-irradiated HaCaT keratinocyte cultures, and in vivo, via a carrageenan-induced paw edema model in Wistar rats. In the in vitro experiments, the authors measured the secretion levels of the pro-inflammatory cytokines IL-1α and IL-6 in cell culture supernatants. HaCaT cells were pretreated with AgNPs for 30 min and subsequently exposed to UVB irradiation at a dose corresponding to the IC_{50} (i.e., the dose reducing cell viability by 50%). Following UVB exposure, the cells received a fresh dose of AgNPs and were incubated for either 24 or 48 h. Supernatants collected at these time points were analysed for cytokine content and compared with non-treated controls. The results showed that phytosynthesized AgNPs induced a transient increase in IL-1α secretion in UVB-irradiated keratinocytes at 24 h, whereas at 48 h IL-1α levels decreased relative to UVB-only treated cells. In contrast, IL-6 secretion was consistently reduced at both time points in AgNP-treated, UVB-exposed keratinocytes. In the in vivo model, rats received a daily oral dose of 0.3 mg AgNPs/kg body weight for 4 consecutive days prior to inflammation induction. This pre-treatment produced an early anti-inflammatory effect, evidenced by reduced cytokine levels (including TNF-α) in hind paw tissue homogenates and decreased paw edema observed two hours after carrageenan injection. Overall, these findings suggest that phytosynthesized AgNPs exhibit rapid and effective anti-inflammatory activity in both in vitro and in vivo experimental systems. Singh et al. [109] demonstrated that green-synthesized AgNPs prepared from *Prunus serrulata* fruit extract reduced the expression of key inflammatory mediators, including prostaglandin E_2 (PGE_2), COX-2, iNOS, and NO. They also observed significant nanoparticle-mediated suppression of LPS-induced NF-κB signaling pathway activation via p38 MAPK in RAW 264.7 macrophages. Similarly, Crisan et al. [110] reported inhibition of NF-κB transcription factor activity by topical AgNPs complexed with a polyphenol-rich Cornus mas extract in human psoriasis plaques.

In addition, recent studies indicate that AgNP-containing biomaterials can directly influence macrophage polarization. AgNPs and AgNP-loaded hydrogels have been shown to suppress macrophages M1-associated markers while upregulating macrophages M2-associated markers, thereby promoting a phenotypic shift that aligns with the resolution of inflammation and initiation of tissue repair [111,112]. This immunoregulatory effect has emerged as an important mechanism contributing to the accelerated healing observed in AgNP-treated wounds.

2.2.2. Effects on Cell Proliferation and Migration

Robust wound closure relies on the proliferation and directed migration of fibroblasts and keratinocytes. The effects of AgNPs on these processes depend on their concentration and surface functionalization.

Low concentrations of AgNPs release trace Ag^+ levels that stimulate fibroblast proliferation and aid wound closure, while simultaneously providing antibacterial protection. In contrast, high AgNP concentrations lead to excessive ion release, causing cytotoxicity through damage to proteins, nucleic acids, and lipids. In an in vitro study on mouse embryonic fibroblasts, Du et al. [113] reported that 16 μM AgNPs stimulated cell proliferation, corroborating the findings of Xu et al. [114], who observed that AgNPs significantly promoted fibroblast proliferation and enhanced wound healing.

Surface functionalization with bioactive molecules can markedly enhance wound healing performance. Long et al. [115] developed a composite sponge incorporating Ag-

NPs decorated with recombinant humanized collagen type III (rhCol III), which exhibited superior haemostatic, wound-repairing, and antimicrobial properties. The porous three-dimensional (3D) shape-memory sponge was constructed from the naturally antibacterial polymer carboxymethyl chitosan (CMC), crosslinked via Schiff base linkages with oxidized starch (OS), and further reinforced by microfibrillated cellulose (MFC). AgNPs were generated in situ within the polymeric matrix by reducing $AgNO_3$ with tannic acid (TA). In brief, TA was added under stirring to a CMC solution containing the silver precursor. The CMC/OS–MFC sponge was prepared via a two-step protocol consisting of a sol–gel process followed by freeze-drying. First, an MFC suspension was added to the AgNP-containing CMC solution, followed by sequential addition of OS to induce crosslinking, and finally rhCol III, which formed hydrogen bonds with the MFC. The resulting hydrogel was freeze-dried to produce a compressible, biodegradable sponge that could be delivered via syringe injection, enabling treatment of narrow and deep wounds. The sponges' ability to promote cell proliferation and migration was assessed in vitro using a scratch assay. After 48 h of incubation, the wound closure rate in the rhCol III/AgNP sponge group reached 77.3%, compared with 43.4% for sponges containing AgNPs alone. Additionally, an in vivo diabetic rat full-thickness skin wound model infected with bacteria was used to evaluate wound repair efficacy. Rats treated with rhCol III/AgNP-decorated sponges achieved complete wound closure within 14 days, whereas control groups still exhibited a residual wound area of approximately 17% of the original size at the same time point [115].

Gaikwad et al. [116] formulated three nanogels by incorporating AgNPs mycosynthesized from *Fusarium oxysporum* into Carbopol at concentrations of 0.1, 0.5, and 1 mg g^{-1}, and evaluated them in vivo in albino Wistar rats. All three silver nanogels demonstrated pronounced effects on cell proliferation and wound healing in incision, excision, and burn wound models. The 0.1 mg g^{-1} AgNP nanogel showed the most notable wound-healing activity in excision wounds, whereas the 1 mg g^{-1} formulation achieved superior outcomes in burn wound care. Histological examination of the healed tissues revealed no signs of toxicity or adverse effects. Lower-concentration nanogels also promoted wound healing and hair follicle regeneration.

Liu et al. [117] investigated the effects of AgNPs on keratinocytes and fibroblasts using a surgical wound model on murine dorsal skin. Wound healing involves two key processes: re-epithelialization and wound contraction. Re-epithelialization is a complex, multistep process driven by keratinocyte migration and proliferation in the epidermal layer. Wound contraction, which minimizes the open wound area, involves pulling the surrounding tissue toward the wound center and occurs primarily in the dermal layer, driven by α-smooth muscle actin (α-SMA) produced by myofibroblasts. In infection-free clean wounds, wound closure occurred significantly faster in animals treated with AgNPs compared to those receiving the standard 1% silver sulfadiazine (SSD) cream. To examine the effects of AgNPs on each cell type separately, keratinocytes and fibroblasts were isolated and cultured ex vivo. AgNP treatment produced a marked increase in keratinocyte proliferation relative to control, and this effect persisted for up to 7 days, thereby accelerating re-epithelialization. Conversely, fibroblast cultures exhibited a reduction in cell numbers. This decrease was not due to AgNP cytotoxicity, as the 3-(4,5-dimethyl thiazol-2-yl)-2,5-diphenyltetrazolium bromide (MTT) assay showed that at concentrations below 100 μM, AgNPs were relatively non-toxic to fibroblasts. However, AgNP-treated fibroblasts showed significantly reduced collagen and hydroxyproline production in the culture supernatants, suggesting that AgNPs altered the normal fibroblast phenotype. Immunohistochemistry (IHC) staining confirmed that the apparent inhibition of fibroblast proliferation was due to AgNP-induced maturation and differentiation of fibroblasts into myofibroblasts, as

evidenced by significantly elevated α-SMA expression, which contributed to accelerated wound contraction.

2.2.3. Pro-Angiogenic Effects

The proliferative phase of wound healing involves not only fibroblast migration and wound closure but also angiogenesis and neovascularization. These processes can be influenced by the size, surface functionalization, and concentration of AgNPs. AgNPs have been shown to promote angiogenesis by upregulating vascular endothelial growth factor (VEGF) and basic fibroblast growth factor (bFGF), as well as activating the PI3K/Akt signalling pathway.

Zhang et al. [118] developed an innovative nanoplatform based on nano-hydroxyapatite (nHEA) to address the challenges posed by inadequate regulation of multiple stages in the wound-healing cascade. This multifunctional system, designed for the treatment of full-thickness infected skin injuries, enabled multi-level therapeutic regulation by covalently incorporating ε-poly-L-lysine–grafted gallic acid (EG) and in situ biosynthesized AgNPs into a multilayered nHEA structure. EG was synthesized from ε-poly-L-lysine (EPL) and gallic acid (GA) via 3-(3-dimethylaminopropyl)carbodiimide hydrochloride (EDC)-mediated amide bond formation. The reaction mixture was then dialyzed and freeze-dried to yield an EG sponge. Sodium hyaluronate (HA) was oxidized with $NaIO_4$ to obtain oxidized HA (OHA). Separately, nanohydroxyapatite (nHA) was surface-functionalized with amino groups by sequential treatment with acidic tetraethyl orthosilicate (TEOS) solution and aminopropyltriethoxysilane (APTES), and then covalently conjugated to OHA through Schiff base formation. To the resulting precipitate, EG and Ag^+ solutions of varying concentrations were added. The mixture was shaken and centrifuged, producing the final nHEA nanoplatform. In infected rat wounds, the release of EG enhanced fibroblast migration and collagen secretion, while the release of Ag^+ and Ca^{2+} provided synergistic antibacterial, anti-inflammatory, and pro-angiogenic effects, the latter through VEGF upregulation. The in vivo efficacy of the nHEA platform was assessed in a full-thickness infected skin defect model in Sprague–Dawley rats. After 7 days of treatment, rats receiving the nHEA nanoplatform showed markedly improved wound healing compared with controls, as evidenced by smaller residual wound areas and lower infection levels.

Mensah et al. [119] incorporated both commercially produced and green-synthesized AgNPs into the network of eggshell membranes (ESM)—a biomaterial with unique physical and mechanical properties—by submerging the ESM in a suspension of ~10 nm AgNPs for 24 h under continuous stirring at 37 °C. ESM was extracted from fresh eggs on treatment with acetic acid at room temperature for 44 h. SEM analysis of AgNPs-incorporated ESM samples revealed a uniform surface deposition of AgNPs while preserving the structural integrity of the ESM. In vitro biocompatibility was evaluated using human dermal fibroblasts (HDFs) and BJ human fibroblast cells. Relative metabolic activity (cell viability) was determined with the CellTiter 96® AQueous One Solution Cell Proliferation Assay, and cytotoxicity was assessed by measuring lactate dehydrogenase (LDH) release. The results showed that ESM samples containing 5 μg/mL AgNPs were highly biocompatible with both fibroblast cell types. Furthermore, a chick chorioallantoic membrane (CAM) assay demonstrated strong pro-angiogenic activity, with a significant increase in vascular branching points. This neovascularization provides an essential framework for the subsequent ECM remodelling phase and tissue repair during wound healing.

2.2.4. Effects on ECM Remodelling Phase

Chronic wounds are often characterized by remodelling defects caused by an imbalance between the degradation of damaged ECM components and the synthesis of new ones.

Ag^+ ions can promote the synthesis of key ECM constituents involved in reconstruction and remodelling, such as type III collagen and elastin, by stimulating fibroblast proliferation and migration [120]. In addition, AgNPs have been shown to inhibit overactive MMPs and upregulate the expression of tissue inhibitor of metalloproteinase-1 (TIMP-1) [121], thereby helping to restore the balance between ECM synthesis and degradation.

Seo et al. [122] reported enhanced wound healing and muscle regeneration in a zebrafish in vivo laser-induced skin wound model. The highest wound healing percentage (WHP) was observed in the group treated with AgNPs by immersion, reaching 36.6% at five days post-wounding. By comparison, the WHP was 23.7% in the group receiving AgNPs via direct skin application, and only 18.32% in the untreated control group at the same time point. In the AgNP immersion group, pronounced aggregation of immune cells near the wound edges was observed, along with epidermal cell differentiation into well-developed skin. Muscle tissue also showed near-complete regeneration. Transcriptional analysis during the healing process revealed that AgNP treatment led to downregulation of IL-1β, TNF-α, and MMP-9/MMP-13 expression and upregulation of antioxidant enzymes, such as SOD. Collectively, these effects contributed to a balanced ECM reconstruction and a reduction in both inflammation and oxidative stress.

For better clarity, the most important effects of AgNPs throughout the wound healing process have been gathered in Figure 2.

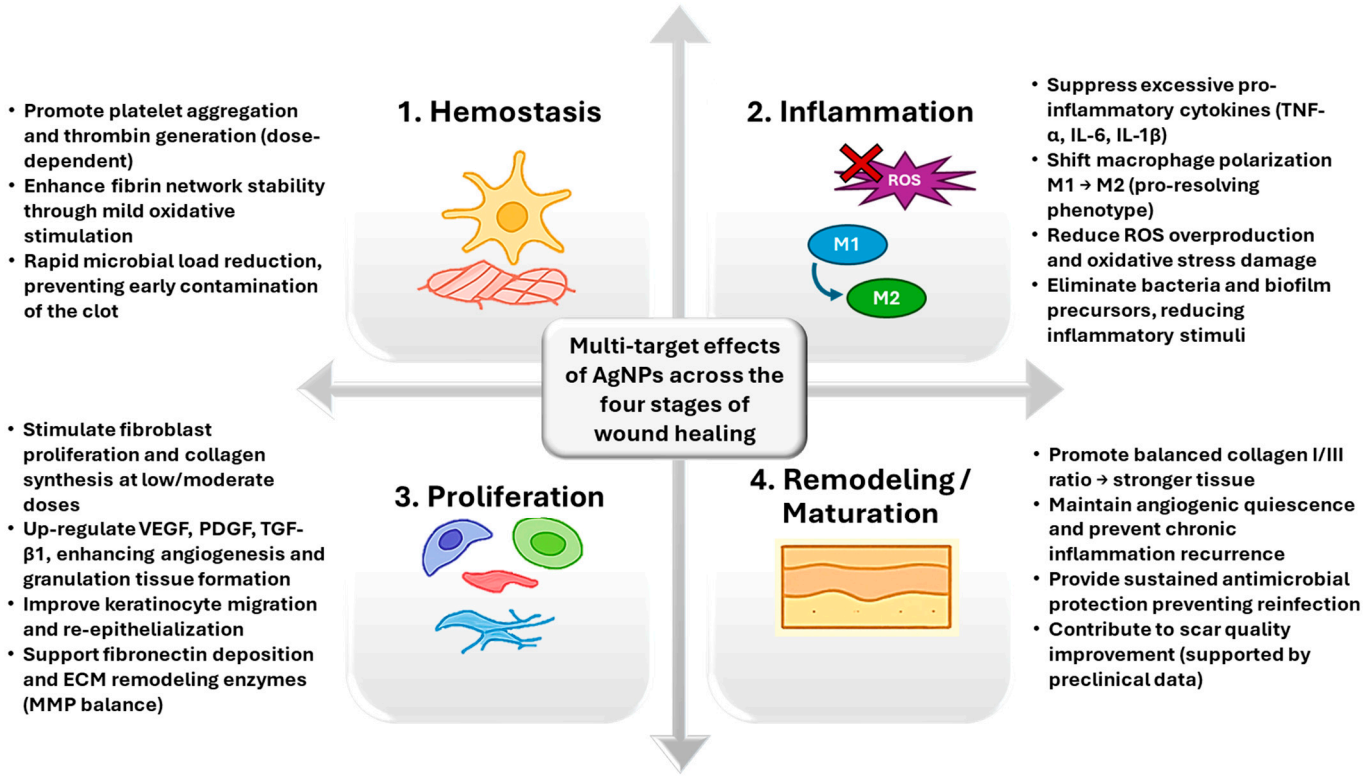

Figure 2. Overview of AgNP effects during the different wound healing stages.

3. AgNPs-Based Nanocomposite Materials for Wound Care

3.1. AgNPs-Loaded Hydrogels

Hydrogels are 3D cross-linked polymer networks that absorb large amounts of water, creating a moist and supportive environment [123]. Their ability to mimic the ECM, along with their biocompatibility, high permeability, and tunable mechanical properties, makes them ideal for wound care by providing a moist healing environment for dry, minimally exudative wounds, supporting cells, and delivering therapeutic agents. Natural

polymer–based hydrogels, such as those derived from chitosan or hyaluronic acid, can be incorporated with in situ-generated AgNPs via reduction of silver salts, thereby enhancing their biocompatibility.

Raho and co-workers [124] developed a composite hydrogel composed of regenerated silk fibroin (RSF) stabilized with sodium carboxymethyl cellulose (CMC-Na) and loaded with AgNPs. The AgNPs were generated in situ via the photoreduction of $AgNO_3$, mediated by the redox-active tyrosine residues in Bombyx mori fibroin under UV irradiation [125,126]. Upon UV excitation, the phenolic side chains of tyrosine donate electrons to reduce Ag^+ ions to metallic silver, while simultaneously stabilizing the resulting nanoparticles through coordination with protein functional groups. The composite hydrogels (CoHy) loaded with AgNPs in the 50–200 nm size range (mean size 92 nm) demonstrated a high fluid-absorption capacity, taking up 20–30 g of fluid per gram of dry material. CoHy prepared with 1 or 2 mg of crystalline $AgNO_3$ per mL of RSF solution showed no in vitro cytotoxicity toward rat bone marrow mesenchymal stem cells (BMSCs). Antimicrobial activity, assessed by agar diffusion tests, revealed clear inhibition zones against a large plethora of pathogenic microorganisms, including *E. coli*, *S. aureus*, *S. epidermidis*, methicillin-resistant Staphylococcus aureus (MRSA), *P. aeruginosa*, *Candida albicans*, and fluconazole-resistant *Candida albicans* (FRCA). Notably, CoHy without AgNPs supported high cell proliferation, underscoring the intrinsic regenerative potential of the RSF/CMC matrix. Among the tested formulations, CoHy loaded with 1 mg/mL of $AgNO_3$ provided the optimal balance between tissue-regenerative properties, cytocompatibility, and antimicrobial activity. In a similar approach, Ruffo et al. [127] developed a biocompatible CMC-based hydrogel loaded with in situ–green-synthesized AgNPs, using an aqueous mixture of olive leaf and Camellia sinensis (green tea) dry extracts as reducing agents, for the treatment of diabetic foot ulcers (DFUs). In diabetic patients, foot ulcers arise from neuropathy, peripheral vascular disease, and ischemia. When infected, these ulcers pose a serious clinical challenge, with an increased risk of progressing to gangrene and amputation due to the patient's impaired immune response. Motivated by the need to control and treat DFUs, the authors prepared a CMC–AgNP hydrogel, which was freeze-dried to yield a flexible, porous structure. The wound-healing potential of the hydrogel was evaluated through in vitro and ex vivo assays. After 24 h of incubation, the hydrogel maintained high viability of 3T3 fibroblast cells (88%). It exhibited potent antibacterial activity against *E. coli* (MIC = 5.15 μg/mL), *S. aureus* (MIC = 30 μg/mL), and *P. aeruginosa* (MIC = 27 μg/mL). Safety and skin compatibility were assessed using the Human Cell Line Activation Test (h-CLAT) and the EpiDerm™ reconstructed human epidermis (RhE) assay, both of which confirmed the absence of skin sensitization or irritation. In a wound-healing scratch assay, treatment with 100 μg/mL of hydrogel resulted in 75 ± 0.3% wound closure after 24 h. Furthermore, ex vivo testing of enzyme inhibition demonstrated that the hydrogel downregulated the activity of myeloperoxidase (MPO)—an enzyme released by neutrophils that produces the potent bactericidal agent hypochlorous acid (HOCl), but which can also cause oxidative tissue damage. The hydrogel also inhibited collagenase activity, thereby supporting ECM preservation and promoting tissue regeneration [127].

Chen et al. [128] developed an injectable hydrogel derived from a decellularized dermal matrix of 6-month-old domestic swine, loaded with GA–capped silver AgNPs for the treatment of MRSA–infected wounds. The acellular dermal matrix was digested with pepsin and then acidified with hydrochloric acid to pH 2 to ensure complete digestion, yielding a homogenate. This homogenate was sequentially treated in an ice bath with pre-cooled phosphate-buffered saline (PBS) and NaOH solutions to adjust the pH to 7.2. The resulting "pre-hydrogel" was combined under continuous stirring with a concentrated solution of GA-capped AgNPs, producing the final acellular dermal matrix hydrogel, designated

Ag@ADMH. Ag@ADMH exhibited excellent biocompatibility and provided sustained release of antimicrobial AgNPs from the three-dimensional dermal scaffold. Quantitative real-time PCR (qPCR) analysis revealed downregulation of iNOS expression, a marker of M1 macrophages, and increased expression of CD206, a marker of M2 macrophages. This indicated a polarization shift from the pro-inflammatory M1 macrophage phenotype to the pro-healing M2 phenotype, which promotes fibroblast migration and proliferation. Such modulation supports the transition from the inflammatory to the proliferative phase of wound healing, thereby enhancing tissue repair and reducing inflammation [129].

Another type of composite hydrogel dressing based on AgNPs was developed by Zhou and co-workers [130]. First, they synthesized a water-soluble adenine-functionalized chitosan derivative (CS-A) via amidation of chitosan (CS) with 3-(9-adeninyl) propionic acid (A-COOH). The resulting CS-A sponge dressing exhibited broad-spectrum wound-healing properties, including suppression of inflammatory cell infiltration, stimulation of neovascularization—attributed to the incorporated adenine nucleotide, which can activate angiogenic factors and promote cell proliferation—enhancement of collagen deposition, and regeneration of epithelial tissue. To improve the mechanical strength and self-healing capacity of the hydrogel, the authors synthesized a star-shaped, eight-armed crosslinker through a two-step process: (i) thiol–ene click reaction between allyloxypolyethylene glycol (PEG) and thiol-functionalized polyhedral oligomeric silsesquioxane (POSS-8SH), followed by (ii) Steglich esterification with 4-carboxybenzaldehyde [131]. The resulting eight-armed POSS-PEG-CHO crosslinker was then used to crosslink the AgNP-impregnated CS-A via Schiff base linkages formed between aldehyde (CHO) groups on the crosslinker and amino (NH_2) groups on the CS-A chains. The AgNP-impregnated CS-A solution was first prepared by mixing the CS-A sponge with an aqueous $AgNO_3$ solution at a 1:1 volume ratio, enabling in situ AgNPs formation. This AgNPs-loaded CS-A/POSS-PEG composite self-healing hydrogel demonstrated excellent cell proliferation support and significantly accelerated wound closure in infected wound models. Treated wounds displayed reduced inflammatory cell infiltration, increased collagen deposition, enhanced angiogenesis, and more rapid epithelial regeneration, as confirmed by immunofluorescence staining assays and histological analysis [130].

To address the heterogeneity among published studies and to quantitatively synthesize AgNP performance, we compiled a summary of representative AgNP-based systems tested in wound-healing–relevant models. Table 5 presents the nanoparticle size, silver concentration or dose, and the corresponding biological outcomes reported in the cited studies.

Table 5. Overview of representative AgNP-based systems used in wound-healing–relevant models.

AgNP System/Formulation	AgNP Size (nm)	Ag Concentration/Dose	Model (In Vitro/In Vivo)	Main Observed Biological Outcomes	Ref.
Dispersed AgNPs	9 nm	16, 32, or 100 μM AgNPs	in vitro: mouse embryonic fibroblasts	16 μM AgNPs stimulated fibroblast proliferation; Concentration-dependent switch from pro-regenerative to toxic effects	[113]
CMC/OS/MFC sponge decorated with rhCol III and in situ TA-reduced AgNPs	n.r.	n.r. ($AgNO_3$ reduced in situ)	in vitro scratch assay; in vivo diabetic rat full-thickness infected wounds	rhCol III/AgNP sponge: 77.3% scratch closure at 48 h vs. 43.4% for AgNP sponge without rhCol III; Complete wound closure by day 14 in infected diabetic rats vs. ~17% residual area in controls.	[115]

Table 5. *Cont.*

AgNP System/Formulation	AgNP Size (nm)	Ag Concentration/Dose	Model (In Vitro/In Vivo)	Main Observed Biological Outcomes	Ref.
Carbopol nanogels with mycosynthesized AgNPs	n.r.	0.1, 0.5, 1 mg g^{-1} AgNPs in nanogels	in vivo: Wistar rat incision, excision, and burn wound models	All three doses improved healing; 0.1 mg g^{-1} most effective in excision wounds, 1 mg g^{-1} best in burn wounds; histology showed good regeneration and no toxicity, highlighting dose-dependent optimization.	[116]
Dispersed AgNPs	5–15 nm (mean 10 nm)	1 mM AgNPs dispersion ≤100 µM non-toxic to fibroblasts (MTT); in vivo dose not numerically specified	in vivo: mouse surgical wounds; ex vivo keratinocytes and fibroblasts	AgNP treatment accelerated wound closure vs. 1% SSD; increased keratinocyte proliferation up to day 7; induced fibroblast differentiation to α-SMA^+ myofibroblasts, enhancing wound contraction without cytotoxicity below 100 µM	[117]
Eggshell membrane (ESM) biomaterial loaded with commercial/green AgNPs	~10 nm	5 µg/mL AgNPs in ESM samples	in vitro: human dermal fibroblasts and BJ fibroblasts; ex ovo CAM assay	Strong pro-angiogenic response in CAM with increased vascular branching, supporting ECM remodeling and later repair	[119]
RSF/CMC-Na composite hydrogel (CoHy) with UV-photoreduced AgNPs	50–200 nm (mean ~92 nm)	1 or 2 mg $AgNO_3$ per mL RSF solution (in situ AgNP formation)	in vitro: rat BMSCs; antimicrobial tests	Broad-spectrum antimicrobial activity; 1 mg/mL $AgNO_3$ (mean 92 nm) gave best balance of cytocompatibility and antibacterial performance	[124]
CMC hydrogel with in situ green-synthesized AgNPs	6.87–8.51 nm	MICs: 5.15 µg/mL (*E. coli*); 30 µg/mL (*S. aureus*); 27 µg/mL (*P. aeruginosa*); 100 µg/mL hydrogel in scratch assay	in vitro: 3T3 fibroblasts, scratch assay; ex vivo DFU-relevant assays	88% fibroblast viability; Strong antibacterial activity at low µg/mL range; 100 µg/mL hydrogel gave ~75% scratch closure at 24 h; reduced MPO and collagenase activity, supporting ECM preservation and regeneration.	[127]
Injectable hydrogel from decellularized swine dermis loaded with GA-capped AgNPs (Ag@ADMH)	8.763 ± 1.221 nm	0.43% silver within Ag@ADMH	in vivo: MRSA-infected wound model	Sustained AgNP release from dermal matrix; Downregulated iNOS (M1 marker) and upregulated CD206 (M2 marker), indicating M1→M2 macrophage polarization; Enhanced fibroblast migration/proliferation and transition from inflammatory to proliferative phase.	[128]

Table 5. *Cont.*

AgNP System/Formulation	AgNP Size (nm)	Ag Concentration/Dose	Model (In Vitro/In Vivo)	Main Observed Biological Outcomes	Ref.
Bilayer electrospun PCL/PVA patch co-loaded with vitamins B12/C and AgNPs	n.r.	n.r.	in vivo: rat full-thickness dorsal skin wounds	Showed stronger inhibition of *S. aureus* and *E. coli* than fibers without AgNPs Maintained > 93% cell viability, and led to faster wound closure Improved epithelialization and collagen deposition vs. dressings without AgNPs/vitamins	[132]
PHB/CS nanofibrous scaffold containing curcumin-derived biogenic AgNPs	Average 19.83 nm	0.25–1%wt AgNPs in the matrix	in vitro: fibroblast compatibility and antibacterial assays	Enhanced antibacterial activity (notably vs. *S. aureus*), indicating suitability as an antibacterial, pro-healing scaffold	[133]

n.r.—not reported.

3.2. AgNPs-Loaded Fiber-Based Composites

Another valuable nanoplatform for wound dressings is represented by electrospun composite nanofibers. These materials offer several advantages that fulfil the main requirements of an efficient wound dressing. They can provide and maintain a moist wound environment while simultaneously absorbing excess wound exudates, which helps accelerate healing. Their intrinsic or functionalized antibacterial properties help reduce the risk of infection. Furthermore, electrospun composite nanofibers possess favourable mechanical properties that closely mimic the interwoven network of collagen and elastin fibers found in the natural ECM. This structural similarity not only reinforces the mechanical stability of the wound site but also guides the directional migration of fibroblasts along the fiber axis, thereby promoting cell adhesion, proliferation, and ultimately tissue regeneration [134–140]. Liu et al. [141] developed a biomimetic composite wound dressing based on electrospun nanofibrous chitosan (CS) incorporating AgNPs and curcumin (Cur), which demonstrated synergistic antibacterial and wound-healing activities. In their design, the hydroxyl groups of curcumin, encapsulated within the hydrophobic cavity of β-cyclodextrin (β-CD), served as a reducing agent for $AgNO_3$, while β-CD simultaneously acted as a capping agent, leading to the formation of Cur@β-CD/AgNPs complexes. These complexes were then incorporated into a solution of CS dissolved in dilute acetic acid, with polyethylene glycol (PEG) added to improve spinnability and biocompatibility, yielding a 2 wt% homogeneous Cur@β-CD/AgNPs/CS/PEG solution that was subsequently electrospun. The resulting electrospun nanofibrous scaffolds exhibited a swelling ratio of 432%, highlighting their ability to maintain a moist wound environment while absorbing excess exudates. Biodegradation studies showed that the degradation rate of the scaffolds matched the pace of new tissue formation, indicating suitability for wound healing. Haemolysis and cytotoxicity assays further confirmed their excellent biocompatibility. Antibacterial activity, evaluated by zone-of-inhibition assays and optical density measurements, demonstrated that the Cur@β-CD/AgNPs/CS/PEG dressings were effective against both Gram-positive and Gram-negative bacteria. This enhanced effect was attributed to the synergistic antibacterial action of sustained curcumin release and exposed silver, surpassing the performance of conventional AgNP-based dressings. Moreover, histological analysis using hematoxylin and eosin (H&E) and Masson's trichrome (MT) staining revealed the most uniform collagen deposition in wounds treated with the Cur@β-CD/AgNPs/CS/PEG dressings compared to

control groups [141]. Yang et al. [142] fabricated Janus nanofibers with two distinct "faces" using side-by-side electrospinning, a process in which two polymer solutions flow in parallel through a specially designed homemade acentric spinneret. One solution (A) consisted of PVP dissolved in a 9:1 (*v*/*v*) ethanol–acetic acid mixture and loaded with ciprofloxacin CIP) (10 wt% relative to PVP). The other solution (B) comprised ethyl cellulose (EC) dissolved in a 1:1 (*v*/*v*) ethanol–acetone mixture containing nanodispersed AgNPs. The novel PVP-CIP//EC-AgNPs Janus nanofibers exhibited markedly stronger antibacterial activity against both *S. aureus* and *E. coli* compared with conventional fiber-based wound dressings. The dual-face design enabled rapid release of >90% CIP antibiotic within 30 min, providing immediate antibacterial protection, while the EC–AgNPs side ensured sustained long-term activity [142]. Mobarakeh et al. [132] investigated the effect of co-delivering vitamins and AgNPs on wound healing. Using a co-spinning technique, they fabricated a bilayered electrospun polycaprolactone/polyvinyl alcohol (PCL/PVA) patch. To this end, they prepared two solutions (S1 and S2, respectively). S1 was obtained by dissolving PCL in a chloroform/ethanol mixture (7:3, *v*/*v*) at a final concentration of 12% *w*/*v*. The second solution, S2, was prepared by dissolving PVA in distilled water at 10% *w*/*v*, followed by the addition of specific amounts of the hydrophilic vitamins B12 and C, and mixing to ensure uniform distribution of the vitamins throughout the PVA solution. AgNPs were then dispersed into this mixture by thorough stirring. Further, the composite wound dressings were fabricated in a two-step process. First, PCL nanofibers were electrospun for 4 h. Then, a second layer was deposited by simultaneously electrospinning the PVA/vitamin/AgNP solution for 1 h. Afterward, the PCL feed was stopped, and electrospinning of the PVA solution continued for an additional 5 h. The wound-healing efficacy of the prepared dressings was evaluated in vivo using a murine model. Circular wounds were created on the dorsal skin of rats, which were divided into three groups according to the applied treatment: G0 (no wound dressing), G1 (wound dressing without vitamins and AgNPs), and G2 (wound dressing loaded with vitamins and AgNPs). The wound closure process was monitored for 14 days. Mechanical testing showed that incorporating AgNPs (G2) increased the elastic modulus compared with the control dressing (G1), indicating enhanced mechanical strength and stability under external forces. Antibacterial assays (disk diffusion method) showed significantly greater inhibition of *S. aureus* and *E. coli* by G2 than by G1. Cytotoxicity testing using the MTT assay confirmed high cell viability (>93%, $p > 0.05$), suggesting good biocompatibility. In vivo, G2-treated wounds showed accelerated closure, improved epithelialization, and enhanced collagen deposition, as confirmed by histological analysis [132]. Biogenic AgNPs, synthesized using curcumin as a reducing agent, were incorporated by Sarıipek [133] into a nanofibrous, biocompatible poly(3-hydroxybutyrate)/chitosan (PHB/CS) scaffold. The addition of curcumin-derived AgNPs to the PHB/CS matrix resulted in a reduction in the nanofiber diameter, enhanced hydrophilicity and wettability, and improved thermal stability. Furthermore, antibacterial activity—particularly against *S. aureus*—was synergistically enhanced by the combined effects of CS and AgNPs. These findings suggest that Cur-AgNP-loaded PHB/CS nanofibrous scaffolds hold promise for applications in antibacterial therapy, wound healing, and tissue engineering.

3.3. Sponge and Foam Composites Incorporating AgNPs

The porous three-dimensional architecture of sponge and foam composites enhances their ability to absorb and retain wound exudate. This property is particularly advantageous in wound healing, as effective exudate management helps maintain a moist wound environment, supporting tissue regeneration and preventing complications such as infection. These materials can absorb and hold large amounts of wound fluid within their interconnected pores, a feature especially beneficial for highly exuding wounds, where

traditional dressings may fail. AgNPs can be incorporated into sponges either by blending or through in situ synthesis, performed before or during lyophilization. In the freeze-drying method used to fabricate wound sponges, a polymeric solution is first frozen to form ice crystals, which are then removed by sublimation. This process yields a porous, sponge-like structure suitable for advanced wound care. An important advantage of this technique is that it preserves the biological activity of sensitive agents such as antimicrobials or growth factors, which can subsequently be released from the porous matrix in a sustained manner [143,144]. For instance, Lu et al. [145] fabricated a sponge dressing by in situ reduction of $AgNO_3$ within a chitosan (CS)/L-glutamic acid (L-GA) matrix containing hyaluronic acid (HA), using freeze-drying. The composite exhibited an interconnected porous structure with pore sizes of 50–200 μm and incorporated AgNPs measuring 5–20 nm, along with a rough surface morphology. The sponge displayed a liquid-absorption capacity exceeding 10 times its dry weight, underscoring its strong potential for exudate management, while its rough surface promoted fibroblast adhesion. In vitro, the dressing demonstrated effective antibacterial activity against *E. coli* and *S. aureus*, with no cytotoxicity in L929 fibroblasts at low AgNP concentrations. In vivo studies in a rabbit model further confirmed accelerated wound healing, as evidenced by enhanced wound contraction, reduced healing time, and rapid re-epithelialization [145]. To overcome the limitation of AgNP toxicity at effective concentrations, Zhou et al. [146] developed a chitosan (CS) composite sponge dressing incorporating in situ iturin-synthesized AgNPs. Iturin is a lipopeptide with antifungal activity, composed of a cyclic heptapeptide linked to a β-amino fatty acid chain. The tyrosine residues within the cyclic peptide can reduce $AgNO_3$ under irradiation, leading to the formation of iturin-stabilized AgNPs [147]. Using a previously reported method [148], Zhou et al. fabricated an iturin–AgNP–CS composite sponge by freeze-drying. The resulting dressing exhibited markedly enhanced antibacterial and wound-healing properties compared with commercially available AgNP-loaded dressings. In a murine full-thickness infected wound model, the composite sponge achieved effective bacterial control by day 4. Accelerated wound contraction was evident by day 7, followed by nearly complete tissue repair by day 16, with the re-epithelialization rate exceeding 90%. Histological analysis further confirmed increased formation of subcutaneous connective tissue and fibroblasts, along with pronounced neovascularization and collagen fiber deposition. Hydrogel no systemic organ toxicity was observed [146].

The primary objective in wound management is to control bleeding and achieve haemostasis, particularly in irregular, deep, non-compressible wounds, as subsequent infection can pose a serious risk to the patient's life. Therefore, the development of new, more effective haemostatic materials is a priority. Among these, shape-memory haemostatic sponges offer important advantages: they can be easily delivered and secured in deep, small wounds through simple compression. Once in place, they absorb blood, expand to their original shape, and form a physical barrier that effectively stops further bleeding. Dong et al. developed a shape-memory composite haemostatic sponge incorporating AgNPs to provide antibacterial activity. However, a key challenge is preventing the rapid release of AgNPs, which can lead to toxic side effects. Thus, effective immobilization within the scaffold and controlled release at the wound site are essential. To address this, Dong et al. [149] constructed a hydroxyethyl cellulose (HEC)/soy protein isolate (SPI) composite sponge (EHSS). The EHSS was prepared by cross-linking HEC and SPI using epichlorohydrin (ECH) [150,151]. Next, a mussel-inspired surface modification was applied to regulate the in situ–generated AgNP release. Specifically, dopamine (DA) was oxidatively polymerized under alkaline conditions, producing a polydopamine (PDA) coating on the EHSS that incorporated AgNPs (EHP@Ag). This antibacterial, shape-memory haemostatic sponge enabled the slow and sustained release of AgNPs. Compared with classical gauze and a

commercial gelatine haemostatic sponge, the EHP@Ag sponge demonstrated markedly improved haemostatic performance in both a rat liver prick injury model and a rat liver non-compressible haemorrhage model, with a haemostasis time of 22.75 ± 3.86 s and blood loss of 285.25 ± 24.93 mg [149]. Furthermore, EHP@Ag was non-toxic to L929 fibroblasts and HUVECs (Human Umbilical Vein Endothelial Cells), while exhibiting excellent antibacterial activity against *E. coli*, *S. aureus*, and MRSA [149].

3.4. Film and Membrane Composites Loaded with AgNPs

Films and membranes are an emerging class of wound dressings that offer several advantages. Their semi-permeable nature provides a physical barrier against external microbes while simultaneously maintaining a moist environment conducive to wound healing and permitting gas exchange (e.g., oxygen) to support cellular function. Various fabrication methods have been employed, including solvent casting, spin casting, salt leaching, microfluidic spinning, dip coating, and layer-by-layer assembly [152]. Films derived from natural macromolecules, such as polypeptides and proteins (keratin, fibroin, gelatine) and polysaccharides (pectin), have attracted considerable attention owing to their high biocompatibility, biodegradability, and low immunogenicity, combined with good mechanical properties, cell-adhesion capability, and versatility in fabrication. In addition, these natural polymers can be functionalized by conjugation with biologically active molecules, such as antibacterial, antioxidant, and anti-inflammatory agents, thereby enhancing their therapeutic efficacy. For instance, Benkhira et al. [153] developed an innovative hydrogel film composed of amidated pectin (AP), which modulates gelling properties, gelatine (GE), and oxidized tannic acid (OTA). OTA served both as a reducing and chelating agent and contributed to cross-linking by conjugating its quinone groups to the free amino groups in GE. In situ–reduced AgNPs were uniformly dispersed throughout the hydrogel matrix. The resulting dressing (AP:GE@OTA/Ag) exhibited enhanced tensile strength and excellent water and moisture management, as demonstrated by high fluid retention capacity (90.96% at 2 h), water retention (91.69% at 2 h), and a water vapor transmission rate of 1903.29 $g/m^2/day$. The biopolymer film containing 1.02 ± 0.13 $\mu g/cm^2$ AgNPs showed strong antibacterial activity against *S. aureus* and *E. coli* while maintaining NIT-1 mouse insulinoma cell viability. Moreover, in vivo assays using a Wistar albino rat model demonstrated that AP:GE@OTA0.5%/Ag supported rapid and complete skin regeneration within 12 days [153]. Li et al. [154] reported that glycoproteins extracted from the medicinal insect Periplaneta americana L. (PAGP), previously shown to promote wound healing [155], can act as a green reducing agent for $AgNO_3$ to produce ultrasmall AgNPs (8.8 ± 2.8 nm). These AgNPs were subsequently incorporated into a nanofibrous film (AgNPs@PP) via electrospinning, using a solution containing 150 mg/mL PVA, 100 mg/mL PAGP, and 300 mg/L AgNPs mixed in a 20:4:1 volume ratio. The resulting AgNPs@PP nanofiber film demonstrated superior wound healing efficacy compared with films containing only AgNPs or only PAGP. The enhanced performance was attributed to a synergistic effect: PAGP promoted M2 macrophage polarization, while AgNPs provided strong antibacterial activity. The authors further proposed that PAGP shares sequence or domain similarity with epidermal growth factor (EGF), enabling it to bind the epidermal growth factor receptor (EGFR). This interaction may activate downstream signalling pathways that drive cell migration, proliferation, and M2 macrophage polarization, thereby accelerating wound repair. In vivo studies using a rat wound model infected with faecal bacteria confirmed that topical application of AgNPs@PP accelerated tissue repair, upregulated TGF-β1 expression, and enhanced collagen deposition, as demonstrated by immunohistochemical staining [154]. Additionally, AgNPs@PP suppressed the growth of *S. aureus* and *E. coli* while exhibiting good mechanical strength. An interesting recent study by Gollapudi et al. [156] reported the in situ synthesis of AgNPs

on the surface of a dialdehyde cellulose nanofibril/polyquaternium-10 (DACNF/PQ) binary complex. DACNF was prepared by sodium periodate ($NaIO_4$) oxidation of cellulose nanofibrils (CNF), which introduced dialdehyde groups onto the CNF surface. PQ, short for polyquaternium-10 is a polymeric quaternary ammonium salt derived from hydroxyethyl cellulose (HEC) through reaction with 2,3-epoxypropyltrimethylammonium chloride. The dialdehyde groups on DACNF acted as effective reducing agents for Ag^+ ions, while the DACNF/PQ complex served synergistically as a stabilizing template, enabling controlled growth and uniform deposition of ultrafine AgNPs (average size ~10.3 nm). In addition, the positive charge of PQ imparted strong antibacterial properties by disrupting the negatively charged bacterial membrane through electrostatic and hydrogen-bonding interactions. The controlled release of AgNPs further enhanced the antibacterial activity of the films, which showed improved efficacy against *S. aureus* and *E. coli*. Importantly, the nanocomposite films exhibited no toxicity toward human skin fibroblast cells, demonstrated high biocompatibility, and possessed excellent tensile strength (9.78 $\pm$ 0.21 MPa), highlighting their potential as wound-healing materials [156].

3.5. Smart Responsive Wound Dressings Incorporating AgNPs

Stimuli-responsive wound dressings are an emerging class of "smart" platforms that couple antimicrobial efficacy with spatiotemporal control over release. In these systems, embedded silver reservoirs—typically AgNPs that provide Ag^+ ions—and/or co-therapeutics are liberated on demand in response to wound-relevant cues. Key trigger stimuli include: (i) pH-responsive systems exploiting the fact that chronic/infected wound beds often show neutral-to-alkaline surface pH while harbouring acidic microdomains in biofilms; polymer networks (e.g., chitosan/alginate, polyacrylic acid, catechol-modified gels) can be tuned to accelerate Ag^+ release in either regime; (ii) Enzyme-responsive dressings integrate cleavable peptide/gelatine motifs sensitive to elevated levels of MMPs or bacterial proteases, triggering matrix degradation and silver release specifically in protease-rich lesions; (iii) Thermo-responsive systems based on phase-transition polymers (notably poly(N-isopropylacrylamide)—PNIPAM) and copolymers adjusted to respond around ~38–40 °C) increase release with infection-associated local warming; (iv) ROS-responsive platforms incorporate thioketal or peroxide-labile linkers (or ROS-degradable backbones) that disassemble under oxidative stress, simultaneously moderating excess ROS and releasing AgNPs; (v) light-responsive dressings embed photothermal/photocatalytic components (e.g., polydopamine–Ag, plasmonic hybrids) to enable near-infrared (NIR)-triggered hyperthermia and accelerated payload release. Collectively, these modalities aim to deliver silver and other therapeutic agents only when and where needed, improving antibacterial performance while limiting cytotoxicity and supporting tissue repair [105,157,158].

A major challenge in wound care is the management of chronic diabetic wounds, in which persistent infection, sustained inflammation, and poor angiogenesis impede healing. To address these barriers, Hu et al. [159] engineered pH-responsive, dual-crosslinked, mussel-inspired hydrogels co-encapsulating AgNPs and the pro-angiogenic drug deferoxamine (DFO). First, oxidized dextran (OD) bearing aldehyde groups was conjugated to dopamine (DA) via Schiff-base linkages (OD–DA). In parallel, a water-soluble quaternary ammonium chitosan (HTCC) was prepared by reacting chitosan (in aqueous acetic acid) with glycidyl trimethylammonium chloride (GTMAC) [160]. Mixing OD–DA and HTCC at alkaline pH (~8.5) in the presence of sodium periodate ($NaIO_4$) yielded a double-crosslinked network comprising (i) reversible imine (Schiff-base) bonds between OD aldehydes and HTCC amines, and (ii) catechol-driven crosslinking initiated by oxidation of DA to dopamine-quinone (DAQ), followed by quinone-mediated Michael/Schiff reactions and semiquinone free radical coupling, forming polydopamine-like crosslinks [161,162]

that confer strong adhesion. AgNPs and DFO were co-encapsulated during gel formation. Under acidic niches of infected diabetic wounds, the imine bonds hydrolyse, loosening the network and accelerating the release of silver species (Ag^+ from AgNPs reservoirs) and DFO. The cationic HTCC together with Ag^+ provides effective antibacterial activity against *S. aureus* and *E. coli* and helps control inflammation, while DFO, by chelating Fe^{2+} in prolyl-hydroxylase domain (PHD) enzymes, prevents HIF-1α hydroxylation and degradation, thereby upregulating VEGF and promoting neovascularization at the wound site [148]. Haidari et al. [163] developed a pH-responsive hydrogel that releases embedded AgNPs as the environment shifts from acidic to neutral/alkaline, as in many infected wounds. The gel is formed by free-radical copolymerization of methacrylic acid (MAA) and acrylamide (AAm), crosslinked with N,N′-methylenebisacrylamide (MBAm). As pH rises above ~5, deprotonation of MAA carboxylic groups increases network charge and swelling, accelerating AgNPs/Ag^+ release. Consistent with this mechanism, Ag release was restricted at pH 4 but substantially higher at pH 7.4 and 10. The AgNPs-loaded hydrogel showed no significant cytotoxicity to human skin fibroblasts, as indicated by metabolic/live-dead assays, and was antibacterial against Gram-positive *Staphylococcus epidermidis* and Gram-negative *P. aeruginosa* [163].

Qi et al. [164] developed polydopamine–silver (PDA@Ag) hybrid plasmonic nanoparticles by leveraging PDA's catechol groups, which act as both coordination sites for Ag^+ and reductants, enabling in situ nucleation and growth of AgNPs on the PDA surface. The resulting Ag-decorated PDA nanoparticles exhibited a photothermal conversion efficiency (PCE) of 38.2%, more than twice that of pure PDA (16.6%), confirming their suitability as efficient photothermal agents for NIR-triggered local hyperthermia applications. The PDA@Ag nanoparticles were subsequently incorporated into a cationic guar gum (CG) hydrogel matrix via simple blending to obtain the CG/PDA@Ag composite hydrogel. The CG network further enhanced antibacterial performance owing to its abundant hydroxyl and quaternary ammonium functional groups, which can nonselectively capture bacteria through noncovalent electrostatic, van der Waals, and hydrophobic interactions, leading to partial bacterial killing. In vitro, the CG/PDA@Ag hydrogel demonstrated potent antibacterial activity against both Gram-negative *E. coli* (99.9%) and Gram-positive *S. aureus* (99.8%). In vivo, it showed excellent bactericidal efficacy in a rat wound infection model, highlighting its potential as a multifunctional photothermal–antibacterial wound dressing [164].

Abdali and coworkers [165] fabricated thermoresponsive antimicrobial wound dressings embedded with in situ generated AgNP that exhibited excellent tensile properties, high wound exudate absorption capacity, and easy removability from the wound surface. The thermoresponsive matrix comprised a semi-interpenetrating polymer network (semi-IPN) of crosslinked PNIPAM and linear thermoplastic polyurethane (TPU) elastomer. The fabrication was straightforward and involved simultaneous thiol-ene click radical polymerization of pentaerythritol tetra (3-mercaptopropionate) (PETMP), N,N′-methylenebisacrylamide, and N-isopropyl acrylamide monomers initiated by azosisobutyronitrile (AIBN) and one electron transfer reaction to an impregnated $AgNO_3$ solution to produce homogenously dispersed AgNPs. In brief, TPU was dissolved in N,N-dimethylacetamide, mixed with the other precursors, and heated under vacuum at 90 °C for 12 h to complete the polymerization. The water vapor transmission rate (WVTR) of the resulting membranes ranged from 300 to 500 g m^{-2} day^{-1}. AgNP-containing dressings exhibited slightly higher WVTR values, attributed to their lower crosslinking density, indicating improved capacity for wound exudate management. Both Ag-loaded and Ag-free membranes demonstrated good cytocompatibility with human dermal fibroblasts, as confirmed by MTT assays. Dressings containing 0.05 wt% metallic silver (quantified by X-ray fluorescence analysis) exhibited strong in vitro antimicrobial activity against *S. aureus*, *P. aeruginosa*, and *C. albicans* [165].

Wu et al. [166] devised an NIR-triggered anti-biofilm strategy using photothermally responsive polydopamine (PDA) nanoparticles surface-modified with AgNPs and curcumin (Cur) and then overcoated with a phase-change material (PCM), namely 1-tetradecanol. The AgNPs were anchored on PDA surface as previously described by coordinative fixation and in situ reduction of silver ions, while Cur was loaded through π–π stacking (and associated noncovalent interactions) with PDA The resulting PDA@Ag@Cur (PAC) nanoparticles were subsequently coated by simple mixing with ethanolic 1-tetradecanol to yield a uniform PCM outer layer. This coating suppresses premature release until NIR-induced heating drives the PCM's rapid solid–liquid transition. The final PDA@Ag@Cur@PCM (PACP) nanoplatform exhibited stable photothermal cycling over five heating–cooling rounds and a photothermal conversion efficiency of 38.2%. Upon 808 nm irradiation, the PCM melts, enabling Cur diffusion and promoting Ag^+ release from surface-bound AgNPs. Curcumin acts as a quorum-sensing (QS) inhibitor, disrupting cell-to-cell communication and biofilm formation, while Ag^+ provides broad-spectrum bactericidal activity; local hyperthermia further potentiates both effects. Consistently, the PACP + NIR group produced the greatest reduction in colony-forming units (CFU) and the lowest bacterial survival relative to control + NIR and PAC + NIR groups; near-complete suppression of colony growth was observed with PACP + NIR, indicating a strong synergistic antibacterial effect from combined photothermal heating, Ag^+ release, and QS inhibition [166].

An ingenious multifunctional enzyme-responsive nanosystem targeting chronic infected wounds treatment was reported by Chen et al. [167]. The platform has a core–shell morphology comprising an AgNP-loaded dendritic mesoporous silica nanoparticle (DMSN) core (D@Ag) surrounded by a cationic liposomal shell. DMSNs (32.7 ± 1.32 nm) featured a central–radial pore architecture and high surface area, favouring loading and release compared with conventional mesoporous silica. Ag^+ ions were first adsorbed electrostatically within the pores and then reduced in situ to Ag^0, yielding D@Ag. Notably, the synthesis employed bis[3-(triethoxysilyl)propyl]tetrasulfide (BTESPT; also TESPT), whose polysulfide bridge is consistent with participating in interfacial Ag^+ reduction under ammoniacal conditions while concurrently providing Ag–S anchoring sites for nascent nanoparticles. The D@Ag core was subsequently overcoated with a cationic liposomal shell functionalized with the EGFR-targeting peptide GE11 and co-loaded with resveratrol (Res), forming "silicasomes" (LR-D@Ag). These silicasomes were dispersed in a gelatin-methacryloyl (GelMA) hydrogel covalently crosslinked by photoinitiated radical polymerization to afford a composite, enzyme-degradable dressing. In infected wounds, matrix metalloproteinase-9 (MMP-9) cleaves the GelMA network, triggering on-demand release of Ag^+ and Res. The released cargo provided antibacterial, anti-inflammatory, haemostatic, and pro-regenerative effects. Notably, intracellular MRSA clearance rate reached 83.75% in BJ fibroblasts and 88.14% in HaCaT keratinocytes [167].

In recent years, considerable attention has focused on dual- and multi-stimuli-responsive delivery systems [168], which gain added functionality by combining multiple release triggers within a single nanoplatform, as follows:

i. On-demand antimicrobial release: Cargo is liberated only under infection-like cues, aligning with the wound's dynamic microenvironment.
ii. Greater antibacterial potency with less silver: Localized, pulsed release—augmented by NIR photothermal effects—enhances killing (including biofilms) while minimizing total silver exposure and host–cell cytotoxicity.
iii. Improved selectivity and safety: Gating release by pathophysiological cues (acid/alkaline shifts, oxidative stress, temperature) confines activity to the wound site and limits off-target/systemic effects.

iv. Adaptability to heterogeneous wounds: Multiple triggers address spatial and temporal variability (surface alkalinity vs. acidic biofilm pockets; fluctuating ROS), sustaining efficacy as conditions evolve.
v. Synergistic mechanisms: Combining chemical cues (pH/ROS) with physical inputs (NIR heat) accelerates bacterial eradication, dampens inflammation, and may shorten time-to-closure.
vi. Fewer dressing changes and better adherence: Sustained, stimulus-triggered cargo delivery can extend wear time and simplify care.
vii. Theragnostic potential: Some platforms pair triggers with sensing (e.g., pH-induced colour change), enabling real-time monitoring alongside therapy.

To create a multifunctional dressing that couples on-demand silver release with self-healing, tissue adhesion, and antioxidant activity, Wang et al. [169] synthesized a nanocomposite hydrogel by crosslinking 3-aminophenylboronic-acid–modified hyaluronic acid (HB) with black chokeberry (Aronia melanocarpa) extract (BCE). Because both hyaluronic acid (HA) and the polyphenol-rich BCE (proanthocyanidins, cyanidin glycosides, quercetin derivatives) present vicinal diols/catechols, they form dynamic covalent boronate esters with the boronic-acid groups on HB, acting as multivalent crosslinkers. BCE also serves as a green reductant for $AgNO_3$, enabling in situ AgNP formation. Mechanical performance depended on BCE content; at 3% BCE (with 20 mM $AgNO_3$), the hydrogel reached a compressive stress of ~36 kPa at 60% strain (35.96 $\pm$ 2.11 kPa). The hydrogel is dual-responsive: (i) acidic pH cleaves boronate esters, and (ii) hyaluronidase (HAase) degrades HA—together promoting on-demand release of silver species (predominantly Ag^+ from AgNPs reservoirs). In vitro, HB–BCE/Ag showed targeted antibacterial activity, achieving bactericidal rates of 99.12 $\pm$ 0.08% against MRSA and 99.32 $\pm$ 0.13% against *S. aureus*. In a rat full-thickness MRSA-infected wound model, the hydrogel accelerated healing, with significantly smaller wound areas versus controls by day 12. Transcriptomic analysis indicated up-regulation of CDH1 (E-cadherin) and down-regulation of CXCL1/CXCL2, consistent with strengthened epithelial integrity and attenuated inflammation. Overall, the pH/HAase-responsive HB–BCE/Ag hydrogels exhibited antioxidant, adhesive, self-healing, and biocompatible properties, along with strong antibacterial activity, inflammation control, collagen deposition, and promotion of angiogenesis in vivo [169].

Srikhao et al. [170] fabricated carboxymethyl starch (cassava-waste)/PVA/glycerol hydrogels embedding tannic-acid–capped AgNPs (H-AgNPs) to enable combined pH- and NIR-photothermal–triggered release of tannic acid (TA). TA served as a bioreductant for $AgNO_3$, a capping/stabilizing agent for AgNPs, as well as a therapeutic wound healing agent due to its antibacterial, anti-inflammatory, and haemostatic effects [171,172]. Photothermal therapy (PTT) uses near-infrared (NIR) light absorbed by a photothermal agent to generate local heat, damaging bacterial membranes and denaturing proteins, with the important advantage that thermal bacteria killing shows a lower propensity for resistance development. Ag-based nanostructures can act as photothermal agents [173–175], generating local heat through localized surface plasmon resonance, which further destabilizes the polymer matrix, facilitating TA release. In acidic medium (pH $\approx$ 5.5), formulations prepared with 200 mM $AgNO_3$ released the highest amount of TA, and release increased further under NIR irradiation, consistent with temperature-enhanced diffusion and weakened polymer–polyphenol interactions. Increasing AgNPs loading improved antibacterial and mechanical performance; the H-AgNPs-200 formulation achieved ~100% kill of *E. coli* and 98.2% of *S. aureus* under NIR, while maintaining high mammalian-cell viability [159]. Unlike PTT—which converts NIR light into local hyperthermia to kill bacteria—photodynamic therapy (PDT) uses photosensitizers that, upon light excitation, generate ROS that oxidize vital biomolecules and cause bacterial death. Although some platforms use separate wave-

lengths for optimal PTT and PDT, this is not essential: single NIR absorbers can deliver both effects. Addressing this, Du et al. [176] created a mesoporous-silica–modified Ag_2S quantum-dots (QDs) hydrogel that integrates PTT, PDT, and controlled Ag^+ release under a single nanoplatform. Ag_2S QDs, prepared from $AgNO_3$ and Na_2S, were coated with mesoporous silica ($mSiO_2$) and functionalized with 3-(trimethoxysilyl)propyl methacrylate (MPS) to introduce surface polymerizable C=C groups, then covalently embedded in a poly(N-isopropylacrylamide-co-acrylamide) network using N,N′-methylenebis(acrylamide) (BIS) as crosslinker and ammonium persulfate (APS) as initiator. Upon 808 nm NIR irradiation, the QDs generate heat and ROS (PTT + PDT), while the PNIPAM-based volume-phase transition modulates diffusion and enables controlled, continuous Ag^+ release from the Ag_2S reservoir—an intentional and important contributor to antibacterial activity. This multi-hit synergy (heat + ROS + Ag^+) produced ~99.7% kill of *E. coli* and 99.8% of MRSA within 4 min. In a BALB/c mouse full-thickness MRSA-infected wound model, the hydrogel accelerated closure with increased collagen deposition and angiogenesis and showed low cytotoxicity toward Vero cells and NIH 3T3 mouse embryonic fibroblasts with no significant in vivo toxicity at the tested doses [176].

Shi et al. [177] prepared an injectable, self-healing, pH/ROS-dual-responsive hydrogel embedding AgNPs, built from phenylboronic-acid–modified hyaluronic acid and plant-derived tannic acid (TA). Hyaluronic acid was first coupled to 2-aminophenylboronic acid (2-APBA) using 1-ethyl-3-(3-dimethyl aminopropyl)carbodiimide (EDC)/hydroxybenzotriazole (HOBt) as the coupling agent to yield HA-PBA. Separately, a 1 wt% TA solution (neutralized with sodium carbonate) was mixed 1:1 with 1 wt% $AgNO_3$ to generate TA-reduced, TA-capped AgNPs (with partial catechol→quinone oxidation); adding extra TA stabilized the dispersion. Blending this AgNP dispersion (with excess TA) into a 2 wt% HA-PBA solution produced a homogeneous AgNP-loaded dynamic gel. Gelation is driven by dynamic covalent boronate esters between TA catechols/diols and PBA groups on HA-PBA, whose reversibility imparts self-healing. Crucially, when PBA is conjugated via 2-APBA, the amide carbonyl oxygen can coordinate intramolecularly to boron (O→B), stabilizing the tetrahedral boronate and strengthening diol binding even at mildly acidic pH—thus enabling hydrogel formation with TA. In contrast, 3-APBA–modified HA, which lacks this intramolecular stabilization, complexes with TA only into nanoparticles, not a bulk gel as reported by the authors [177–179]. Release studies using fluorescein isothiocyanate labelled bovine serum albumin (FITC–BSA) as a model drug showed faster release at pH 7.2 (chronic-wound-like) than at pH 5.0 (healthy skin), attributed to progressive catechol oxidation to quinone, which weakens TA–protein interactions and loosens boronate crosslinks. At pH 7.2 in the presence of H_2O_2 (ROS model), oxidative disruption of boronate linkages further accelerated network erosion, giving the fastest cargo release (pH/ROS dual responsiveness). Both the neat and AgNP-loaded HA-PBA–TA hydrogels were cytocompatible, as proved by L929 cell viability and live/dead staining assays, and showed low-haemolytic toxicity, and antioxidant activity as revealed by the 2,2-diphenyl-1-picryl-hydrazyl-hydrate (DPPH) scavenging and ROS-staining assays [177].

Haidari et al. [180] designed a dual pH- and temperature-responsive hydrogel incorporating ultrasmall AgNPs for infection-triggered, on-demand antimicrobial release. Upon bacterial infection, the wound microenvironment typically shifts from acidic to alkaline, which initiates Ag^+ release. This process is further modulated by temperature responsiveness, which tunes the hydrogel's LCST to match the dynamic thermal changes in infected wounds. The hydrogel was synthesized by free radical copolymerization of NIPAM and acrylic acid (AA), using APS and BIS as the initiator and crosslinker, respectively. Ultrasmall AgNPs (2.91 $\pm$ 0.35 nm) were produced by reducing an MSA-complexed silver nitrate precursor with $NaBH_4$ and subsequently embedded into the PNIPAM-PAA network. At

elevated pH, deprotonation of carboxylic groups in the PAA segments induces electrostatic repulsion and hydrogel swelling, enabling Ag^+ diffusion. Incorporation of acrylic acid also increased the LCST from 32 °C (pure PNIPAM) to 36.5 °C, near physiological temperature, due to hydrogen bonding that stabilizes the hydrated, expanded polymer chains. During infection, local temperature elevations of 2–5 °C promote polymer–polymer hydrophobic interactions, expelling water, and driving hydrogel collapse, thereby enhancing Ag^+ release. LCST remained largely unaffected within the tested pH range (4–10). Ag^+ release was strongly pH-dependent, being minimal under acidic conditions (pH < 5.5) and substantially enhanced at alkaline pH (>7.4). This behaviour aligned with antibacterial efficacy: over 95% of *S. epidermidis* and *P. aeruginosa* were eradicated in vitro at pH 7.4 and pH 10. In an *S. aureus*-infected mouse wound model, the PNIPAM-PAA-AgNP hydrogel achieved accelerated wound closure, enhanced re-epithelialization, and increased collagen deposition compared with PNIPAM-PAA and SSD controls. Cytocompatibility assays (resazurin) and live/dead staining on human fibroblasts (HFFs) and keratinocytes (HaCaTs) confirmed negligible toxicity, underscoring the hydrogel's strong potential for clinical translation as a stimuli-responsive wound dressing [180].

Rapid adhesion to wet tissue—limiting bleeding and restoring haemostasis—is a key requirement for wound dressings. Khadem et al. [181] developed a bioadhesive, dual-crosslinked hydrogel nanocomposite (CAO/ATR) that is colorimetric pH-responsive and incorporates functionalized AgNPs. The CAO network is formed from carboxyethyl chitosan (CEC) and oxidized sodium alginate (OSA). In a typical preparation, separate aqueous solutions of CEC (2 wt%) and OSA (4 wt%) are prepared. To the CEC solution, the authors added $CaCl_2$ (4 wt% relative to total polymer) as a noncovalent/ionic crosslinker and adipic acid dihydrazide (ADH, 8 wt%) as a covalent crosslinker (hydrazone formation with OSA aldehydes). In parallel, tannic-acid–capped AgNPs are prepared, then functionalized with a 50 *v*/*v*% red-cabbage (RC) anthocyanin aqueous–ethanolic extract, yielding ATR nanoparticles [182]. ATR dispersions are mixed into the OSA solution (with sonication) and finally combined with the CEC phase under vigorous vortex mixing to produce homogeneous CAO/ATR hydrogels. The incorporation of 1% wt ATR into CAO significantly increased the elasticity of CAO hydrogel, as demonstrated by the results of cyclic compression tests, while almost a threefold increase in the compression strength of CAO was observed. The hybrid CAO/ATR hydrogel also demonstrated better haemostatic properties than CAO, reducing the clotting time. Moreover, the CAO/ATR effectively inhibited the growth of *E. coli* and *S. aureus* in an in vitro test carried out by the disk diffusion method and was compatible with L929 fibroblasts. Importantly, anthocyanins from RC confer a naked-eye pH response, enabling simple visual monitoring of wound status [181].

Selected stimuli-responsive AgNPs-loaded wound dressings are collected in Table 6.

Table 6. AgNPs-loaded stimuli-responsive wound dressings.

Composition	Stimuli	Properties and Effects	References
Dual-crosslinked, mussel-inspired hydrogels based on oxidized dextran (OD), dopamine (DA), and water-soluble quaternary ammonium chitosan (HTCC) co-loaded with deferoxamine (DFO)	pH	Antibacterial activity against *S. aureus* and *E. coli*; controls inflammation, promotes neovascularization	[159]
Methacrylic acid (MAA)—acrylamide (AAm), crosslinked with N,N′-methylenebisacrylamide (MBAm) copolymer hydrogel	pH	Antibacterial against *Staphylococcus epidermidis* and *P. aeruginosa*; no significant cytotoxicity to human skin fibroblasts	[163]

Table 6. *Cont.*

Composition	Stimuli	Properties and Effects	References
Polydopamine (PDA)@Ag plasmonic nanoparticles embedded in a cationic guar gum (CG) hydrogel matrix (CG/PDA@Ag)	NIR	Antibacterial activity against both Gram-negative *E. coli* (99.9%) and Gram-positive *S. aureus* (99.8%); excellent bactericidal efficacy in a rat wound infection model	[164]
Semi-interpenetrating polymeric membrane composed of crosslinked PNIPAM and linear thermoplastic polyurethane (TPU) elastomer	Temperature	Excellent tensile properties, high wound exudate absorption capacity, and easy re-movability from the wound surface; increased water vapor transmission rate (WVTR); good cytocompatibility with human dermal fibroblasts; in vitro antimicrobial activity against *S. aureus*, *P. aeruginosa*, and *C. albicans*	[165]
Polydopamine (PDA) nanoparticles surface-modified with AgNPs and curcumin (Cur) and then overcoated with the phase-change material (PCM), 1-tetradecanol (PDA@Ag@Cur@PCM)	NIR/temperature	Stable photothermal cycling over five heating–cooling rounds; QS inhibition; suppression of colony growth; broad-spectrum bactericidal activity; local hyperthermia	[166]
Core/shell (D@Ag/LR) silicasomes comprising a dendritic mesoporous silica nanoparticle (DMSN) core (D@Ag) surrounded by a cationic liposomal shell functionalized with the EGFR-targeting peptide GE11 and co-loaded with resveratrol (Res); silicasomes were dispersed in an enzyme-responsive gelatin-methacryloyl (GelMA) covalently crosslinked hydrogel	Enzymes (MMP-9)	Antibacterial, anti-inflammatory, haemostatic, and pro-regenerative; clearance rate of intracellular *MRSA* reached 83.75% in BJ fibroblasts and 88.14% in HaCaT keratinocytes	[167]
3-aminophenylboronic-acid–modified hyaluronic acid (HB) crosslinked with black chokeberry (BCE) extract (HB—BCE/Ag)	pH/hyaluronidases (HAas)	Bactericidal rates of 99.12 ± 0.08% against *MRSA* and 99.32 ± 0.13% against *S. aureus*; antioxidant, adhesive, self-healing, and biocompatible properties; up-regulation of CDH1 (E-cadherin) and down-regulation of CXCL1/CXCL2; inflammation control, collagen deposition, and promotion of angiogenesis in a rat full-thickness *MRSA*-infected wound model	[169]
Carboxymethylated starch (cassava-waste)/PVA/glycerol hydrogels embedding tannic-acid (TA)–capped AgNPs (H-AgNPs)	NIR/pH	H-AgNPs-200 formulation achieved ~100% kill of *E. coli* and 98.2% of *S.* under NIR, while maintaining high mammalian-cell viability	[170]
Platelet-inspired biodegradable hydrogel based on GelMA, TA, polyphosphate (PolyP), and gallic acid functionalized AgNPs (Gel/PP-TA-Ag)	NIR	Better haemostatic effect than commercial gauze in the mice-bleeding model; 97.57% of methicillin-resistant *MRSA* and 95.99% of *E. coli* are eliminated in vitro; 91.76% of *MRSA* in wounds is removed in vivo; reduced inflammation; improved collagen deposition and angiogenesis	[173]
Biocompatible polysaccharide carrageenan (Carr) embedded with gallic acid functionalized AgNPs (GA-Ag NP hydrogel)	NIR	Sterilization property against *E. coli* and *S. aureus*; biosafety; accelerated wound healing in *S. aureus*-infected mice	[174]

Table 6. *Cont.*

Composition	Stimuli	Properties and Effects	References
Mesoporous-silica–modified Ag_2S quantum-dots (QDs) hydrogel covalently embedded in a poly(N-isopropylacrylamide-co-acrylamide) network	NIR (PTT + PDT)	Produced ~99.7% kill of *E. coli* and 99.8% of MRSA within 4 min; accelerated wound closure and increased collagen deposition and angiogenesis in vivo in a BALB/c mouse full-thickness MRSA-infected wound model; low cytotoxicity towards Vero cells and NIH 3T3 mouse embryonic fibroblasts	[176]
Injectable, self-healing hydrogel built from phenylboronic-acid–modified hyaluronic acid (HA-PBA) and AgNPs-capped plant-derived TA	pH/ROS	Faster drug release at pH 7.2 (chronic-wound-like) than at pH 5.0 (healthy skin); the fastest cargo release rate was reached at pH 7.2 in the presence of H_2O_2; antioxidant activity, low haemolytic toxicity, cytocompatibility towards L929 cells	[177]
PNIPAM-polyacrylic acid (PAA) copolymer hydrogel embedded with ultrasmall AgNPs	pH/temperature	Over 95% of *S. epidermidis* and *P. aeruginosa* eradicated in vitro at pH 7.4 and pH 10; accelerated wound closure, enhanced re-epithelialization, and increased collagen deposition in an in vivo *S. aureus*-infected mouse wound model; cytocompatibility with human fibroblasts (HFFs) and keratinocytes (HaCaTs)	[180]
Dual crosslinked nanocomposite hydrogel (CAO/ATR) built up from carboxyethyl chitosan (CEC), oxidized sodium alginate (OSA), and TA-capped AgNPs functionalized with red-cabbage anthocyanin aqueous–ethanolic extract (ATR)	colorimetric pH-responsive	Bioadhesive, haemostatic properties, inhibition of the growth of *E. coli* and *S. aureus* in vitro; simple visual monitoring of wound status	[181,182]

4. In Vivo Fate and Safety Profile of AgNP-Based Nanocomposites in Wound Therapeutics

A first step in translating the significant, promising potential of AgNPs-based composite nanoplatforms for enhanced wound therapy is the correct and comprehensive evaluation of their safety and biocompatibility. Beyond simple cytotoxicity assays, this assessment should encompass dose- and time-dependent silver ion release under realistic wound conditions (pH, chloride, proteins, and exudate), nanoparticle agglomeration and surface corona formation, and their consequences for keratinocytes, fibroblasts, endothelial, and immune cells [23]. Particular attention is needed for oxidative stress, mitochondrial dysfunction, pro-inflammatory signalling, delayed re-epithelialization, and genotoxic endpoints, alongside hemocompatibility and sensitization/irritation potential of both the nanophase and the dressing matrix/co-excipients. Because biological effects are tightly linked to particle size, shape, coating, and charge, rigorous physicochemical characterization (size distribution, surface chemistry, zeta potential) must be paired with dissolution and transformation studies (e.g., sulfidation) in simulated wound fluid. Percutaneous absorption, tissue biodistribution, and clearance should be quantified for repeated applications and in vulnerable populations (e.g., extensive burns, paediatrics, diabetics), with attention to cumulative silver burden and rare outcomes such as argyria [183]. Finally, environmental fate of released silver, manufacturing batch consistency in ion release, and compliance with device/biocompatibility standards (e.g., ISO 10993 series, risk management per ISO 14971)

and good laboratory practices are essential to establish a risk–benefit profile robust enough to justify clinical trials and eventual clinical use [184].

4.1. Pharmacokinetics of Topical AgNPs Formulations

After topical application to a wound, the in vivo fate of AgNPs involves sequential processes of absorption, biodistribution, biotransformation, and excretion. Each of these steps is shaped by the interplay between wound microenvironmental factors (such as exudate composition, pH, and protein content) and intrinsic nanoparticle properties (including size, shape, surface chemistry, charge, and ion-release kinetics) [105,185]. Because the skin barrier is compromised during inflammation, penetration from the epidermis into the dermis is facilitated. Ultrasmall particles (~10 nm or smaller), owing to their high specific surface area and reactivity, cross endothelial layers more efficiently—by transcytosis or paracellular leakage—than larger counterparts [186]. Increased vascular permeability at the wound site, combined with lymphatic drainage, further enhances absorption into the systemic circulation and subsequent distribution [185].

Upon contact with wound exudate or body fluids, AgNPs undergo oxidative dissolution, releasing bioactive Ag^+ ions from metallic silver. These ions exhibit a high binding affinity for chloride anions and thiol-containing proteins, forming sparingly soluble AgCl and Ag–protein complexes, respectively. This binding modulates the concentration of free, bioavailable Ag^+ at the wound–dressing interface and contributes to a sustained, controlled release of silver ions over time [187]. The strong interaction of Ag^+ with insoluble ECM proteins, primarily collagen and elastin, explains why much of the topically applied silver remains localized at the site of administration or in adjacent tissues. Conversely, binding of Ag^+ to soluble proteins and peptides in extracellular fluids enables systemic translocation of silver as protein- or peptide-bound complexes, which circulate to distant organs.

Once systemically absorbed, AgNPs exhibit organ-selective biodistribution. Particles in the ~5–20 nm range preferentially accumulate in the liver, spleen, and kidneys [188]. In a rabbit model, silver levels in these organs peaked around day 2 after a single topical application and subsequently declined, whereas repeated applications led to persistently elevated concentrations over time [105]. Following dressing removal, tissue silver levels returned toward baseline [105]. Size and surface charge further influence central nervous system exposure: in animal studies, <20 nm and positively charged AgNPs cross the blood–brain barrier (BBB) more effectively than larger or neutral/negatively charged particles [189]. In a rat burn-wound model, where wound dressings containing silver nanocrystals were changed weekly, Pfurtscheller et al. reported blood silver levels of 62 μg/kg and 168 μg/kg at weeks 3 and 6, respectively [190,191]. After 6 weeks, ex vivo analysis by inductively coupled plasma mass spectrometry revealed silver accumulation in parenchymal organs (μg/kg): 3469 in the spleen, 3186 in the kidney, and 2022 in the liver. Silver was also detected in the brain, testis, lung, heart, and muscle tissue [190]. Moiemen et al. reported, in a group of six burn patients treated with nanocrystalline silver dressings (Acticoat/Acticoat Absorbent), a median maximum serum silver concentration of 200.3 μg/L, reached at a median of 9.5 days after the initial application [192]. Serum levels declined following cessation of treatment. In a separate study investigating systemic silver absorption in 30 patients with relatively small burns (median postoperative wound size 12% of total body surface area), the same group observed a median maximum serum silver concentration of 56.8 μg/L, occurring at a median of 9 days during Acticoat therapy; no biochemical or hematological signs of toxicity were detected [193]. Trop et al. [194] reported a plasma silver concentration of 107 μg/kg after 7 days of Acticoat treatment (approximately 35 mg Ag/kg body weight per day) in a 17-year-old patient with 30% mixed-depth burns. A prospective study involving 20 patients with a mean burned body

surface area of 27.68% was conducted at the Burn Treatment Unit of Londrina University. The mean time interval between injury and hospital admission was 18.66 h. Patients treated with topical 1% SSD cream exhibited mean serum silver concentrations that were approximately 14-, 48-, 77-, and 117-fold higher than those of healthy controls (0.13 μg/L) on days 1, 3, 5, and 10, respectively [195]. In one patient, the peak serum silver concentration reached 72.58 μg/L on day 10, which was 558 times higher than that of the controls [182]. Serum silver analysis in a 19-year-old woman treated with Flammazine® (1% SSD) for deep second-degree thermal burns of the lower limbs revealed a concentration of 440 μg/L (normal < 0.5 μg/L), accompanied by urinary silver excretion of 12 μg/L (normal = 0) [196]. Elevated silver concentrations were detected in both blood (196 μg/L) and urine (149 μg/L) in a 61-year-old woman who had been treated with SSD cream (200 g/day; about 9 mg silver/kg bw/day) for three weeks for extensive pyoderma gangrenosum lesions on the legs [197]. In a clinical study involving 40 patients with chronic wounds treated with various silver-containing dressings, increased serum silver levels correlated strongly with wound surface area. The authors suggested that systemic absorption was likely related to enhanced wound vascularization during granulation tissue formation under conditions of inadequate arterial perfusion [198].

For topically administered silver, understanding its dermal transformation and metabolism is essential. In a porcine model, multiple silver species—including elemental silver (Ag), silver oxide (AgO), silver chloride (AgCl), silver nitrate ($AgNO_3$), silver(I) oxide (Ag_2O), and small silver clusters (Ag_{2-6})—were identified within the epidermis following exposure to silver nanocrystals [199]. The brown to brown-black particulate deposits observed in the skin ranged from 10 nm to 1000 nm in size [191]. Moreover, in patients with both localized and systemic argyria, the deposited particles were composed predominantly of silver sulfide (Ag_2S) and silver selenide (Ag_2Se) [191]. Deposition of silver sulfide (Ag_2S) and silver selenide (Ag_2Se) in tissues results from well-recognized metabolic biotransformation pathways. Because of their strong affinity for thiolate groups in peptides and proteins, free Ag^+ ions are rapidly sequestered as silver–protein complexes, a process that plays a crucial role in mitigating cytotoxicity and contributing to detoxification mechanisms. For example, absorbed Ag^+ ions are initially bound by glutathione (GSH), after which glutathione-S-transferases (GSTs) catalyse the transfer of silver to other sulphur-containing proteins. These resulting complexes are eventually internalized and processed within lysosomes [187]. In biological media rich in glutathione or protein cysteine residues, the resulting Ag–S–R complexes (where R denotes a protein or peptide moiety) can undergo thiolate → sulphide ligand exchange [200,201], leading to the formation of silver sulphide according to the reaction:

$$2Ag{-}S{-}R + H_2S \rightarrow Ag_2S\downarrow + 2R{-}SH \quad (3)$$

Biogenic hydrogen sulphide (H_2S/HS^-) is produced in mammals primarily via the cystathionine-β-synthase (CBS)-catalysed condensation of cysteine and homocysteine [202,203]. If free Ag^+ ions remain present, they can also react directly with sulphide anions (HS^-) to yield Ag_2S. Over time, sulphur atoms within deposited Ag_2S particles can be replaced by selenium, resulting in the formation of silver selenide—a compound that is more stable and even less soluble than silver sulphide [200,204]. Formation of these insoluble silver compounds drastically reduces the bioavailability of silver ions, thereby contributing to the enhanced biosafety of silver-based nanotherapeutics [191].

Multiple clinical and kinetic studies indicate that systemic silver is cleared slowly, with blood/serum concentrations remaining detectable for months and a terminal decline that can extend to ~200 days or longer [192,193,205,206]. This prolonged persistence is consistent with extensive binding of Ag^+ to plasma proteins and low-molecular-mass

thiols (e.g., albumin, metallothionein, glutathione), which limits glomerular filtration and slows tissue redistribution. Silver is eliminated via both hepatobiliary (faecal) and renal routes. With topical AgNP wound dressings, most silver stays local and is shed with skin turnover; any silver that does enter the bloodstream is cleared mainly via the faces, with the kidney/urine as a secondary route [187].

4.2. Toxicity of Topically Administered AgNPs

We have already outlined the principal mechanisms underlying the pharmacological and toxicological activities AgNPs. For more detailed information, readers are referred to an excellent comprehensive review that discusses cellular uptake, interference with normal metabolic and signalling pathways, and the resulting biological effects observed both in vitro and in vivo [207]. In brief, nanosized silver (AgNPs) enters cells predominantly via endocytic pathways (e.g., clathrin-/caveolae-dependent endocytosis and macropinocytosis). Very small silver species (dissolved Ag^+ or ultrasmall clusters) may also cross membranes by passive diffusion or ion transport, but larger particles/aggregates are less readily internalized and tend instead to engage cell-surface receptors, thereby activating signalling cascades including those involving p21-activated kinases (PAKs), mitogen-activated protein kinases (MAPKs), and protein phosphatase 2A (PP2A) even without extensive uptake. AgNPs exposure can induce lipid peroxidation, leading to plasma-membrane damage and increased LDH release. It can also elevate ROS and trigger apoptotic signalling, via extrinsic (death-receptor) and/or intrinsic (mitochondrial) pathways. By perturbing cellular redox systems—including reduced glutathione (GSH) and antioxidant enzymes such as SOD and CAT—AgNPs frequently activate oxidative-stress response programs (e.g., Nrf2–ARE target genes). Genotoxic effects reported with AgNPs include DNA strand breaks, oxidative base lesions, chromosomal aberrations, and epigenetic alterations (e.g., DNA methylation changes, histone-tail modifications, and non-coding RNA dysregulation), often secondary to oxidative stress. At the mitochondrial level, AgNPs can cause loss of membrane potential ($\Delta\Psi m$), decreased ATP production, and cytochrome-c–mediated intrinsic apoptosis [208]. At higher or prolonged doses, AgNPs may induce endoplasmic reticulum (ER) stress and the unfolded protein response, and enhance ER–mitochondria contacts (mitochondria-associated membranes), facilitating Ca^{2+} transfer from ER to mitochondria and elevating mitochondrial Ca^{2+}, which further promotes mitochondrial dysfunction [207,208].

Here, we focus on selected clinical case reports describing adverse effects and toxicological outcomes following treatment with topical silver nanoparticle (AgNP)-based wound dressings.

Hepatotoxicity, evidenced by elevated liver enzyme activities that did not correlate with serum silver concentrations, was reported by Coombs et al. [209] in patients treated with SSD, and by Trop et al. [194] following the use of nanocrystalline silver dressings for one week (approximately 35 mg silver/kg body weight/day). In the latter study, liver enzyme levels returned to normal once silver exposure was discontinued [194].

McCague and Joe [210] reported the case of a 56-year-old woman who developed toxic epidermal necrolysis (TEN) involving 70% of the total body surface area following cotrimoxazole therapy. Upon admission, she presented with clinical sepsis, which was managed successfully with vancomycin and piperacillin/tazobactam over several days. Initially, the wounds were treated with a topical double antibiotic and 3% bismuth tribromophenate petroleum gauze. Subsequently, they were covered with a silver-containing soft silicone foam dressing. The initial serum silver concentration was 190 μg/L, which rose to 249 μg/L after 1 week, coinciding with the onset of acute leukopenia that prompted removal of the dressing. The leukocyte count returned to normal within seven days; however, the patient's skin gradually turned grey, and in the following days and weeks, she developed acute

kidney injury and ultimately multiple organ failure. The authors attributed the acute leukopenia and argyria to the silver-containing soft silicone foam dressing, which may also have contributed to the renal failure [210].

Aktepe et al. [211] reported evidence of oxidative stress and extensive DNA damage in jewellery workers occupationally exposed to silver particles. Silver-induced genotoxicity was assessed using the alkaline comet assay to quantify DNA strand breaks in peripheral blood mononuclear leukocytes. In parallel, serum total antioxidant status (TAS), total oxidant status (TOS), total thiol content, and ceruloplasmin levels were measured colorimetrically and compared with those of non-exposed healthy controls. The study found that the mean DNA damage values in leukocytes were significantly higher in the exposed workers than in the control group [211].

In summary, topical silver formulations are generally regarded as safe, with few reports of local or systemic toxicity and only rare cases of localized argyria observed at standard therapeutic doses. However, caution has to be taken in patients with extensive wound areas, as the use of large quantities of silver-based preparations can lead to significant local and systemic accumulation, potentially resulting in serious adverse effects, particularly in individuals with multiple comorbidities or impaired excretory function.

5. Clinical Translation Challenges for Silver-Based Nanoformulations in Wound Care: A Decade of Clinical Evidence

Despite the relatively abundant and promising silver-based nanoformulations, numerous key obstacles remain in translating these materials from experimental research into clinically approved, routinely used wound-care therapies. The major "bench-to-bedside" hurdles are summarized below:

(1) Formulation variability & standardization. AgNP size, shape, surface coating, loading, and release kinetics differ widely across products, making direct comparisons and dosing recommendations difficult.

(2) Dose, exposure, and pharmacokinetics/pharmacodynamics (PK/PD) in wounds. Local Ag^+ flux depends on exudate volume, pH, proteins, and biofilm presence, meaning that identical dressings can deliver markedly different exposures. Robust local PK/PD models linking silver release to antibacterial efficacy and host safety are still lacking.

(3) Safety window in real patients. Silver can be cytotoxic to keratinocytes/fibroblasts at high local concentrations. Systemic absorption increases with large total burn surface area (TBSA), prolonged application, and barrier disruption, raising concerns about argyria, hepatic/renal toxicity, and paediatric safety. Routine therapeutic monitoring (e.g., serum Ag) remains unstandardized.

(4) Efficacy against biofilms in vivo. Strong in vitro antibacterial effects often fail to translate clinically. Biofilm architecture, wound matrix binding, and ion scavenging (by chloride or thiol groups) can diminish efficacy. Demonstrating biofilm clearance and healing benefit in randomized controlled trials (RCTs) remains challenging.

(5) Comparative effectiveness & endpoints. Clinical trials frequently involve heterogeneous wounds and inconsistent outcome measures (e.g., bioburden reduction vs. time-to-healing vs. pain or odor control). Well-powered, blinded RCTs with clinically meaningful endpoints and head-to-head comparisons against standard care are needed.

(6) Resistance, tolerance & microbiome impact. Although classical resistance to silver is uncommon, tolerance mechanisms (efflux, sequestration, biofilm protection) and co-selection with antibiotic resistance are concerns. The influence of AgNPs on the skin and wound microbiome remains poorly understood.

(7) Regulatory pathway clarity. Consistent requirements for nano-specific characterization, risk assessment, and post-market surveillance are still evolving across jurisdictions. Silver dressings straddle device/drug/combination categories, since their mechanism of action may be partly physical (covering the wound, absorbing exudate, maintaining moisture) and partly pharmacological (antibacterial). This overlap creates regulatory grey zones, complicating product approval and standardization.
(8) Manufacturing, quality control, and reproducibility. Scale-up must tightly control particle size distribution, surface chemistry, endotoxin levels, residual reagents, and batch-to-batch consistency. Protein corona formation during storage or use can alter biological behaviour.
(9) Assay interference & measurement. Silver (in both nanoparticulate and ionic forms) can interfere with colorimetric and fluorescence assays, complicating cytotoxicity, ROS, and microbiological testing. Reliable speciation methods, such as Single Particle Inductively Coupled Plasma Mass Spectrometry (sp-ICP-MS), can distinguish metallic Ag^0 nanoparticles, dissolved Ag^+ ions, and protein-bound complexes, quantifying each form—essential for understanding toxicokinetics, release behaviour, and biological safety. However, such methods are not yet routine in clinical laboratories.
(10) Integration with standard wound care. Compatibility with debridement, negative pressure, enzymatic agents, and adjunct antimicrobials requires clearly defined protocols to prevent over-treatment or neutralization of effect.
(11) Long-term outcomes & scarring. Evidence remains limited regarding how nanosilver influences re-epithelialization quality, scarring, and tissue function over longer healing periods, beyond early bioburden reduction.
(12) Cost-effectiveness & stewardship. Premium products must show value vs. simpler dressings. Antimicrobial stewardship principles should guide when to start/stop silver-based treatment. Clinicians should use clinical indicators (not habit or routine) to decide when to apply (infection or high-risk indicators) and when to discontinue silver dressings (the wound is clean and granulating), minimizing unnecessary exposure.
(13) Environmental & occupational considerations. Silver release into wastewater and potential aerosolization during handling (e.g., sprays, powders, or cutting dry foams) pose ecotoxicological and occupational safety concerns that institutions must carefully evaluate.

Wound dressings that successfully complete preclinical evaluation and advance to clinical trials are tested in carefully selected human subjects, according to the study design and predefined inclusion criteria. In the following section, several selected clinical trials from the past decade are briefly presented together with their main outcomes, while additional studies are summarized in Table 7. Further illustrative examples are provided in references [212–214].

In 2017, Meekul et al. [215] reported the results of a randomized controlled trial (RCT) evaluating the effects of an alginate-silver dressing on wound healing in patients with necrotizing fasciitis admitted between April 2013 and May 2016. Patients were randomized into two groups: one treated with silver alginate dressings (Ag group) and the other with normal saline solution gauze (NSS group). The primary outcomes included the duration of wound bed preparation, length of hospital stay, total wound-care cost, and pain score. The mean time for wound bed preparation was remarkably shorter in the Ag group (21.39 days) compared with the NSS group (31.87 days). Similarly, the mean hospital stay was shorter in the Ag group (20.99 days) than in the NSS group (29.19 days). While total hospitalization costs did not differ significantly between groups, pain scores were significantly lower in patients treated with silver alginate dressings.

Metcalf and Bowler [216] evaluated the impact of a next-generation antibiofilm hydrofiber dressing (AQUACEL™ Ag^+ Extra; [AQAg$^+$E]) on hard-to-heal wounds. The study included 65 patients with wounds of 1 week to 20 years' duration (mean duration: 12 months). All patients had previously received various single or combined wound treatments, most frequently: standard silver dressings alone (26%), iodine dressings alone (23%), antibiotics alone (12%), polyhexamethylene biguanide (PHMB) products alone (11%), silver dressings with antibiotics (9%), and silver dressings with PHMB products (6%). Despite these prior interventions, 47 patients (72%) had stagnant wounds, 15 (23%) had deteriorating wounds, and 3 were unrecorded at baseline. Following a mean of 4.2 weeks of treatment (range: 1–11 weeks) with the antibiofilm dressing AQUACEL™ Ag^+ Extra, 11 wounds (17%) achieved complete closure, 40 (62%) showed improvement, 9 (14%) remained stagnant, and 5 (8%) deteriorated. The antibiofilm hydrofiber dressing incorporates the metal-chelating agent ethylenediaminetetraacetic acid (EDTA) and the quaternary ammonium surfactant benzethonium chloride, which act synergistically with silver ions at pH 5.5 to disrupt biofilm structure and enhance antimicrobial efficacy [217].

Wang et al. [218] published in 2022 a study investigating the effects of silver ion dressings on chronic refractory wounds with complex pathogenesis. A total of 80 patients treated in their department between June 2019 and January 2022 were enrolled and randomly assigned to two groups of 40 patients each. The control group received conventional wound care, whereas the study group was treated with a silver alginate dressing. Patients in the study group demonstrated faster wound healing (mean healing time: 25 days) compared with the control group (29 days). Likewise, the time to granulation and complete epithelialization was shorter in the study group than in the control group. Zhang et al. [219] conducted a retrospective study evaluating the efficacy of AgNPs combined with thermoplastic polyurethane (TPU/NS) in the postoperative management of diabetic patients with open fractures of the lower extremities. A total of 98 diabetic patients treated between June 2015 and December 2021 were enrolled and divided into two groups: a control group receiving traditional dressings (n = 57) and an observation group treated with TPU/NS dressings (n = 41). Wound secretions were collected on postoperative day 7 and analysed for bacterial culture positive rates. Venous blood samples were obtained on days 1, 3, 7, and 10, and analysed for white blood cell count (WBC), neutrophil count (NEU), erythrocyte sedimentation rate (ESR), C-reactive protein (CRP), and the inflammatory cytokines IL-6 and tumour TNF-α. The bacterial positive rate was lower in the TPU/NS group than in the control group, accompanied by reductions in ESR, NEU, CRP, IL-6, and TNF-α levels. In addition, the time to dressing change completion, stopping of wound exudation, overall wound healing time, and mean visual analogue scale (VAS) pain score were all shorter or lower in the TPU/NS group compared with controls. Furthermore, the incidence of adverse reactions after treatment was 17.07% in the TPU/NS group—approximately half that observed in the control group (35.09%).

Hurd et al. [220] published the results of a retrospective study conducted between March 2016 and March 2018, involving 2572 patients with various chronic wounds, including diabetic foot ulcers, venous leg ulcers, pressure injuries, surgical wounds, and burns. Of these, 330 patients were treated using an Integrated Care Bundle (ICB) that included nanocrystalline silver (NCS) dressings, while the remaining 2242 patients received non-bundle wound management without NCS. The mean wound healing time, regardless of wound type, was more than halved in the NCS/ICB group (10.46 weeks) compared with the non-ICB group (25.49 weeks). Moreover, the mean dressing change interval was longer in the NCS/ICB group (every 3.98 days) than in the non-ICB group (every 1.87 days), reflecting a lower dressing change frequency and contributing to a substantial reduction in wound-care costs ($1251 vs. $6488 per patient).

In a clinical trial published in 2021, Wang et al. [221] investigated the effects of a non-adhesive hydrophilic polyurethane foam dressing containing silver salts incorporated into the matrix (Biatain® Ag, Coloplast, Humlebaek, Denmark) on the healing of diabetic foot ulcers (DFUs). A total of 60 adult patients with type 2 diabetes mellitus and Wagner Grade 1–2 DFUs were enrolled according to the following inclusion criteria: wound area ≥ 1 cm^2, ankle–brachial index (ABI) > 0.7 in the affected foot, and skin perfusion pressure (SPP) ≥ 30 mm Hg. Exclusion criteria included malignancy near the ulcer, allergy to dressing components, osteomyelitis or other severe infections, uncontrolled abscess or cellulitis, human immunodeficiency virus (HIV) infection, other uncontrolled medical conditions, or inability to wear offloading devices. Patients were randomly assigned to one of two groups: a treatment group receiving the silver ion–releasing non-adhesive polyurethane foam dressing, and a control group treated with 1% SSD cream, applied once or twice daily for four weeks. The silver-releasing foam dressing demonstrated superior healing efficacy compared with SSD cream, as indicated by a significantly greater reduction in wound area (76.43 $\pm$ 7.41% vs. 27.00 $\pm$ 4.95%, $p < 0.05$) and a higher weekly wound-healing rate during the first three weeks of treatment in the Biatain® Ag group compared with the control group.

Dissemond et al. [222] analyzed electronic medical records and patient charts to compare the outcomes of hard-to-heal wounds—including venous leg ulcers (VLUs), DFUs, and pressure injuries (PIs)—in patients treated with either AQUACEL® Ag Advantage/Ag$^+$ Extra (AQUACEL® Ag$^+$) (Convatec, Deeside, UK) or Cutimed® Sorbact® (Essity, Philadelphia, PA, USA). The combined study population included 200 patients treated with AQUACEL® Ag$^+$ and 150 patients treated with Sorbact, recruited from wound-care centres in Germany and the United States. In the German cohort, complete wound healing was achieved in 54% of patients treated with AQUACEL® Ag$^+$, while 46% showed wound improvement. In comparison, among the Sorbact group, 37% achieved complete healing and 55% showed improvement. No major complications occurred in either treatment arm. However, a significantly higher proportion of patients required surgical intervention in the Sorbact group (11% vs. 0%; $p = 0.039$). In the USA cohort, a statistically significant difference in wound outcomes was also observed between the two treatments. The proportion of completely healed or improved wounds was 96% in the AQUACEL® Ag$^+$ group compared with 91% in the Sorbact group ($p = 0.036$). Specifically, complete healing occurred in 48% of AQUACEL® Ag$^+$–treated wounds versus 35% with Sorbact, while improvement without complete closure occurred in 48% and 56% of patients, respectively. Using multinomial logistic regression, the authors found that patients treated with AQUACEL® Ag$^+$ were 3.53 times more likely to achieve complete wound healing than those treated with Sorbact ($p = 0.033$).

In 2024, Chan et al. [223] conducted a prospective, randomized, controlled, single-centre clinical trial to evaluate the efficacy of a novel FDA-cleared wireless electroceutical dressing (WED) in disrupting biofilm infections in burns, which contribute to nearly 60% of burn-related mortality. Unlike topical pharmaceutical formulations, the WED is powered by a silver–zinc (Ag–Zn) electrochemical couple that generates a low-intensity electric field (approximately 1 V)—a level safe for human tissue but disruptive to bacterial physiology. Bacterial adhesion, proliferation, and aggregation, which are critical early steps in biofilm formation, depend on electroactive signalling pathways mediated by ion channels that facilitate cell-to-cell communication among bacteria. Moreover, both defence mechanisms leading to bacterial resistance and offensive mechanisms enhancing virulence are influenced by electrical and redox signalling [224]. For example, pyocyanin, a redox-active and electrically conductive virulence factor produced by *P. aeruginosa*, promotes biofilm persistence and host tissue injury [225]. When activated by moisture, the WED

(Procellera™, Vomaris Innovations, Inc., Fountain Hills, AZ, USA) generates transient micromolar levels of superoxide anion radicals ($O_2\bullet^-$) that further inhibit bacterial growth and biofilm development. A total of 38 burn patients were enrolled and randomly assigned to receive either the WED (Procellera™) or standard-of-care (SoC) dressings, including silver nylon, SSD ointment, bacitracin, 5% sulfamylon solution, xeroform, Manuka honey, or other antimicrobials. After one week of treatment, biofilm formation was evaluated by SEM. Minimal or no biofilm formation was observed in 52% of wounds treated with Procellera™, compared with only 24% in the SoC group ($p < 0.05$), indicating a significant reduction in biofilm development with the WED treatment.

Table 7. Summary of clinical trials conducted in the past decade on commercial AgNPs-based dressings for wound treatment (extracted from reference [213]).

Dressings	Clinical Method Summary	Quantitative Results	Year (Ref.)
Aquacel Ag	The study was designed to evaluate the systemic absorption of silver in patients (criteria: silver levels > 0.5 µg/mL) with chronic inflammatory wounds and its association with silver toxicity. The study was a longitudinal, observational, multicenter, open-label pilot study using 40 elderly (patients mostly female, average age 74.3 years).	Dressing changed every 2 days between the initial day and day 28 of the treatment period. Mean wound surface area reduction was 22.8% ($p = 0.041$), along with a decrease in the fibrin percentage (beneficial for wound healing) between day 0 and day 28. Half the patients showed increased silver levels. There was no argyria or systemic toxicity. Elimination of silver from the body was slow and could lead to cumulative toxicity, especially in elderly patients. The study recommends against long-term silver dressing use.	2018 [198]
Aquacel® Ag^+ Extra™ (All patients previously managed with traditional silver (26%), iodine (23%) or polyhexamethylene biguanide (PHMB) (11%) containing products or systemic antibiotics (12%))	The study recruited 65 patients with wounds ranging in duration from 1 week to 20 years (median duration: 12 months). 47 cases (72%) had stagnant wounds, and 15 cases (23%) had deteriorating wounds, while 3 wounds were not recorded; observations were made for 1–11 weeks. Participants also had clinical signs of infection or critical colonization.	Observations were as follows: 17% of wounds healed, 62% of wounds showed improvement, 14% of wounds remained the same, and 8% of wounds deteriorated. Moderate exudate (52% n = 24) and high exudate (37% n = 34) levels before treatment led to low (31%, n = 20) and moderate (43% n = 28) levels, respectively, after treatment. Biofilms were observed in 49% and slough in 42% of wounds. After applying the dressing, the wound bed tissue was 63% granulated. Healthy wound bed tissues increased from 33% to 67% after treatment. Necrotic, slough biofilm reduced from 92% to 40% following treatment. Peri-wound skin health improved in 67% of cases.	2020 [216]
Acticoat™ Flex 7 (nano-Ag) with dressings without nano Ag	Retrospective study: 330 patients and 2242 patients in the control group in community centers with various types of wounds, including pressure injuries, diabetic foot ulcers, and venous leg ulcers (used Bates–Jensen Wound Assessment Tool).	Sustained silver release over 7 days. The mean time between dressing changes was 3.98 days vs. 1.87 days in control ($p < 0.01$), reducing nurse visits. The mean healing time for wounds treated with Acticoat 7 was significantly shorter (10.46 weeks) compared to wounds with a control dressing (25.49 weeks). Only 0.9% of patients treated with Acticoat 7 dressing developed a systemic infection, compared to 3% in the comparative group. Potential for bias and no control for confounding variables, e.g., concurrent treatments.	2021 [220]

Table 7. *Cont.*

Dressings	Clinical Method Summary	Quantitative Results	Year (Ref.)
Biatain® Ag Non-Adhesive Foam versus silver sulfadiazine	60 adult patients diagnosed with type 2 diabetes mellitus with diabetic foot ulcers (DFU) measuring at least 1 cm^2 were recruited. Treatment Group: Biatain® Ag Non-Adhesive Foam dressing applied at least every two days (38 patients). Control Group: 1% SSD cream applied once or twice per day (22 patients) A 4-week study, where debridement was performed during weekly visits, if necessary.	*Enterococcus faecalis* and *Staphylococcus aureus* were isolated from the wound culture in both groups. The proportion of the wound healed at week 4 in the SSD group was 27.00 ± 4.95%, while Biatain was 76.43 ± 7.41% ($p < 0.0001$). Silver foam facilitated wound closure faster than SSD in the patient population with HbA1c > 7% (59.94 ± 8.00% vs. 14.21 ± 3.72%, $p = 0.027$) and in patients with positive microbial isolates in their wound culture (60.87 ± 4.06% vs. 37.50 ± 5.89%, $p = 0.020$).	2021 [221]
Biatain alginate Ag versus gauze (some with iodoform)	40 patients in observation and 40 patients in the control group. Debridement and Biatain Alginate Ag were applied to the wounds. Dressing changed every 1 to 3 days. Assessment at 7, 14 days, and 1 month after treatment. The study observed the frequency of dressing changes, granulation tissue growth, wound formation, and healing time.	Pain score (VAS) was significantly different between the Bitain and the control group ($p < 0.05$). Better outcomes in wound scar healing were observed as compared to the control group ($p < 0.05$). Enhanced granulation tissue growth was significantly higher in the observation vs. the control. Bacterial load was significantly lower than in the control group.	2022 [218]
Aquacel Ag^+ versus Sorbact dressing (Cutimed Sorbact, Essity, retains exudate, no release of any antimicrobials)	Retrospective Patient Chart Audit with 350 patient charts: 200 with Aquacel Ag^+ and 150 with Sorbact. Data analyzed separately for Germany and the US (DFU and venous leg ulcers).	Unclear why specific dressings were chosen for specific patients. Germany: Wound percent reduction and wound closure comparable; greater proportion of Sorbact users needed surgery (0 vs. 11%, $p = 0.039$). US: Wounds were worsening before the use of Aquacel (49% vs. 34%, $p = 0.01$), regression analysis suggests that it was 3.53 times more likely to have wound healed in Aquacel cohort ($p = 0.033$).	2023 [222]
Acticoat versus Standard of Care (SoC)	Prospective, open-labeled, randomized, placebo-controlled trial for acute diabetes-related foot ulcers, with 63 patients with Acticoat and 55 with SoC. The primary endpoint was the proportion of ulcers healed at 12 weeks.	Observation of ulcers healed at 12 weeks: 75% in the control group and 69% in the silver group ($p = 0.49$). No significant difference in complete ulcer healing ($p = 0.53$), osteomyelitis, need for amputation or antibiotic treatment between the silver and control groups.	2023 [226]
Acticoat™ vs. Aquacel Ag	A single-blind, randomized controlled study in a Pediatric Emergency Department, included 89 children with superficial or mid-dermal burns (<10% TBSA),who were randomized to receive either the Acticoat™ (n = 45) or Aquacel® Ag (n = 44) dressings.	No significant difference between the groups in terms of percentage epithelialization by day 10, with Acticoat™ showing 93 ± 14% and Aquacel® Ag showing 94 ± 17% ($p = 0.89$). No significant difference in infection and escalation of care. Aquacel® Ag dressings (59) required significantly fewer dressing changes compared to Acticoat (102) ($p = 0.03$)	2016 [227]

Table 7. *Cont.*

Dressings	Clinical Method Summary	Quantitative Results	Year (Ref.)
Procellera™ + SoC versus SoC (moleskin and Tegaderm)	A prospective randomized controlled two-arm Clinical Study for blister management. The study involved 80 Ranger recruits as participants in a 14-day study.	No significant difference in wound healing rates between the SoC group and the SoC + Procellera group ($p = 0.528$). No significant difference in pain management between the SoC and SoC + Procellera groups.	2017 [228]
Mepilex A vs. Suprathel (DL-polylactic Acid membrane)	A prospective randomized controlled trial comparing the outpatient treatment of pediatric and adult partial-thickness burns. 29 adults and 33 pediatric patients (almost equally split between two dressings). TBSA: 1–29% in Meiplex Ag and 1–20% in Suprathel group.	The median time to complete reepithelialization was 12 days for both groups ($p = 0.75$). Suprathel reported better overall scar quality, and Mepilex Ag increased the stiffness of burned skin at 1 month post-burn. Patients experienced less pain with Suprathel (only for the first 5 days, $p = 0.03$).	2018 [229]
Silverlon vs. SSD or mafenide acetate (considered topical antimicrobials)	A 10-year retrospective analysis on a total of 987 combat burn casualties, with 184 patients in Group 1 (Silverlon) and 803 in Group 2 (topical antimicrobial); 49% of the cohort had third-degree burns.	The incidence of wound infection was 5.4% in Group 1 and 9.5% in Group 2 ($p = 0.08$), the overall mortality rate did not differ significantly between the groups (8% in Group 1). The incidence of bacteremia was 4.3% in Group 1 and 5.5% in Group 2, showing no significant difference ($p = 1.0$). The application of topical antimicrobials was painful.	2018 [230]
Acticoat Flex 3 vs. 1% SSD	A randomized, single-center, single-blind trial involving 100 adults aged 18–65 with second-degree burns.	Reepithelization: Acticoat: 48% (24/50 patients), SSD: 52% (26/50 patients) ($p = 0.56$). Number of dressing changes: Acticoat fewer than SSD ($p < 0.001$)	2022 [231]
Procellera™ versus SoC	A single-center prospective, randomized controlled clinical trial with 38 patients with dermal burn/traumatic wounds. Procellera dressing compared with SOC: silver nylon, SSD ointment, bacitracin, xeroform, 5% sulfamylon solution, and Manuka honey, observations at 7-day.	In 52% of the Procellera-treated wounds, little to no biofilm could be detected by scanning electron microscopy compared to only 24% of SoC-treated wounds; Procellera lowered the increase in biofilm versus SoC ($p < 0.05$).	2024 [223]

Although several clinical studies demonstrate encouraging outcomes for AgNP-based wound dressings, the overall evidence base remains limited by small sample sizes, heterogeneous wound types, inconsistent comparators, and short follow-up periods. Most trials lack standardized endpoints such as time to complete closure, patient-reported outcomes, or systematic microbiological assessment. As a result, the current clinical literature, while promising, is not yet sufficiently robust to allow definitive conclusions regarding comparative effectiveness across wound categories. Moreover, to date, relatively few AgNP-based systems have completed formal regulatory review as distinct nanomedical products, underscoring the need for harmonized standards in characterization and manufacturing.

6. Conclusions and Future Perspective

Silver nanoparticle-integrated composite wound dressings have emerged as one of the most promising innovations in advanced wound management. Their unique combination of broad-spectrum antibacterial, anti-inflammatory, antioxidant, and proangiogenic properties supports all key stages of the wound-healing cascade—hemostasis, inflammation, proliferation, and remodeling. In addition, AgNPs exhibit a lower propensity to induce bac-

terial resistance than conventional antibiotics, making them highly attractive for managing chronic and infected wounds.

Despite these advantages, the safe and reproducible clinical translation of AgNP-based nanocomposites remains an ongoing challenge. Each stage of their developmental pathway—from rational design and synthesis to clinical validation and large-scale manufacturing—presents specific scientific, regulatory, and practical barriers (Figure 3).

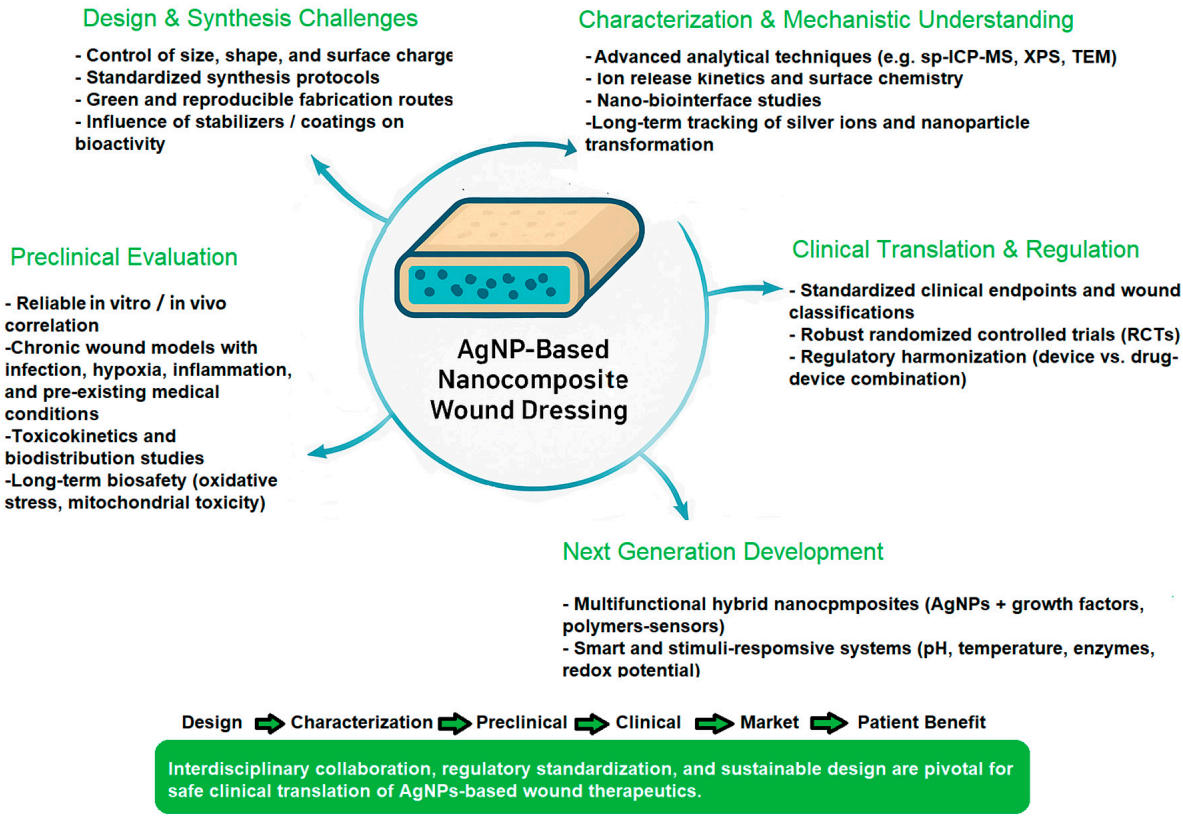

Figure 3. Key future challenges and development pathways for AgNP-based nanocomposite wound dressings.

At the design and synthesis stage, precise control of particle size, shape, surface charge, and the stabilizing matrix composition is essential to ensure predictable ion-release profiles and consistent biological performance. However, batch-to-batch variability and lack of standardized synthetic protocols remain major limitations. Furthermore, surface coatings and capping agents, while necessary for colloidal stability, may alter biological interactions and toxicity, highlighting the need for comprehensive surface chemistry characterization. In this regard, future perspectives lean towards broader implementation of green synthesis methods, such as advanced biogenic or solvent-lean routes with tight control of nucleation/growth resistance [133,232].

In the preclinical phase, multimodal evaluation encompassing in vitro cytocompatibility, oxidative stress balance, inflammatory signaling, and biofilm inhibition must be complemented by relevant in vivo wound models that replicate the complexity of chronic wounds, including impaired vascularization and infection dynamics. Moreover, toxicokinetic studies are essential to elucidate the biodistribution, accumulation, and clearance of silver species, as well as their potential effects on distant organs. To improve translational relevance, toxicological studies using animal models with pre-existing conditions such as obesity, asthma, or hypertension, which may increase susceptibility to silver exposure, should also be conducted. Moreover, it would also be of interest to implement harmonized

test batteries that resolve particle vs. ionic silver contributions (e.g., speciation analytics), interference-aware in vitro assays, chronic/repeat-dose models, and host-microbiome impacts resistance. Multi-site interlaboratory studies and reporting checklists should enable comparability and inform exposure-minimizing designs without compromising efficacy.

The clinical translation phase faces additional obstacles. Only a limited number of AgNP-containing dressings have advanced to well-designed randomized controlled trials (RCTs), and reported outcomes often vary due to heterogeneous wound types, inconsistent endpoints, and small sample sizes. Regulatory classification further complicates progress: depending on their intended mechanism of action, silver-based dressings may be classified as medical devices, drug–device combinations, or even pharmacologically active formulations, creating ambiguity in approval pathways and safety requirements. Clinical trials could benefit from the use of patient-centered endpoints (time-to-closure, pain, exudate control, infection recurrence, quality of life), incorporating pragmatic designs and health-economic evaluation to support adoption in real-world settings [233,234].

At the manufacturing and commercialization level, achieving scalable, reproducible, and cost-effective production while maintaining stringent quality control (QC) and environmental safety remains a challenge. One promising strategy is to integrate manufacturing optimization with life-cycle assessment and measures that minimize downstream silver release (e.g., enhanced matrix binding, triggered capture) to lessen environmental impact. Moreover, standardized protocols for nanoparticle characterization—including ion release kinetics, colloidal stability, and batch uniformity—are essential to satisfy both regulatory and clinical reliability standards. This requires prioritizing Good Manufacturing Practices (GMP), applying Quality by Design (QbD) principles, and performing comprehensive batch-to-batch characterization in line with regulatory expectations for device, drug, and combination products. [235–237].

Looking forward, future research should prioritize the development of multifunctional hybrid nanocomposites that combine AgNPs with biopolymers, growth factors, or smart-responsive materials capable of controlled release, real-time wound monitoring, and stimuli-responsive antimicrobial action. For instance, the development of on-demand systems that couple Ag release to wound-relevant triggers (pH, ROS, proteases, temperature, or electrical/magnetic stimuli) represents a promising avenue for further advances in the field. Such systems could minimize unnecessary cytotoxic Ag^+ release, thereby reducing host toxicity and limiting the risk of bacterial tolerance or resistance. In addition, Ag-based nanosystems co-delivering orthogonal functionalities (e.g., localized anti-inflammatories, quorum-sensing inhibitors, matrix-remodeling enzymes, oxygen carriers, angiogenic cues, or analgesics) could be engineered to address specific wound-phase needs and ensure mechanistic complementarity rather than additive silver exposure.

Integration of biosensors and electroceutical components (e.g., silver–zinc microcurrents) may further enhance antimicrobial efficacy while promoting angiogenesis and tissue regeneration. In particular, closed-loop platforms incorporating both sensing and actuation—for example, impedance or optical biofilm monitoring linked to feedback-controlled dosing—can optimize therapeutic efficacy while minimizing cytotoxicity and resistance-driving selection pressure [238,239].

Additionally, advanced analytical tools—including single-particle ICP-MS, synchrotron-based imaging, and omics technologies—will be indispensable for elucidating nano–bio interactions, filling current knowledge gaps on AgNPs' mechanisms of action, and ensuring biosafety [240]. In particular, transcriptomic, proteomic, and metabolomic analyses—including single-cell and spatial modalities—represent powerful strategies to characterize host–pathogen–biofilm responses to specific Ag formulations. Such datasets

can identify predictive biomarkers, guide dose/regimen optimization, and enable patient stratification (e.g., inflammatory or biofilm-dominant phenotypes) [241–243].

Ultimately, successful translation of AgNP-based wound dressings from the laboratory to the clinic will require interdisciplinary collaboration among materials scientists, clinicians, toxicologists, and regulatory authorities. Establishing harmonized international standards for characterization, safety evaluation, and clinical efficacy will be crucial to advance the next generation of nanocomposite wound therapeutics—safe, effective, and accessible for widespread clinical use. Executing on these priorities will convert the proven antimicrobial value of silver into predictable, durable healing across diverse wound etiologies while safeguarding patients and the environment.

Author Contributions: Conceptualization, P.C.B., A.-G.N., A.A. and A.M.G.; methodology, P.C.B., A.-G.N., D.A. and A.A.; writing—original draft preparation, P.C.B., A.-G.N., A.M.G., D.A. and A.A.; writing—review and editing, P.C.B., A.-G.N., D.A. and A.M.G. All authors have read and agreed to the published version of the manuscript.

Funding: This research received no external funding.

Institutional Review Board Statement: Not applicable.

Informed Consent Statement: Not applicable.

Data Availability Statement: No new data were created or analyzed in this study.

Conflicts of Interest: The authors declare no conflicts of interest.

Abbreviations

The following abbreviations are used in this manuscript:

AgNPs	Silver nanoparticles
ROS	Reactive oxygen species
RNS	Reactive nitrogen species
VEGF	Vascular endothelial growth factor
bFGF	Basic fibroblast growth factor
ECM	Extracellular matrix
MMP	Matrix metalloproteinase
TIMP	Tissue inhibitor of metalloproteinase
HIF-1	Hypoxia-inducible factor-1
NO	Nitric oxide
iNOS	Inducible nitric oxide synthase
NF-κB	Nuclear factor kappa-light-chain-enhancer of activated B cells
MAPK	Mitogen-activated protein kinase
PI3K	Phosphatidylinositol 3-kinase
Akt	Protein kinase B
SOD	Superoxide dismutase
CAT	Catalase
IHC	Immunohistochemistry
SSD	Silver sulfadiazine
CAM	Chorioallantoic membrane
QC	Quality control

References

1. Mihai, M.M.; Dima, M.B.; Dima, B.; Holban, A.M. Nanomaterials for Wound Healing and Infection Control. *Materials* **2019**, *12*, 2176. [CrossRef]
2. Morton, L.M.; Phillips, T.J. Wound healing and treating wounds: Differential diagnosis and evaluation of chronic wounds. *J. Am. Acad. Dermatol.* **2016**, *74*, 589–605. [CrossRef]

3. Percival, N.J. Classification of Wounds and their Management. *Surg. Oxf. Int. Ed.* **2002**, *20*, 114–117. [CrossRef]
4. Lazarus, G.S.; Cooper, D.M.; Knighton, D.R.; Margolis, D.J.; Pecoraro, R.E.; Rodeheaver, G.; Robson, M.C. Definitions and guidelines for assessment of wounds and evaluation of healing. *Arch. Dermatol.* **1994**, *130*, 489–493. [CrossRef] [PubMed]
5. Chhabra, S.; Chhabra, N.; Kaur, A.; Gupta, N. Wound Healing Concepts in Clinical Practice of OMFS. *J. Maxillofac. Oral Surg.* **2017**, *16*, 403–423. [CrossRef]
6. Diegelmann, R.F.; Evans, M.C. Wound healing: An overview of acute, fibrotic and delayed healing. *Front. Biosci.* **2004**, *9*, 283–289. [CrossRef]
7. Young, A.; McNaught, C.-E. The physiology of wound healing. *Surgery* **2011**, *29*, 475–479. [CrossRef]
8. Greaves, N.S.; Ashcroft, K.J.; Baguneid, M.; Bayat, A. Current understanding of molecular and cellular mechanisms in fibroplasia and angiogenesis during acute wound healing. *J. Dermatol. Sci.* **2013**, *72*, 206–217. [CrossRef]
9. Monika, P.; Chandraprabha, M.N.; Rangarajan, A.; Waiker, P.V.; Chidambara Murthy, K.N. Challenges in Healing Wound: Role of Complementary and Alternative Medicine. *Front. Nutr.* **2021**, *8*, 791899. [CrossRef]
10. Whittam, A.J.; Maan, Z.N.; Duscher, D.; Wong, V.W.; Barrera, J.A.; Januszyk, M.; Gurtner, G.C. Challenges and Opportunities in Drug Delivery for Wound Healing. *Adv. Wound Care* **2016**, *5*, 79–88. [CrossRef]
11. Frykberg, R.G.; Banks, J. Challenges in the Treatment of Chronic Wounds. *Adv. Wound Care* **2015**, *4*, 560–582. [CrossRef]
12. Tarnuzzer, R.W.; Schultz, G.S. Biochemical analysis of acute and chronic wound environments. *Wound Repair Regen.* **1996**, *4*, 321–325. [CrossRef]
13. Sutcliffe, J.E.S.; Thrasivoulou, C.; Serena, T.E.; Madden, L.; Richards, T.; Phillips, A.R.J.; Becker, D.L. Changes in the extracellular matrix surrounding human chronic wounds revealed by 2-photon imaging. *Int. Wound J.* **2017**, *14*, 1225–1236. [CrossRef]
14. Landén, N.X.; Li, D.; Ståhle, M. Transition from inflammation to proliferation: A critical step during wound healing. *Cell. Mol. Life Sci.* **2016**, *73*, 3861–3885. [CrossRef] [PubMed]
15. Hong, W.X.; Hu, M.S.; Esquivel, M.; Liang, G.Y.; Rennert, R.C.; McArdle, A.; Paik, K.J.; Duscher, D.; Gurtner, G.C.; Lorenz, H.P.; et al. The Role of Hypoxia-Inducible Factor in Wound Healing. *Adv. Wound Care* **2014**, *3*, 390–399. [CrossRef] [PubMed]
16. Hunt, M.; Torres, M.; Bachar-Wikstrom, E.; Wikstrom, J.D. Cellular and molecular roles of reactive oxygen species in wound healing. *Commun. Biol.* **2024**, *7*, 1534. [CrossRef] [PubMed]
17. Ukaegbu, K.; Allen, E.; Svoboda, K.K.H. Reactive Oxygen Species and Antioxidants in Wound Healing: Mechanisms and Therapeutic Potential. *Int. Wound J.* **2025**, *22*, e70330. [CrossRef]
18. Cano Sanchez, M.; Lancel, S.; Boulanger, E.; Neviere, R. Targeting Oxidative Stress and Mitochondrial Dysfunction in the Treatment of Impaired Wound Healing: A Systematic Review. *Antioxidants* **2018**, *7*, 98. [CrossRef]
19. Tan, M.L.L.; Chin, J.S.; Madden, L.; Becker, D.L. Challenges faced in developing an ideal chronic wound model. *Expert Opin. Drug Discov.* **2023**, *18*, 99–114. [CrossRef]
20. Caley, M.P.; Martins, V.L.; O'Toole, E.A. Metalloproteinases and Wound Healing. *Adv. Wound Care* **2015**, *4*, 225–234. [CrossRef]
21. Tyavambiza, C.; Meyer, M.; Meyer, S. Cellular and Molecular Events of Wound Healing and the Potential of Silver Based Nanoformulations as Wound Healing Agents. *Bioengineering* **2022**, *9*, 712. [CrossRef]
22. Naganthran, A.; Verasoundarapandian, G.; Khalid, F.E.; Masarudin, M.J.; Zulkharnain, A.; Nawawi, N.M.; Karim, M.; Che Abdullah, C.A.; Ahmad, S.A. Synthesis, Characterization and Biomedical Application of Silver Nanoparticles. *Materials* **2022**, *15*, 427. [CrossRef]
23. Kaya, M.; Akdaşçi, E.; Eker, F.; Bechelany, M.; Karav, S. Recent Advances of Silver Nanoparticles in Wound Healing: Evaluation of In Vivo and In Vitro Studies. *Int. J. Mol. Sci.* **2025**, *26*, 9889. [CrossRef]
24. Verma, R.K.; Nagar, V.; Sharma, A.; Mavry, B.; Kumari, P.; Lohar, S.; Singhal, A.; Prajapati, M.K.; Singh, A.; Awasthi, K.K.; et al. Green Synthesized Nanoparticles Targeting Antimicrobial Activities. *Biointerface Res. Appl. Chem.* **2023**, *13*, 469. [CrossRef]
25. El Shanshoury, A.E.R.R.; Sabae, S.Z.; El Shouny, W.A.; Elsaied, H.E.; Badr, H.M.; Abo-Shady, A.M. Biomimetic Synthesis of Silver Nanoparticles Using New Aquatic Species of *Bacillus*, *Alcaligenes*, and *Paenibacillus* and their Potential Antibiofilm Activity against Biofilm-Forming *Escherichia coli*. *Lett. Appl. NanoBioSci.* **2023**, *12*, 127. [CrossRef]
26. Abdussalam-Mohammed, W.; Abraheem, M.S.; Ettarhouni, Z.O.; Dakhil, O.O.; Mezoughi, A.B. Novel Compatible Silver Nanoparticles Functionalized by Vitamin C and its Derivatives: Characterization and their Antibacterial Activity against *Escherichia coli* and *Staphylococcus aureus*. *Biointerface Res. Appl. Chem.* **2023**, *13*, 590. [CrossRef]
27. Narayanaswamy, S.; Bhaskar, R.; Jayadevappa, R.K.K.; Ramachandran, S.K.M.; Prasad, M.A. A Comprehensive Review on the Antimicrobial and Photocatalytic Properties of Green Synthesized Silver Nanoparticles. *Lett. Appl. NanoBioSci.* **2023**, *12*, 140. [CrossRef]
28. Abbaszadegan, A.; Ghahramani, Y.; Gholami, A.; Hemmateenejad, B.; Dorostkar, S.; Nabavizadeh, M.; Sharghi, H. The Effect of Charge at the Surface of Silver Nanoparticles on Antimicrobial Activity against Gram-Positive and Gram-Negative Bacteria: A Preliminary Study. *J. Nanomater.* **2015**, *2015*, 720654. [CrossRef]

29. Godoy-Gallardo, M.; Eckhard, U.; Delgado, L.M.; de Roo Puente, Y.J.D.; Hoyos-Nogués, M.; Gil, F.J.; Perez, R.A. Antibacterial approaches in tissue engineering using metal ions and nanoparticles: From mechanisms to applications. *Bioact. Mater.* **2021**, *6*, 4470–4490. [CrossRef]
30. Sadoq, B.E.; Britel, M.R.; Bouajaj, A.; Maâlej, R.; Abid, M.; Douiri, H.; Touhami, F.; Maurady, A.; Touhami, A. A Review on Antibacterial Activity of Nanoparticles. *Biointerface Res. Appl. Chem.* **2023**, *13*, 405. [CrossRef]
31. Zhang, Q.; Hu, Y.; Masterson, C.M.; Jang, W.; Xiao, Z.; Bohloul, A.; Garcia-Rojas, D.; Puppala, H.L.; Bennett, G.; Colvin, V.L. When function is biological: Discerning how silver nanoparticle structure dictates antimicrobial activity. *iScience* **2022**, *25*, 104475. [CrossRef]
32. Lok, C.N.; Ho, C.M.; Chen, R.; He, Q.Y.; Yu, W.Y.; Sun, H.; Tam, P.K.; Chiu, J.F.; Che, C.M. Silver nanoparticles: Partial oxidation and antibacterial activities. *J. Biol. Inorg. Chem.* **2007**, *12*, 527–534. [CrossRef]
33. Xiu, Z.M.; Zhang, Q.B.; Puppala, H.L.; Colvin, V.L.; Alvarez, P.J. Negligible particle-specific antibacterial activity of silver nanoparticles. *Nano Lett.* **2012**, *12*, 4271–4275. [CrossRef]
34. Le Ouay, B.; Stellacci, F. Antibacterial activity of silver nanoparticles: A surface science insight. *Nano Today* **2015**, *10*, 339–354. [CrossRef]
35. Pareek, V.; Gupta, R.; Panwar, J. Do physico-chemical properties of silver nanoparticles decide their interaction with biological media and bactericidal action? A review. *Mater. Sci. Eng. C* **2018**, *90*, 739–749. [CrossRef]
36. AshaRani, P.V.; Low Kah Mun, G.; Hande, M.P.; Valiyaveettil, S. Cytotoxicity and genotoxicity of silver nanoparticles in human cells. *ACS Nano* **2009**, *3*, 279–290. [CrossRef]
37. Ho, C.M.; Yau, S.K.; Lok, C.N.; So, M.H.; Che, C.M. Oxidative dissolution of silver nanoparticles by biologically relevant oxidants: A kinetic and mechanistic study. *Chem. Asian J.* **2010**, *5*, 285–293. [CrossRef] [PubMed]
38. Menichetti, A.; Mavridi-Printezi, A.; Mordini, D.; Montalti, M. Effect of Size, Shape and Surface Functionalization on the Antibacterial Activity of Silver Nanoparticles. *J. Funct. Biomater.* **2023**, *14*, 244. [CrossRef]
39. Raza, M.A.; Kanwal, Z.; Rauf, A.; Sabri, A.N.; Riaz, S.; Naseem, S. Size- and Shape-Dependent Antibacterial Studies of Silver Nanoparticles Synthesized by Wet Chemical Routes. *Nanomaterials* **2016**, *6*, 74. [CrossRef]
40. Wu, Y.; Yang, Y.; Zhang, Z.; Wang, Z.; Zhao, Y.; Sun, L. A facile method to prepare size-tunable silver nanoparticles and its antibacterial mechanism. *Adv. Powder Technol.* **2018**, *29*, 407–415. [CrossRef]
41. Skandalis, N.; Dimopoulou, A.; Georgopoulou, A.; Gallios, N.; Papadopoulos, D.; Tsipas, D.; Theologidis, I.; Michailidis, N.; Chatzinikolaidou, M. The Effect of Silver Nanoparticles Size, Produced Using Plant Extract from Arbutus unedo, on Their Antibacterial Efficacy. *Nanomaterials* **2017**, *7*, 178. [CrossRef]
42. Balu, S.K.; Andra, S.; Damiri, F.; Sivaramalingam, A.; Sudandaradoss, M.V.; Kumarasamy, K.; Bhakthavachalam, K.; Ali, F.; Kundu, M.K.; Rahman, M.H.; et al. Size-Dependent Antibacterial, Antidiabetic, and Toxicity of Silver Nanoparticles Synthesized Using Solvent Extraction of *Rosa indica* L. Petals. *Pharmaceuticals* **2022**, *15*, 689. [CrossRef]
43. Hileuskaya, K.; Ladutska, A.; Kulikouskaya, V.; Kraskouski, A.; Novik, G.; Kozerozhets, I.; Kozlovskiy, A.; Agabekov, V. 'Green' approach for obtaining stable pectin-capped silver nanoparticles: Physico-chemical characterization and antibacterial activity. *Colloids Surf. A Physicochem. Eng. Asp.* **2020**, *585*, 124141. [CrossRef]
44. Ji, H.; Zhou, S.; Fu, Y.; Wang, Y.; Mi, J.; Lu, T.; Wang, X.; Lü, C. Size-controllable preparation and antibacterial mechanism of thermo-responsive copolymer-stabilized silver nanoparticles with high antimicrobial activity. *Mater. Sci. Eng. C Mater. Biol. Appl.* **2020**, *110*, 110735. [CrossRef]
45. Haidari, H.; Bright, R.; Kopecki, Z.; Zilm, P.S.; Garg, S.; Cowin, A.J.; Vasilev, K.; Goswami, N. Polycationic Silver Nanoclusters Comprising Nanoreservoirs of Ag(+) Ions with High Antimicrobial and Antibiofilm Activity. *ACS Appl. Mater. Interfaces* **2022**, *14*, 390–403. [CrossRef] [PubMed]
46. Kittler, S.; Greulich, C.; Diendorf, J.; Köller, M.; Epple, M. Toxicity of Silver Nanoparticles Increases during Storage Because of Slow Dissolution under Release of Silver Ions. *Chem. Mater.* **2010**, *22*, 4548–4554. [CrossRef]
47. Lomelí-Rosales, D.A.; Zamudio-Ojeda, A.; Cortes-Llamas, S.A.; Velázquez-Juárez, G. One-step synthesis of gold and silver non-spherical nanoparticles mediated by Eosin Methylene Blue agar. *Sci. Rep.* **2019**, *9*, 19327. [CrossRef]
48. Titkov, A.I.; Logutenko, O.A.; Bulina, N.V.; Yukhin, Y.M.; Lyakhov, N.Z. Synthesis of nonspherical nanoparticles by reducing silver neodecanoate extract with benzyl alcohol. *Theor. Found. Chem. Eng.* **2017**, *51*, 557–562. [CrossRef]
49. Hong, X.; Wen, J.; Xiong, X.; Hu, Y. Shape effect on the antibacterial activity of silver nanoparticles synthesized via a microwave-assisted method. *Environ. Sci. Pollut. Res. Int.* **2016**, *23*, 4489–4497. [CrossRef]
50. Goyal, D.; Kaur, G.; Tewari, R.; Kumar, R. Correlation of edge truncation with antibacterial activity of plate-like anisotropic silver nanoparticles. *Environ. Sci. Pollut. Res. Int.* **2017**, *24*, 20429–20437. [CrossRef]
51. Seyedpour, S.F.; Arabi Shamsabadi, A.; Khoshhal Salestan, S.; Dadashi Firouzjaei, M.; Sharifian Gh, M.; Rahimpour, A.; Akbari Afkhami, F.; Shirzad Kebria, M.R.; Elliott, M.A.; Tiraferri, A.; et al. Tailoring the Biocidal Activity of Novel Silver-Based Metal Azolate Frameworks. *ACS Sustain. Chem. Eng.* **2020**, *8*, 7588–7599. [CrossRef]

52. Shaikh, S.; Nazam, N.; Rizvi, S.M.D.; Ahmad, K.; Baig, M.H.; Lee, E.J.; Choi, I. Mechanistic Insights into the Antimicrobial Actions of Metallic Nanoparticles and Their Implications for Multidrug Resistance. *Int. J. Mol. Sci.* **2019**, *20*, 2468. [CrossRef]
53. Armentano, I.; Arciola, C.R.; Fortunati, E.; Ferrari, D.; Mattioli, S.; Amoroso, C.F.; Rizzo, J.; Kenny, J.M.; Imbriani, M.; Visai, L. The interaction of bacteria with engineered nanostructured polymeric materials: A review. *Sci. World J.* **2014**, *2014*, 410423. [CrossRef]
54. Jiang, W.; Kim, B.Y.S.; Rutka, J.T.; Chan, W.C.W. Nanoparticle-mediated cellular response is size-dependent. *Nat. Nanotechnol.* **2008**, *3*, 145–150. [CrossRef]
55. Ramalingam, B.; Parandhaman, T.; Das, S.K. Antibacterial Effects of Biosynthesized Silver Nanoparticles on Surface Ultrastructure and Nanomechanical Properties of Gram-Negative Bacteria viz. *Escherichia coli* and *Pseudomonas aeruginosa*. *ACS Appl. Mater. Interfaces* **2016**, *8*, 4963–4976. [CrossRef] [PubMed]
56. Buszewski, B.; Railean-Plugaru, V.; Pomastowski, P.; Rafińska, K.; Szultka-Mlynska, M.; Golinska, P.; Wypij, M.; Laskowski, D.; Dahm, H. Antimicrobial activity of biosilver nanoparticles produced by a novel Streptacidiphilus durhamensis strain. *J. Microbiol. Immunol. Infect.* **2018**, *51*, 45–54. [CrossRef] [PubMed]
57. Biao, L.; Tan, S.; Wang, Y.; Guo, X.; Fu, Y.; Xu, F.; Zu, Y.; Liu, Z. Synthesis, characterization and antibacterial study on the chitosan-functionalized Ag nanoparticles. *Mater. Sci. Eng. C Mater. Biol. Appl.* **2017**, *76*, 73–80. [CrossRef]
58. Huma, Z.E.; Gupta, A.; Javed, I.; Das, R.; Hussain, S.Z.; Mumtaz, S.; Hussain, I.; Rotello, V.M. Cationic Silver Nanoclusters as Potent Antimicrobials against Multidrug-Resistant Bacteria. *ACS Omega* **2018**, *3*, 16721–16727. [CrossRef]
59. Zhao, R.; Lv, M.; Li, Y.; Sun, M.; Kong, W.; Wang, L.; Song, S.; Fan, C.; Jia, L.; Qiu, S.; et al. Stable Nanocomposite Based on PEGylated and Silver Nanoparticles Loaded Graphene Oxide for Long-Term Antibacterial Activity. *ACS Appl. Mater. Interfaces* **2017**, *9*, 15328–15341. [CrossRef] [PubMed]
60. Alsammarraie, F.K.; Wang, W.; Zhou, P.; Mustapha, A.; Lin, M. Green synthesis of silver nanoparticles using turmeric extracts and investigation of their antibacterial activities. *Colloids Surf. B Biointerfaces* **2018**, *171*, 398–405. [CrossRef]
61. Nakamura, S.; Ando, N.; Sato, M.; Ishihara, M. Ultraviolet Irradiation Enhances the Microbicidal Activity of Silver Nanoparticles by Hydroxyl Radicals. *Int. J. Mol. Sci.* **2020**, *21*, 3204. [CrossRef]
62. Quinteros, M.A.; Cano Aristizábal, V.; Dalmasso, P.R.; Paraje, M.G.; Páez, P.L. Oxidative stress generation of silver nanoparticles in three bacterial genera and its relationship with the antimicrobial activity. *Toxicol. Vitr.* **2016**, *36*, 216–223. [CrossRef] [PubMed]
63. Dąbrowska-Bouta, B.; Sulkowski, G.; Strużyński, W.; Strużyńska, L. Prolonged Exposure to Silver Nanoparticles Results in Oxidative Stress in Cerebral Myelin. *Neurotox. Res.* **2019**, *35*, 495–504. [CrossRef]
64. Nallathamby, P.D.; Lee, K.J.; Desai, T.; Xu, X.H. Study of the multidrug membrane transporter of single living *Pseudomonas aeruginosa* cells using size-dependent plasmonic nanoparticle optical probes. *Biochemistry* **2010**, *49*, 5942–5953. [CrossRef]
65. Halder, S.; Yadav, K.K.; Sarkar, R.; Mukherjee, S.; Saha, P.; Haldar, S.; Karmakar, S.; Sen, T. Alteration of Zeta potential and membrane permeability in bacteria: A study with cationic agents. *Springerplus* **2015**, *4*, 672. [CrossRef]
66. Holt, K.B.; Bard, A.J. Interaction of silver(I) ions with the respiratory chain of *Escherichia coli*: An electrochemical and scanning electrochemical microscopy study of the antimicrobial mechanism of micromolar Ag+. *Biochemistry* **2005**, *44*, 13214–13223. [CrossRef]
67. Kaur, P.; Vadehra, D.V. Mechanism of resistance to silver ions in Klebsiella pneumoniae. *Antimicrob. Agents Chemother.* **1986**, *29*, 165–167. [CrossRef] [PubMed]
68. Gordon, O.; Vig Slenters, T.; Brunetto, P.S.; Villaruz, A.E.; Sturdevant, D.E.; Otto, M.; Landmann, R.; Fromm, K.M. Silver coordination polymers for prevention of implant infection: Thiol interaction, impact on respiratory chain enzymes, and hydroxyl radical induction. *Antimicrob. Agents Chemother.* **2010**, *54*, 4208–4218. [CrossRef]
69. Slavin, Y.N.; Asnis, J.; Häfeli, U.O.; Bach, H. Metal nanoparticles: Understanding the mechanisms behind antibacterial activity. *J. Nanobiotechnol.* **2017**, *15*, 65. [CrossRef]
70. Nikaido, H. Porins and specific diffusion channels in bacterial outer membranes. *J. Biol. Chem.* **1994**, *269*, 3905–3908. [CrossRef]
71. Pugsley, A.P.; Schnaitman, C.A. Outer membrane proteins of *Escherichia coli*. VII. Evidence that bacteriophage-directed protein 2 functions as a pore. *J. Bacteriol.* **1978**, *133*, 1181–1189. [CrossRef]
72. Franci, G.; Falanga, A.; Galdiero, S.; Palomba, L.; Rai, M.; Morelli, G.; Galdiero, M. Silver nanoparticles as potential antibacterial agents. *Molecules* **2015**, *20*, 8856–8874. [CrossRef]
73. Li, X.Z.; Nikaido, H.; Williams, K.E. Silver-resistant mutants of *Escherichia coli* display active efflux of Ag+ and are deficient in porins. *J. Bacteriol.* **1997**, *179*, 6127–6132. [CrossRef]
74. Radzig, M.A.; Nadtochenko, V.A.; Koksharova, O.A.; Kiwi, J.; Lipasova, V.A.; Khmel, I.A. Antibacterial effects of silver nanoparticles on gram-negative bacteria: Influence on the growth and biofilms formation, mechanisms of action. *Colloids Surf. B Biointerfaces* **2013**, *102*, 300–306. [CrossRef] [PubMed]
75. Girma, A. Alternative mechanisms of action of metallic nanoparticles to mitigate the global spread of antibiotic-resistant bacteria. *Cell Surf.* **2023**, *10*, 100112. [CrossRef]
76. Mikhailova, E.O. Silver Nanoparticles: Mechanism of Action and Probable Bio-Application. *J. Funct. Biomater.* **2020**, *11*, 84. [CrossRef]

77. Mikhailova, E.O. Green Silver Nanoparticles: An Antibacterial Mechanism. *Antibiotics* **2025**, *14*, 5. [CrossRef]
78. Rai, M.K.; Deshmukh, S.D.; Ingle, A.P.; Gade, A.K. Silver nanoparticles: The powerful nanoweapon against multidrug-resistant bacteria. *J. Appl. Microbiol.* **2012**, *112*, 841–852. [CrossRef] [PubMed]
79. Yamanaka, M.; Hara, K.; Kudo, J. Bactericidal actions of a silver ion solution on *Escherichia coli*, studied by energy-filtering transmission electron microscopy and proteomic analysis. *Appl. Environ. Microbiol.* **2005**, *71*, 7589–7593. [CrossRef]
80. Modi, S.K.; Gaur, S.; Sengupta, M.; Singh, M.S. Mechanistic insights into nanoparticle surface-bacterial membrane interactions in overcoming antibiotic resistance. *Front. Microbiol.* **2023**, *14*, 1135579. [CrossRef]
81. Behdad, R.; Pargol, M.; Mirzaie, A.; Karizi, S.Z.; Noorbazargan, H.; Akbarzadeh, I. Efflux pump inhibitory activity of biologically synthesized silver nanoparticles against multidrug-resistant Acinetobacter baumannii clinical isolates. *J. Basic Microbiol.* **2020**, *60*, 494–507. [CrossRef]
82. Abdolhosseini, M.; Zamani, H.; Salehzadeh, A. Synergistic antimicrobial potential of ciprofloxacin with silver nanoparticles conjugated to thiosemicarbazide against ciprofloxacin resistant *Pseudomonas aeruginosa* by attenuation of MexA-B efflux pump genes. *Biologia* **2019**, *74*, 1191–1196. [CrossRef]
83. Madhi, M.; Hasani, A.; Mojarrad, J.S.; Rezaee, M.A.; Zarrini, G.; Davaran, S.; Alizadeh, E.; Sheikhalizadeh, V. Impact of chitosan and silver nanoparticles laden with antibiotics on multidrug-resistant *Pseudomonas aeruginosa* and *Acinetobacter baumannii*. *Arch. Clin. Infect. Dis.* **2020**, *15*, e100195. [CrossRef]
84. Sadat Shandiz, S.A.; Montazeri, A.; Abdolhosseini, M.; Hadad Shahrestani, S.; Hedayati, M.; Moradi-Shoeili, Z.; Salehzadeh, A. Functionalization of Ag Nanoparticles by Glutamic Acid and Conjugation of Ag@Glu by Thiosemicarbazide Enhances the Apoptosis of Human Breast Cancer MCF-7 Cells. *J. Clust. Sci.* **2018**, *29*, 1107–1114. [CrossRef]
85. Dedon, P.C.; Plastaras, J.P.; Rouzer, C.A.; Marnett, L.J. Indirect mutagenesis by oxidative DNA damage: Formation of the pyrimidopurinone adduct of deoxyguanosine by base propenal. *Proc. Natl. Acad. Sci. USA* **1998**, *95*, 11113–11116. [CrossRef]
86. Juan, C.A.; Pérez de la Lastra, J.M.; Plou, F.J.; Pérez-Lebeña, E. The Chemistry of Reactive Oxygen Species (ROS) Revisited: Outlining Their Role in Biological Macromolecules (DNA, Lipids and Proteins) and Induced Pathologies. *Int. J. Mol. Sci.* **2021**, *22*, 4642. [CrossRef]
87. Valavanidis, A.; Vlachogianni, T.; Fiotakis, C. 8-hydroxy-2′ -deoxyguanosine (8-OHdG): A critical biomarker of oxidative stress and carcinogenesis. *J. Environ. Sci. Health C Environ. Carcinog. Ecotoxicol. Rev.* **2009**, *27*, 120–139. [CrossRef]
88. Rodríguez-García, A.; García-Vicente, R.; Morales, M.L.; Ortiz-Ruiz, A.; Martínez-López, J.; Linares, M. Protein Carbonylation and Lipid Peroxidation in Hematological Malignancies. *Antioxidants* **2020**, *9*, 1212. [CrossRef] [PubMed]
89. Qian, H.; Zhu, K.; Lu, H.; Lavoie, M.; Chen, S.; Zhou, Z.; Deng, Z.; Chen, J.; Fu, Z. Contrasting silver nanoparticle toxicity and detoxification strategies in Microcystis aeruginosa and Chlorella vulgaris: New insights from proteomic and physiological analyses. *Sci. Total Environ.* **2016**, *572*, 1213–1221. [CrossRef]
90. Nallanthighal, S.; Chan, C.; Murray, T.M.; Mosier, A.P.; Cady, N.C.; Reliene, R. Differential effects of silver nanoparticles on DNA damage and DNA repair gene expression in Ogg1-deficient and wild type mice. *Nanotoxicology* **2017**, *11*, 996–1011. [CrossRef]
91. Xu, L.; Wang, Y.Y.; Huang, J.; Chen, C.Y.; Wang, Z.X.; Xie, H. Silver nanoparticles: Synthesis, medical applications and biosafety. *Theranostics* **2020**, *10*, 8996–9031. [CrossRef] [PubMed]
92. Feng, Q.L.; Wu, J.; Chen, G.Q.; Cui, F.Z.; Kim, T.N.; Kim, J.O. A mechanistic study of the antibacterial effect of silver ions on *Escherichia coli* and *Staphylococcus aureus*. *J. Biomed. Mater. Res.* **2000**, *52*, 662–668. [CrossRef]
93. Ishida, T. Anticancer activities of silver ions in cancer and tumor cells and DNA damages by Ag+-DNA base-pairs reactions. *MOJ Tumor Res.* **2017**, *1*, 8–16.
94. Balaure, P.C.; Grumezescu, A.M. Recent Advances in Surface Nanoengineering for Biofilm Prevention and Control. Part II: Active, Combined Active and Passive, and Smart Bacteria-Responsive Antibiofilm Nanocoatings. *Nanomaterials* **2020**, *10*, 1527. [CrossRef]
95. Agarwal, H.; Gurnani, B.; Pippal, B.; Jain, N. Capturing the micro-communities: Insights into biogenesis and architecture of bacterial biofilms. *BBA Adv.* **2025**, *7*, 100133. [CrossRef]
96. Seebach, E.; Elschner, T.; Kraus, F.V.; Souto-Carneiro, M.; Kubatzky, K.F. Bacterial and Metabolic Factors of Staphylococcal Planktonic and Biofilm Environments Differentially Regulate Macrophage Immune Activation. *Inflammation* **2023**, *46*, 1512–1530. [CrossRef] [PubMed]
97. Rather, M.A.; Gupta, K.; Mandal, M. Microbial biofilm: Formation, architecture, antibiotic resistance, and control strategies. *Braz. J. Microbiol.* **2021**, *52*, 1701–1718. [CrossRef]
98. Tian, H.; Liao, Q.; Liu, M.; Hou, J.; Zhang, Y.; Liu, J. Antibacterial activity of silver nanoparticles target sara through srna-teg49, a key mediator of hfq, in *Staphylococcus aureus*. *Int. J. Clin. Exp. Med.* **2015**, *8*, 5794–5799.
99. Joshi, A.S.; Singh, P.; Mijakovic, I. Interactions of Gold and Silver Nanoparticles with Bacterial Biofilms: Molecular Interactions behind Inhibition and Resistance. *Int. J. Mol. Sci.* **2020**, *21*, 7658. [CrossRef]
100. Fröhlich, K.S.; Gottesman, S. Small Regulatory RNAs in the Enterobacterial Response to Envelope Damage and Oxidative Stress. In *Regulating with RNA in Bacteria and Archaea*; Storz, G., Papenfort, K., Eds.; John Wiley & Sons, Inc.: Hoboken, NJ, USA, 2018; pp. 211–228.

101. Ren, J.; Nong, N.T.; Lam Vo, P.N.; Lee, H.M.; Na, D. Rational Design of High-Efficiency Synthetic Small Regulatory RNAs and Their Application in Robust Genetic Circuit Performance Through Tight Control of Leaky Gene Expression. *ACS Synth. Biol.* **2024**, *13*, 3256–3267. [CrossRef]
102. González-Fernández, S.; Blanco-Agudín, N.; Rodríguez, D.; Fernández-Vega, I.; Merayo-Lloves, J.; Quirós, L.M. Silver Nanoparticles: A Versatile Tool Against Infectious and Non-Infectious Diseases. *Antibiotics* **2025**, *14*, 289. [CrossRef]
103. Cress, B.F.; Englaender, J.A.; He, W.; Kasper, D.; Linhardt, R.J.; Koffas, M.A. Masquerading microbial pathogens: Capsular polysaccharides mimic host-tissue molecules. *FEMS Microbiol. Rev.* **2014**, *38*, 660–697. [CrossRef]
104. Kohanski, M.A.; Dwyer, D.J.; Collins, J.J. How antibiotics kill bacteria: From targets to networks. *Nat. Rev. Microbiol.* **2010**, *8*, 423–435. [CrossRef]
105. Guan, J.; Wang, J.; Zhang, X.; Chi, J.; Ma, Z.; Zhang, X. Silver nanoparticles with multimodal biological activities integrated into advanced material platforms for chronic wound management. *Nanoscale* **2025**, *17*, 18409–18445. [CrossRef] [PubMed]
106. Carvalho-Silva, J.M.; Reis, A.C.D. Anti-inflammatory action of silver nanoparticles in vivo: Systematic review and meta-analysis. *Heliyon* **2024**, *10*, e34564. [CrossRef]
107. Jalil, K.; Ahmad, S.; Islam, N.u.; Muhammad, S.; Jalil, Q.; Ali, A. Excellent antibacterial and anti-inflammatory efficacy of amoxicillin by AgNPs and their conjugates synthesized using *Micromeria biflora* crude flavonoid extracts. *Heliyon* **2024**, *10*, e36752. [CrossRef]
108. Moldovan, B.; David, L.; Vulcu, A.; Olenic, L.; Perde-Schrepler, M.; Fischer-Fodor, E.; Baldea, I.; Clichici, S.; Filip, G.A. In vitro and in vivo anti-inflammatory properties of green synthesized silver nanoparticles using *Viburnum opulus* L. fruits extract. *Mater. Sci. Eng. C Mater. Biol. Appl.* **2017**, *79*, 720–727. [CrossRef]
109. Singh, P.; Ahn, S.; Kang, J.P.; Veronika, S.; Huo, Y.; Singh, H.; Chokkaligam, M.; El-Agamy Farh, M.; Aceituno, V.C.; Kim, Y.J.; et al. In vitro anti-inflammatory activity of spherical silver nanoparticles and monodisperse hexagonal gold nanoparticles by fruit extract of Prunus serrulata: A green synthetic approach. *Artif. Cells Nanomed. Biotechnol.* **2018**, *46*, 2022–2032. [CrossRef] [PubMed]
110. Crisan, D.; Scharffetter-Kochanek, K.; Crisan, M.; Schatz, S.; Hainzl, A.; Olenic, L.; Filip, A.; Schneider, L.A.; Sindrilaru, A. Topical silver and gold nanoparticles complexed with Cornus mas suppress inflammation in human psoriasis plaques by inhibiting NF-κB activity. *Exp. Dermatol.* **2018**, *27*, 1166–1169. [CrossRef] [PubMed]
111. You, C.; Zhu, Z.; Wang, S.; Wang, X.; Han, C.; Shao, H. Nanosilver alleviates foreign body reaction and facilitates wound repair by regulating macrophage polarization. *J. Zhejiang Univ. Sci. B* **2023**, *24*, 510–523. [CrossRef] [PubMed]
112. Chen, Y.; Guan, M.; Ren, R.; Gao, C.; Cheng, H.; Li, Y.; Gao, B.; Wei, Y.; Fu, J.; Sun, J. Improved immunoregulation of ultra-low-dose silver nanoparticle-loaded TiO_2 nanotubes via M2 macrophage polarization by regulating GLUT1 and autophagy. *Int. J. Nanomed.* **2020**, *15*, 2011–2026. [CrossRef]
113. Du, J.; Liu, X.; Wong, C.W.Y.; Lok, C.N.; Yang, Z.; Yuan, Z.; Wong, K.K.Y. Silver nanoparticles promote osteogenic differentiation of mouse embryonic fibroblasts in vitro. *Am. J. Stem Cells* **2023**, *12*, 51–59. [PubMed]
114. Xu, Y.; Zheng, B.; He, J.; Cui, Z.; Liu, Y. Silver nanoparticles promote osteogenic differentiation of human periodontal ligament fibroblasts by regulating the RhoA-TAZ axis. *Cell Biol. Int.* **2019**, *43*, 910–920. [CrossRef] [PubMed]
115. Long, L.Y.; Hu, C.; Liu, W.; Wu, C.; Lu, L.; Yang, L.; Wang, Y.B. Microfibrillated cellulose-enhanced carboxymethyl chitosan/oxidized starch sponge for chronic diabetic wound repair. *Mater. Sci. Eng. C Mater. Biol. Appl.* **2022**, *135*, 112669. [CrossRef] [PubMed]
116. Gaikwad, S.; Birla, S.; Ingle, A.P.; Gade, A.; Ingle, P.; Golińska, P.; Rai, M. Superior in vivo Wound-Healing Activity of Mycosynthesized Silver Nanogel on Different Wound Models in Rat. *Front. Microbiol.* **2022**, *13*, 881404. [CrossRef]
117. Liu, X.; Lee, P.Y.; Ho, C.M.; Lui, V.C.; Chen, Y.; Che, C.M.; Tam, P.K.; Wong, K.K. Silver nanoparticles mediate differential responses in keratinocytes and fibroblasts during skin wound healing. *ChemMedChem* **2010**, *5*, 468–475. [CrossRef]
118. Zhang, S.; He, T.; Zhao, F.; Tan, Q.; Li, D.; Wang, Q.; Xiao, Y.; Zhang, X. Development of a multifunctional nano-hydroxyapatite platform (nHEA) for advanced treatment of severely infected full-thickness skin wounds. *Acta Biomater.* **2024**, *181*, 440–452. [CrossRef]
119. Mensah, R.A.; Trotta, F.; Briggs, E.; Sharifulden, N.S.; Silva, L.V.B.; Keskin-Erdogan, Z.; Diop, S.; Kureshi, A.K.; Chau, D.Y.S. A Sustainable, Green-Processed, Ag-Nanoparticle-Incorporated Eggshell-Derived Biomaterial for Wound-Healing Applications. *J. Funct. Biomater.* **2023**, *14*, 450. [CrossRef]
120. Sabarees, G.; Velmurugan, V.; Tamilarasi, G.P.; Alagarsamy, V.; Raja Solomon, V. Recent Advances in Silver Nanoparticles Containing Nanofibers for Chronic Wound Management. *Polymers* **2022**, *14*, 3994. [CrossRef]
121. Krishnan, N.; Velramar, B.; Ramatchandirin, B.; Abraham, G.C.; Duraisamy, N.; Pandiyan, R.; Velu, R.K. Effect of biogenic silver nanocubes on matrix metalloproteinases 2 and 9 expressions in hyperglycemic skin injury and its impact in early wound healing in streptozotocin-induced diabetic mice. *Mater. Sci. Eng. C Mater. Biol. Appl.* **2018**, *91*, 146–152. [CrossRef]
122. Seo, S.B.; Dananjaya, S.H.S.; Nikapitiya, C.; Park, B.K.; Gooneratne, R.; Kim, T.Y.; Lee, J.; Kim, C.H.; De Zoysa, M. Silver nanoparticles enhance wound healing in zebrafish (*Danio rerio*). *Fish. Shellfish Immunol.* **2017**, *68*, 536–545. [CrossRef]

123. Xue, H.; Zhu, C.; Wang, Y.; Gu, Q.; Shao, Y.; Jin, A.; Zhang, X.; Lei, L.; Li, Y. Stimulus-responsive cellulose hydrogels in biomedical applications and challenges. *Mater. Today Bio* **2025**, *32*, 101814. [CrossRef]
124. Raho, R.; Nguyen, N.Y.; Zhang, N.; Jiang, W.; Sannino, A.; Liu, H.; Pollini, M.; Paladini, F. Photo-assisted green synthesis of silver doped silk fibroin/carboxymethyl cellulose nanocomposite hydrogels for biomedical applications. *Mater. Sci. Eng. C Mater. Biol. Appl.* **2020**, *107*, 110219. [CrossRef]
125. Satheeshkumar, E.; Yang, J. Analyte-induced photoreduction method for visual and colorimetric detection of tyrosine. *Anal. Chim. Acta* **2015**, *879*, 111–117. [CrossRef]
126. Maddinedi, S.B.; Mandal, B.K.; Anna, K.K. Tyrosine assisted size controlled synthesis of silver nanoparticles and their catalytic, in-vitro cytotoxicity evaluation. *Environ. Toxicol. Pharmacol.* **2017**, *51*, 23–29. [CrossRef]
127. Ruffo, M.; Parisi, O.I.; Dattilo, M.; Patitucci, F.; Malivindi, R.; Pezzi, V.; Tzanov, T.; Puoci, F. Synthesis and evaluation of wound healing properties of hydro-diab hydrogel loaded with green-synthetized AGNPS: In vitro and in ex vivo studies. *Drug Deliv. Transl. Res.* **2022**, *12*, 1881–1894. [CrossRef] [PubMed]
128. Chen, S.; Yao, J.; Huo, S.; Xu, C.; Yang, R.; Tao, D.; Fang, B.; Ma, G.; Zhu, Z.; Zhang, Y.; et al. Designing injectable dermal matrix hydrogel combined with silver nanoparticles for methicillin-resistant *Staphylococcus aureus* infected wounds healing. *Nano Converg.* **2024**, *11*, 41. [CrossRef] [PubMed]
129. Sharifiaghdam, M.; Shaabani, E.; Faridi-Majidi, R.; De Smedt, S.C.; Braeckmans, K.; Fraire, J.C. Macrophages as a therapeutic target to promote diabetic wound healing. *Mol. Ther.* **2022**, *30*, 2891–2908. [CrossRef] [PubMed]
130. Zhou, C.; Jiang, T.; Liu, S.; He, Y.; Yang, G.; Nie, J.; Wang, F.; Yang, X.; Chen, Z.; Lu, C. AgNPs loaded adenine-modified chitosan composite POSS-PEG hybrid hydrogel with enhanced antibacterial and cell proliferation properties for promotion of infected wound healing. *Int. J. Biol. Macromol.* **2024**, *267*, 131575. [CrossRef]
131. Li, C.; Jiang, T.; Zhou, C.; Jiang, A.; Lu, C.; Yang, G.; Nie, J.; Wang, F.; Yang, X.; Chen, Z. Injectable self-healing chitosan-based POSS-PEG hybrid hydrogel as wound dressing to promote diabetic wound healing. *Carbohydr. Polym.* **2023**, *299*, 120198. [CrossRef]
132. Iranpour Mobarakeh, A.; Shahmoradi Ramsheh, A.; Khanshan, A.; Aghaei, S.; Mirbagheri, M.S.; Esmaeili, J. Fabrication and evaluation of a bi-layered electrospun PCL/PVA patch for wound healing: Release of vitamins and silver nanoparticle. *Heliyon* **2024**, *10*, e33178. [CrossRef]
133. Bayram Sarıipek, F. Biopolymeric nanofibrous scaffolds of poly(3-hydroxybuthyrate)/chitosan loaded with biogenic silver nanoparticle synthesized using curcumin and their antibacterial activities. *Int. J. Biol. Macromol.* **2024**, *256*, 128330. [CrossRef]
134. Liu, W.; Thomopoulos, S.; Xia, Y. Electrospun nanofibers for regenerative medicine. *Adv. Healthc. Mater.* **2012**, *1*, 10–25. [CrossRef]
135. Chen, S.; Liu, B.; Carlson, M.A.; Gombart, A.F.; Reilly, D.A.; Xie, J. Recent advances in electrospun nanofibers for wound healing. *Nanomedicine* **2017**, *12*, 1335–1352. [CrossRef]
136. Zhang, S.; Yang, W.; Gong, W.; Lu, Y.; Yu, D.G.; Liu, P. Recent progress of electrospun nanofibers as burning dressings. *RSC Adv.* **2024**, *14*, 14374–14391. [CrossRef] [PubMed]
137. Zhao, J.; Chen, L.; Ma, A.; Bai, X.; Zeng, Y.; Liu, D.; Liu, B.; Zhang, W.; Tang, S. Recent advances in coaxial electrospun nanofibers for wound healing. *Mater. Today Bio* **2024**, *29*, 101309. [CrossRef]
138. Lucian, B.I.; Cheregi, C.D.; Sebastian, H.M.; Ruxandra-Florina, B.; Maghiar, L.; Ilarie, B.; Anca, H.; Sachelarie, L.; Mircea-Ioan, S. Electrospun Nanofibers in Wound Healing: Real-World Evaluation of Spincare™ Technology. *Bioengineering* **2025**, *12*, 500. [CrossRef]
139. Yadav, P.D.; Londhe, P.V.; Chavan, S.S.; Mohite, D.D.; Firame, G.B.; Kadam, S.S.; Patil, M.J.; Ansari, M.I. Electrospun composite nanofibers for wound healing: Synthesis, characterization, and clinical potential of biopolymer-based materials. *Discov. Mater.* **2024**, *4*, 99. [CrossRef]
140. Ambekar, R.S.; Kandasubramanian, B. Advancements in nanofibers for wound dressing: A review. *Eur. Polym. J.* **2019**, *117*, 304–336. [CrossRef]
141. Liu, C.; Zhu, Y.; Lun, X.; Sheng, H.; Yan, A. Effects of wound dressing based on the combination of silver@curcumin nanoparticles and electrospun chitosan nanofibers on wound healing. *Bioengineered* **2022**, *13*, 4328–4339. [CrossRef]
142. Yang, J.; Wang, K.; Yu, D.G.; Yang, Y.; Bligh, S.W.A.; Williams, G.R. Electrospun Janus nanofibers loaded with a drug and inorganic nanoparticles as an effective antibacterial wound dressing. *Mater. Sci. Eng. C Mater. Biol. Appl.* **2020**, *111*, 110805. [CrossRef]
143. Kim, J.; Abu Al-Rub, R.K.; Han, S.M. High-resilience conductive PVA+AgNW/PDMS nanocomposite via directional freeze-drying. *Extrem. Mech. Lett.* **2024**, *68*, 102132. [CrossRef]
144. Wu, Y.; Wang, Z.; Xu, L.; Wang, H.; Peng, S.; Zheng, L.; Yang, Z.; Wu, L.; Miao, J.-T. Preparation of silver-plated carbon nanotubes/carbon fiber hybrid fibers by combining freeze-drying deposition with a sizing process to enhance the mechanical properties of carbon fiber composites. *Compos. Part A Appl. Sci. Manuf.* **2021**, *146*, 106421. [CrossRef]
145. Lu, B.; Lu, F.; Zou, Y.; Liu, J.; Rong, B.; Li, Z.; Dai, F.; Wu, D.; Lan, G. In situ reduction of silver nanoparticles by chitosan-l-glutamic acid/hyaluronic acid: Enhancing antimicrobial and wound-healing activity. *Carbohydr. Polym.* **2017**, *173*, 556–565. [CrossRef] [PubMed]

146. Zhou, L.; Zhao, X.; Li, M.; Yan, L.; Lu, Y.; Jiang, C.; Liu, Y.; Pan, Z.; Shi, J. Antibacterial and wound healing-promoting effect of sponge-like chitosan-loaded silver nanoparticles biosynthesized by iturin. *Int. J. Biol. Macromol.* **2021**, *181*, 1183–1195. [CrossRef]
147. Zhao, X.; Wang, K.; Ai, C.; Yan, L.; Jiang, C.; Shi, J. Improvement of antifungal and antibacterial activities of food packages using silver nanoparticles synthesized by iturin A. *Food Packag. Shelf Life* **2021**, *28*, 100669. [CrossRef]
148. Liang, D.; Lu, Z.; Yang, H.; Gao, J.; Chen, R. Novel Asymmetric Wettable AgNPs/Chitosan Wound Dressing: In Vitro and In Vivo Evaluation. *ACS Appl. Mater. Interfaces* **2016**, *8*, 3958–3968. [CrossRef]
149. Dong, Q.; Liang, X.; Chen, F.; Ke, M.; Yang, X.; Ai, J.; Cheng, Q.; Zhou, Y.; Chen, Y. Injectable shape memory hydroxyethyl cellulose/soy protein isolate based composite sponge with antibacterial property for rapid noncompressible hemorrhage and prevention of wound infection. *Int. J. Biol. Macromol.* **2022**, *217*, 367–380. [CrossRef]
150. Zhao, Y.; Li, Y.; Du, Q.; Zhang, Q.; Lv, X.; Yang, Q.; Chang, P.R.; Anderson, D.P.; He, M.; Chen, Y. Shape memory histocompatible and biodegradable sponges for subcutaneous defect filling and repair: Greatly reducing surgical incision. *J. Mater. Chem. B* **2019**, *7*, 5848–5860. [CrossRef]
151. Zhao, Y.; He, M.; Jin, H.; Zhao, L.; Du, Q.; Deng, H.; Tian, W.; Li, Y.; Lv, X.; Chen, Y. Construction of highly biocompatible hydroxyethyl cellulose/soy protein isolate composite sponges for tissue engineering. *Chem. Eng. J.* **2018**, *341*, 402–413. [CrossRef]
152. Ottaviano, L.; Buoso, S.; Zamboni, R.; Sotgiu, G.; Posati, T. Natural Protein Films from Textile Waste for Wound Healing and Wound Dressing Applications. *J. Funct. Biomater.* **2025**, *16*, 20. [CrossRef]
153. Benkhira, I.; Zermane, F.; Cheknane, B.; Trache, D.; Brosse, N.; Paolone, A.; Chader, H.; Sobhi, W. Preparation and characterization of amidated pectin-gelatin-oxidized tannic acid hydrogel films supplemented with in-situ reduced silver nanoparticles for wound-dressing applications. *Int. J. Biol. Macromol.* **2024**, *277*, 134158. [CrossRef] [PubMed]
154. Li, X.; Pang, L.; Duan, J.; Huang, N.; Chen, X.; Huang, W.; Liu, Y.; Fu, C.; Zhang, C.; Tu, H.; et al. Eco-friendly antibacterial electrospinning nanofibrous film containing nano-silver green-synthesized by natural glycoprotein for infected wound healing. *J. Colloid Interface Sci.* **2025**, *683*, 256–268. [CrossRef] [PubMed]
155. Pang, L.; Liao, Q.; Zou, L.; Zhang, C.; Nie, X.; Yi, Z.; Fu, C.; Zhang, J. Two glycoproteins from medicinal insect *Periplaneta americana* (L.) promote diabetic wound healing via macrophage polarization modulation. *Int. J. Biol. Macromol.* **2022**, *209*, 2130–2141. [CrossRef] [PubMed]
156. Gollapudi, K.K.; Dutta, S.D.; Adnan, M.; Taylor, M.L.; Reddy, K.V.N.S.; Alle, M.; Huang, X. Dialdehyde cellulose nanofibrils/polyquaternium stabilized ultra-fine silver nanoparticles for synergistic antibacterial therapy. *Int. J. Biol. Macromol.* **2024**, *280*, 135971. [CrossRef] [PubMed]
157. Jia, X.; Dou, Z.; Zhang, Y.; Li, F.; Xing, B.; Hu, Z.; Li, X.; Liu, Z.; Yang, W.; Liu, Z. Smart Responsive and Controlled-Release Hydrogels for Chronic Wound Treatment. *Pharmaceutics* **2023**, *15*, 2735. [CrossRef]
158. Fauzian, F.; Garmana, A.N.; Mauludin, R. Applications of Nanotechnology-Based Drug Delivery System for Delivering Natural Products into Acute and Chronic Wounds: A Review. *Biointerface Res. Appl. Chem.* **2023**, *13*, 426. [CrossRef]
159. Hu, C.; Long, L.; Cao, J.; Zhang, S.; Wang, Y. Dual-crosslinked mussel-inspired smart hydrogels with enhanced antibacterial and angiogenic properties for chronic infected diabetic wound treatment via pH-responsive quick cargo release. *Chem. Eng. J.* **2021**, *411*, 128564. [CrossRef]
160. Hu, C.; Zhang, F.; Kong, Q.; Lu, Y.; Zhang, B.; Wu, C.; Luo, R.; Wang, Y. Synergistic Chemical and Photodynamic Antimicrobial Therapy for Enhanced Wound Healing Mediated by Multifunctional Light-Responsive Nanoparticles. *Biomacromolecules* **2019**, *20*, 4581–4592. [CrossRef]
161. Della Vecchia, N.F.; Avolio, R.; Alfè, M.; Errico, M.E.; Napolitano, A.; d'Ischia, M. Building-Block Diversity in Polydopamine Underpins a Multifunctional Eumelanin-Type Platform Tunable Through a Quinone Control Point. *Adv. Funct. Mater.* **2013**, *23*, 1331–1340. [CrossRef]
162. Burzio, L.A.; Waite, J.H. Cross-linking in adhesive quinoproteins: Studies with model decapeptides. *Biochemistry* **2000**, *39*, 11147–11153. [CrossRef]
163. Haidari, H.; Kopecki, Z.; Sutton, A.T.; Garg, S.; Cowin, A.J.; Vasilev, K. pH-Responsive "Smart" Hydrogel for Controlled Delivery of Silver Nanoparticles to Infected Wounds. *Antibiotics* **2021**, *10*, 49. [CrossRef]
164. Qi, X.; Huang, Y.; You, S.; Xiang, Y.; Cai, E.; Mao, R.; Pan, W.; Tong, X.; Dong, W.; Ye, F.; et al. Engineering Robust Ag-Decorated Polydopamine Nano-Photothermal Platforms to Combat Bacterial Infection and Prompt Wound Healing. *Adv. Sci.* **2022**, *9*, e2106015. [CrossRef]
165. Abdali, Z.; Yeganeh, H.; Solouk, A.; Gharibi, R.; Sorayya, M. Thermoresponsive antimicrobial wound dressings via simultaneous thiol-ene polymerization and in situ generation of silver nanoparticles. *RSC Adv.* **2015**, *5*, 66024–66036. [CrossRef]
166. Wu, M.; Liu, M.; Feng, G.; Jia, R.; Chen, R.; Li, Y.; Yan, G.; Qiu, Z.J. NIR-triggered temperature-sensitive polydopamine nanosystem with rapid phase transition for on-demand release to enhance antibacterial and antibiofilm performance. *Colloids Surf. B Biointerfaces* **2025**, *255*, 114901. [CrossRef]

167. Chen, Y.; Xing, Y.; Han, J.; Liu, S.; Xiang, X.; Shen, J.; Du, X.; Ma, X. Multifunctional MMP9-responsive silicasomes-GelMA hydrogels with bacteria-targeting capability and tissue restoration function for chronic wound infection. *Chem. Eng. J.* **2023**, *475*, 146246. [CrossRef]
168. Michalicha, A.; Belcarz, A.; Giannakoudakis, D.A.; Staniszewska, M.; Barczak, M. Designing Composite Stimuli-Responsive Hydrogels for Wound Healing Applications: The State-of-the-Art and Recent Discoveries. *Materials* **2024**, *17*, 278. [CrossRef]
169. Wang, X.; Huang, J.; Zhao, J.; Peng, L.; Qi, L.; Wu, T.; He, J.; Gao, Y.; Zhou, Y. Dual stimuli-responsive and self-healing hyaluronic acid-based nanocomposite hydrogels for promoting wound healing of methicillin-resistant *Staphylococcus aureus* infection. *Int. J. Biol. Macromol.* **2025**, *320*, 145829. [CrossRef] [PubMed]
170. Srikhao, N.; Theerakulpisut, S.; Chindaprasirt, P.; Okhawilai, M.; Narain, R.; Kasemsiri, P. Green synthesis of nano silver-embedded carboxymethyl starch waste/poly vinyl alcohol hydrogel with photothermal sterilization and pH-responsive behavior. *Int. J. Biol. Macromol.* **2023**, *242*, 125118. [CrossRef] [PubMed]
171. Li, N.; Yang, X.; Liu, W.; Xi, G.; Wang, M.; Liang, B.; Ma, Z.; Feng, Y.; Chen, H.; Shi, C. Tannic Acid Cross-linked Polysaccharide-Based Multifunctional Hemostatic Microparticles for the Regulation of Rapid Wound Healing. *Macromol. Biosci.* **2018**, *18*, e1800209. [CrossRef]
172. Orlowski, P.; Zmigrodzka, M.; Tomaszewska, E.; Ranoszek-Soliwoda, K.; Czupryn, M.; Antos-Bielska, M.; Szemraj, J.; Celichowski, G.; Grobelny, J.; Krzyzowska, M. Tannic acid-modified silver nanoparticles for wound healing: The importance of size. *Int. J. Nanomed.* **2018**, *13*, 991–1007. [CrossRef]
173. Cao, C.; Yang, N.; Zhao, Y.; Yang, D.; Hu, Y.; Yang, D.; Song, X.; Wang, W.; Dong, X. Biodegradable hydrogel with thermo-response and hemostatic effect for photothermal enhanced anti-infective therapy. *Nano Today* **2021**, *39*, 101165. [CrossRef]
174. Liu, Y.; Li, F.; Guo, Z.; Xiao, Y.; Zhang, Y.; Sun, X.; Zhe, T.; Cao, Y.; Wang, L.; Lu, Q.; et al. Silver nanoparticle-embedded hydrogel as a photothermal platform for combating bacterial infections. *Chem. Eng. J.* **2020**, *382*, 122990. [CrossRef]
175. Melo, R.M.; Albuquerque, G.M.; Monte, J.P.; Pereira, G.A.L.; Pereira, G. Recent Advances in the Application of Silver Nanoparticles for Enhancing Phototherapy Outcomes. *Pharmaceuticals* **2025**, *18*, 970. [CrossRef]
176. Du, T.; Xiao, Z.; Cao, J.; Wei, L.; Li, C.; Jiao, J.; Song, Z.; Liu, J.; Du, X.; Wang, S. NIR-activated multi-hit therapeutic Ag(2)S quantum dot-based hydrogel for healing of bacteria-infected wounds. *Acta Biomater.* **2022**, *145*, 88–105. [CrossRef]
177. Shi, W.; Kong, Y.; Su, Y.; Kuss, M.A.; Jiang, X.; Li, X.; Xie, J.; Duan, B. Tannic acid-inspired, self-healing, and dual stimuli responsive dynamic hydrogel with potent antibacterial and anti-oxidative properties. *J. Mater. Chem. B* **2021**, *9*, 7182–7195. [CrossRef]
178. Terriac, L.; Helesbeux, J.-J.; Maugars, Y.; Guicheux, J.; Tibbitt, M.W.; Delplace, V. Boronate Ester Hydrogels for Biomedical Applications: Challenges and Opportunities. *Chem. Mater.* **2024**, *36*, 6674–6695. [CrossRef]
179. Deng, C.C.; Brooks, W.L.A.; Abboud, K.A.; Sumerlin, B.S. Boronic Acid-Based Hydrogels Undergo Self-Healing at Neutral and Acidic pH. *ACS Macro Lett.* **2015**, *4*, 220–224. [CrossRef] [PubMed]
180. Haidari, H.; Vasilev, K.; Cowin, A.J.; Kopecki, Z. Bacteria-Activated Dual pH- and Temperature-Responsive Hydrogel for Targeted Elimination of Infection and Improved Wound Healing. *ACS Appl. Mater. Interfaces* **2022**, *14*, 51744–51762. [CrossRef] [PubMed]
181. Khadem, E.; Kharaziha, M.; Salehi, S. Colorimetric pH-responsive and hemostatic hydrogel-based bioadhesives containing functionalized silver nanoparticles. *Mater. Today Bio* **2023**, *20*, 100650. [CrossRef]
182. Khadem, E.; Kharaziha, M. Red cabbage anthocyanin- functionalized tannic acid-silver nanoparticles with pH sensitivity and antibacterial properties. *Mater. Chem. Phys.* **2022**, *291*, 126689. [CrossRef]
183. Edwards-Jones, V. Silver nanoparticles: An overview of scientific toxicity and safety data and introduction of a new dressing, Venus Ag. *Wounds UK* **2022**, *18*, 22.
184. Kumar, S.S.D.; Rajendran, N.K.; Houreld, N.N.; Abrahamse, H. Recent advances on silver nanoparticle and biopolymer-based biomaterials for wound healing applications. *Int. J. Biol. Macromol.* **2018**, *115*, 165–175. [CrossRef]
185. Xu, M.; Qi, Y.; Liu, G.; Song, Y.; Jiang, X.; Du, B. Size-Dependent In Vivo Transport of Nanoparticles: Implications for Delivery, Targeting, and Clearance. *ACS Nano* **2023**, *17*, 20825–20849. [CrossRef] [PubMed]
186. Panja, P.; Jana, N.R. Arginine-Terminated Nanoparticles of <10 nm Size for Direct Membrane Penetration and Protein Delivery for Straight Access to Cytosol and Nucleus. *J. Phys. Chem. Lett.* **2020**, *11*, 2363–2368. [CrossRef] [PubMed]
187. Walker, M.; Parsons, D. The biological fate of silver ions following the use of silver-containing wound care products—A review. *Int. Wound J.* **2014**, *11*, 496–504. [CrossRef]
188. Schleh, C.; Semmler-Behnke, M.; Lipka, J.; Wenk, A.; Hirn, S.; Schäffler, M.; Schmid, G.; Simon, U.; Kreyling, W.G. Size and surface charge of gold nanoparticles determine absorption across intestinal barriers and accumulation in secondary target organs after oral administration. *Nanotoxicology* **2012**, *6*, 36–46. [CrossRef]
189. Trickler, W.J.; Lantz, S.M.; Murdock, R.C.; Schrand, A.M.; Robinson, B.L.; Newport, G.D.; Schlager, J.J.; Oldenburg, S.J.; Paule, M.G.; Slikker, W., Jr.; et al. Silver nanoparticle induced blood-brain barrier inflammation and increased permeability in primary rat brain microvessel endothelial cells. *Toxicol. Sci.* **2010**, *118*, 160–170. [CrossRef]
190. Pfurtscheller, K.; Petnehazy, T.; Goessler, W.; Bubalo, V.; Kamolz, L.P.; Trop, M. Transdermal uptake and organ distribution of silver from two different wound dressings in rats after a burn trauma. *Wound Repair Regen.* **2014**, *22*, 654–659. [CrossRef]

191. Hadrup, N.; Sharma, A.K.; Loeschner, K. Toxicity of silver ions, metallic silver, and silver nanoparticle materials after in vivo dermal and mucosal surface exposure: A review. *Regul. Toxicol. Pharmacol.* **2018**, *98*, 257–267. [CrossRef]
192. Moiemen, N.S.; Shale, E.; Drysdale, K.J.; Smith, G.; Wilson, Y.T.; Papini, R. Acticoat dressings and major burns: Systemic silver absorption. *Burns* **2011**, *37*, 27–35. [CrossRef]
193. Vlachou, E.; Chipp, E.; Shale, E.; Wilson, Y.T.; Papini, R.; Moiemen, N.S. The safety of nanocrystalline silver dressings on burns: A study of systemic silver absorption. *Burns* **2007**, *33*, 979–985. [CrossRef] [PubMed]
194. Trop, M.; Novak, M.; Rodl, S.; Hellbom, B.; Kroell, W.; Goessler, W. Silver-coated dressing acticoat caused raised liver enzymes and argyria-like symptoms in burn patient. *J. Trauma* **2006**, *60*, 648–652. [CrossRef]
195. Mimura, E.C.M.; Favoreto, J.P.M.; Favero, M.E.; Bonifacio, K.L.; Peixe, T.S.; Morita, A.A.; Barbosa, D.S.; Yabe, M.J.S.; Carrilho, A.J.F. Silver serum levels in burned patients treated with silver sulfadiazine and its toxicity on inflammatory cells. *Burns* **2020**, *46*, 1120–1127. [CrossRef] [PubMed]
196. Maitre, S.; Jaber, K.; Perrot, J.-L.; Guy, C.; Cambazard, F. Élévation des taux sériques et urinaires d'argent au cours d'un traitement topique par sulfadiazine argentique (Flammazine®). In Proceedings of the Annales de Dermatologie et de Vénéréologie, Paris, France, 30 June 2002; pp. 217–219.
197. Chaby, G.; Viseux, V.; Poulain, J.F.; De Cagny, B.; Denoeux, J.P.; Lok, C. Insuffisance rénale aiguë après application topique de sulfadiazine argentique. *Ann. Dermatol. Vénéréologie* **2005**, *132*, 891–893. [CrossRef] [PubMed]
198. Brouillard, C.; Bursztejn, A.C.; Latarche, C.; Cuny, J.F.; Truchetet, F.; Goullé, J.P.; Schmutz, J.L. Silver absorption and toxicity evaluation of silver wound dressings in 40 patients with chronic wounds. *J. Eur. Acad. Dermatol. Venereol.* **2018**, *32*, 2295–2299. [CrossRef]
199. Nadworny, P.L.; Landry, B.K.; Wang, J.; Tredget, E.E.; Burrell, R.E. Does nanocrystalline silver have a transferable effect? *Wound Repair Regen.* **2010**, *18*, 254–265. [CrossRef]
200. Liu, J.; Wang, Z.; Liu, F.D.; Kane, A.B.; Hurt, R.H. Chemical Transformations of Nanosilver in Biological Environments. *ACS Nano* **2012**, *6*, 9887–9899. [CrossRef]
201. Miclăuş, T.; Beer, C.; Chevallier, J.; Scavenius, C.; Bochenkov, V.E.; Enghild, J.J.; Sutherland, D.S. Dynamic protein coronas revealed as a modulator of silver nanoparticle sulphidation in vitro. *Nat. Commun.* **2016**, *7*, 11770. [CrossRef]
202. Chen, X.; Jhee, K.H.; Kruger, W.D. Production of the neuromodulator H2S by cystathionine beta-synthase via the condensation of cysteine and homocysteine. *J. Biol. Chem.* **2004**, *279*, 52082–52086. [CrossRef] [PubMed]
203. Omorou, M.; Liu, N.; Huang, Y.; Al-Ward, H.; Gao, M.; Mu, C.; Zhang, L.; Hui, X. Cystathionine beta-Synthase in hypoxia and ischemia/reperfusion: A current overview. *Arch. Biochem. Biophys.* **2022**, *718*, 109149. [CrossRef] [PubMed]
204. Massi, D.; Santucci, M. Human generalized argyria: A submicroscopic and X-ray spectroscopic study. *Ultrastruct. Pathol.* **1998**, *22*, 47–53. [CrossRef]
205. Payne, C.M.; Bladin, C.; Colchester, A.C.; Bland, J.; Lapworth, R.; Lane, D. Argyria from excessive use of topical silver sulphadiazine. *Lancet* **1992**, *340*, 126. [CrossRef]
206. Van de Voorde, K.; Nijsten, T.; Schelfhout, K.; Moorkens, G.; Lambert, J. Long-term use of silver containing nose-drops resulting in systemic argyria. *Acta Clin. Belg.* **2005**, *60*, 33–35. [CrossRef]
207. Cameron, S.J.; Hosseinian, F.; Willmore, W.G. A Current Overview of the Biological and Cellular Effects of Nanosilver. *Int. J. Mol. Sci.* **2018**, *19*, 2030. [CrossRef]
208. Piao, M.J.; Kang, K.A.; Fernando, P.; Herath, H.; Hyun, J.W. Silver nanoparticle-induced cell damage via impaired mtROS-JNK/MnSOD signaling pathway. *Toxicol. Mech. Methods* **2024**, *34*, 803–812. [CrossRef]
209. Coombs, C.J.; Wan, A.T.; Masterton, J.P.; Conyers, R.A.; Pedersen, J.; Chia, Y.T. Do burn patients have a silver lining? *Burns* **1992**, *18*, 179–184. [CrossRef]
210. McCague, A.; Joe, V.C. A Case of Argyria and Acute Leukopenia Associated with the Use of an Antimicrobial Soft Silicone Foam Dressing. *J. Burn Care Res.* **2016**, *37*, e493–e496. [CrossRef]
211. Aktepe, N.; Kocyigit, A.; Yukselten, Y.; Taskin, A.; Keskin, C.; Celik, H. Increased DNA damage and oxidative stress among silver jewelry workers. *Biol. Trace Elem. Res.* **2015**, *164*, 185–191. [CrossRef] [PubMed]
212. Rybka, M.; Mazurek, Ł.; Konop, M. Beneficial Effect of Wound Dressings Containing Silver and Silver Nanoparticles in Wound Healing—From Experimental Studies to Clinical Practice. *Life* **2023**, *13*, 69. [CrossRef]
213. Shrestha, S.; Wang, B.; Dutta, P.K. Commercial Silver-Based Dressings: In Vitro and Clinical Studies in Treatment of Chronic and Burn Wounds. *Antibiotics* **2024**, *13*, 910. [CrossRef]
214. Dias, M.; Zhang, R.; Lammers, T.; Pallares, R.M. Clinical translation and landscape of silver nanoparticles. *Drug Deliv. Transl. Res.* **2025**, *15*, 789–797. [CrossRef]
215. Meekul, J.; Chotirosniramit, A.; Himakalasa, W.; Orrapin, S.; Wongthanee, A.; Pongtam, O.; Kulprachakarn, K.; Rerkasem, K. A Randomized Controlled Trial on the Outcome in Comparing an Alginate Silver Dressing with a Conventional Treatment of a Necrotizing Fasciitis Wound. *Int. J. Low. Extrem. Wounds* **2017**, *16*, 108–113. [CrossRef]

216. Metcalf, D.G.; Bowler, P.G. Clinical impact of an anti-biofilm Hydrofiber dressing in hard-to-heal wounds previously managed with traditional antimicrobial products and systemic antibiotics. *Burns Trauma* **2020**, *8*, tkaa004. [CrossRef]
217. Bowler, P.G.; Parsons, D. Combatting wound biofilm and recalcitrance with a novel anti-biofilm Hydrofiber® wound dressing. *Wound Med.* **2016**, *14*, 6–11. [CrossRef]
218. Wang, R.; Guo, Y.; Li, B.; Zheng, J.; Tang, Z.; Shu, M. Application Effect of Silver-Containing Dressings in the Repair of Chronic Refractory Wounds. *Evid. Based Complement. Altern. Med.* **2022**, *2022*, 3616923. [CrossRef]
219. Zhang, D.; Yao, D.; Ma, R.; Nan, S.; Lv, Y.; Zhu, Y.; Zhu, S. Effect of Silver Nanoparticles with Thermoplastic Polyurethane on Postoperative Rehabilitation of Diabetic Patients with Open Fracture of Lower Extremities. *Front. Surg.* **2022**, *9*, 954155. [CrossRef] [PubMed]
220. Hurd, T.; Woodmansey, E.J.; Watkins, H.M.A. A retrospective review of the use of a nanocrystalline silver dressing in the management of open chronic wounds in the community. *Int. Wound J.* **2021**, *18*, 753–762. [CrossRef] [PubMed]
221. Wang, Y.C.; Lee, H.C.; Chen, C.L.; Kuo, M.C.; Ramachandran, S.; Chen, R.F.; Kuo, Y.R. The Effects of Silver-Releasing Foam Dressings on Diabetic Foot Ulcer Healing. *J. Clin. Med.* **2021**, *10*, 1495. [CrossRef]
222. Dissemond, J.; Aare, K.; Ozer, K.; Gandhi, D.; Ryan, J.L.; DeKoven, M. Aquacel Ag Advantage/Ag+ Extra and Cutimed Sorbact in the management of hard-to-heal wounds: A cohort study. *J. Wound Care* **2023**, *32*, 624–633. [CrossRef]
223. Chan, R.K.; Nuutila, K.; Mathew-Steiner, S.S.; Diaz, V.; Anselmo, K.; Batchinsky, M.; Carlsson, A.; Ghosh, N.; Sen, C.K.; Roy, S. A Prospective, Randomized, Controlled Study to Evaluate the Effectiveness of a Fabric-Based Wireless Electroceutical Dressing Compared to Standard-of-Care Treatment Against Acute Trauma and Burn Wound Biofilm Infection. *Adv. Wound Care* **2024**, *13*, 1–13. [CrossRef] [PubMed]
224. Sen, C.K.; Mathew-Steiner, S.S.; Das, A.; Sundaresan, V.B.; Roy, S. Electroceutical Management of Bacterial Biofilms and Surgical Infection. *Antioxid. Redox Signal.* **2020**, *33*, 713–724. [CrossRef]
225. Rada, B.; Leto, T.L. Pyocyanin effects on respiratory epithelium: Relevance in *Pseudomonas aeruginosa* airway infections. *Trends Microbiol.* **2013**, *21*, 73–81. [CrossRef] [PubMed]
226. Lafontaine, N.; Jolley, J.; Kyi, M.; King, S.; Iacobaccio, L.; Staunton, E.; Wilson, B.; Seymour, C.; Rogasch, S.; Wraight, P. Prospective randomised placebo-controlled trial assessing the efficacy of silver dressings to enhance healing of acute diabetes-related foot ulcers. *Diabetologia* **2023**, *66*, 768–776. [CrossRef] [PubMed]
227. Brown, M.; Dalziel, S.R.; Herd, E.; Johnson, K.; Wong She, R.; Shepherd, M. A Randomized Controlled Study of Silver-Based Burns Dressing in a Pediatric Emergency Department. *J. Burn Care Res.* **2016**, *37*, e340–e347. [CrossRef]
228. Housler, G.J.; Cross, S.; Marcel, V.; Kennedy, D.O.; Husband, M.; Register, A.; Roberts, T.; Grubbs, S.; Dudewicz, D.; Setka, N.; et al. A Prospective Randomized Controlled Two-Arm Clinical Study Evaluating the Efficacy of a Bioelectric Dressing System for Blister Management in US Army Ranger Recruits. *J. Spec. Oper. Med.* **2017**, *17*, 49–58. [CrossRef]
229. Hundeshagen, G.; Collins, V.N.; Wurzer, P.; Sherman, W.; Voigt, C.D.; Cambiaso-Daniel, J.; Nunez Lopez, O.; Sheaffer, J.; Herndon, D.N.; Finnerty, C.C.; et al. A Prospective, Randomized, Controlled Trial Comparing the Outpatient Treatment of Pediatric and Adult Partial-Thickness Burns with Suprathel or Mepilex Ag. *J. Burn Care Res.* **2018**, *39*, 261–267. [CrossRef]
230. Aurora, A.; Beasy, A.; Rizzo, J.A.; Chung, K.K. The Use of a Silver-Nylon Dressing During Evacuation of Military Burn Casualties. *J. Burn Care Res.* **2018**, *39*, 593–597. [CrossRef]
231. Moreira, S.S.; Camargo, M.C.; Caetano, R.; Alves, M.R.; Itria, A.; Pereira, T.V.; Lopes, L.C. Efficacy and costs of nanocrystalline silver dressings versus 1% silver sulfadiazine dressings to treat burns in adults in the outpatient setting: A randomized clinical trial. *Burns* **2022**, *48*, 568–576. [CrossRef]
232. Jiang, X.; Khan, S.; Dykes, A.; Stulz, E.; Zhang, X. Biogenic Synthesis of Silver Nanoparticles and Their Diverse Biomedical Applications. *Molecules* **2025**, *30*, 3104. [CrossRef]
233. Veličković, V.M.; Macmillan, T.; Lones, E.; Arlouskaya, Y.; Prieto, P.A.; Webb, N.; Crompton, A.; Munro, I.; Carvalho, V.F.; Attila, S.; et al. Systematic review and quality assessment of clinical and economic evidence for superabsorbent wound dressings in a population with chronic ulcers. *Int. Wound J.* **2024**, *21*, e14750. [CrossRef]
234. Gould, L.J.; Liu, J.; Wan, R.; Carter, M.J.; Dotson, M.; Driver, V.R. Evidence supporting wound care end points relevant to clinical practice and patients' lives. Part 3: The Patient Survey. *Wound Repair Regen.* **2021**, *29*, 60–69. [CrossRef]
235. Rawal, M.; Singh, A.; Amiji, M.M. Quality-by-Design Concepts to Improve Nanotechnology-Based Drug Development. *Pharm. Res.* **2019**, *36*, 153. [CrossRef]
236. Lin, C.; Huang, X.; Xue, Y.; Jiang, S.; Chen, C.; Liu, Y.; Chen, K. Advances in medical devices using nanomaterials and nanotechnology: Innovation and regulatory science. *Bioact. Mater.* **2025**, *48*, 353–369. [CrossRef]
237. Taleuzzaman, M.; Jahangir, M.A.; Chauhan, S.; Kala, C.; Beg, S. Chapter 19—Good laboratory practice and current good manufacturing practice requirements in the development of cancer nanomedicines. In *Nanoformulation Strategies for Cancer Treatment*; Beg, S., Rahman, M., Choudhry, H., Souto, E.B., Ahmad, F.J., Eds.; Elsevier: Amsterdam, The Netherlands, 2021; pp. 341–352.

238. Vo, D.-K.; Trinh, K.T.L. Advances in Wearable Biosensors for Wound Healing and Infection Monitoring. *Biosensors* **2025**, *15*, 139. [CrossRef] [PubMed]
239. Li, J.; Li, Z.; Xiao, J.; Nie, C. Conformable electrochemical devices for closed-loop wound management. *Front. Bioeng. Biotechnol.* **2023**, *11*, 1331567. [CrossRef] [PubMed]
240. Ferdous, Z.; Nemmar, A. Health Impact of Silver Nanoparticles: A Review of the Biodistribution and Toxicity Following Various Routes of Exposure. *Int. J. Mol. Sci.* **2020**, *21*, 2375. [CrossRef]
241. Huang, Y.; Chen, R.; Chen, Y.; Lü, X. Investigation of molecular mechanisms in silver nanoparticle-induced cytotoxicity from gene to metabolite level. *Sci. Rep.* **2025**, *15*, 26923. [CrossRef]
242. Gao, X.; Li, R.; Yourick, J.J.; Sprando, R.L. Transcriptomic and proteomic responses of silver nanoparticles in hepatocyte-like cells derived from human induced pluripotent stem cells. *Toxicol. Vitr.* **2022**, *79*, 105274. [CrossRef] [PubMed]
243. Vohra, M.; Kour, A.; Kalia, N.P.; Kumar, M.; Sharma, S.; Jaglan, S.; Kamath, N.; Sharma, S. A comprehensive review of genomics, transcriptomics, proteomics, and metabolomic insights into the differentiation of *Pseudomonas aeruginosa* from the planktonic to biofilm state: A multi-omics approach. *Int. J. Biol. Macromol.* **2024**, *257*, 128563. [CrossRef] [PubMed]